E. Ü. FEN BİLİMLERİ ENSTİTÜSÜ

EGE ÜNİVERSİTESİ

YÜKSEK LİSANS TEZİ

PREPARATION AND CHARACTERIZATION OF METAL NANO PARTICLES MODIFIED CARBON NANOTUBE AND POLYMER FILM ELECTRODES AND THEIR ANALYTICAL APPLICATIONS

Çağrı Ceylan BAKIR

Supervised by: Associate Prof. Dr. Zekerya DURSUN

Deparment of Chemistry

Code of dicipline: 405.03.01
Presentation Date: 22.07.2010

Bornova-İZMİR

2010

EGE UNIVERSITY

**GRADUATE SCHOOL OF
NATURAL AND APPLIED SCIENCE**

(MSc THESIS)

PREPARATION AND CHARACTERIZATION OF METAL NANO PARTICLES MODIFIED CARBON NANOTUBE AND POLYMER FILM ELECTRODES AND THEIR ANALYTICAL APPLICATIONS

Çağrı Ceylan BAKIR

Supervised by: Associate Prof. Dr. Zekerya DURSUN

Department of Chemistry

Code of dicipline: 405.03.01
Presentation Date: 22.07.2010

Bornova-İZMİR

2010

Çağrı Ceylan Bakır tarafından **Yüksek Lisans** tezi olarak sunulan "**Preparation and characterization of metal nano particles modified carbon nanotube and polymer film electrodes and their analytical applications**" başlıklı bu çalışma E.Ü. Lisansüstü Eğitim ve Öğretim Yönetmeliği ile E.Ü. Fen Bilimleri Enstitüsü Eğitim ve Öğretim Yönergesi'nin ilgili hükümleri uyarınca tarafımızdan değerlendirilerek savunmaya değer bulunmuş ve **22.07.2010** tarihinde yapılan tez savunma sınavında aday oybirliği/oyçokluğu ile başarılı bulunmuştur.

Jüri Üyeleri: **İmza**

Jüri Başkanı **: Doç. Dr. Zekerya DURSUN.....**

Raportör Üye **: Prof. Dr. F. Nil ERTAŞ .....**

Üye **: Doç. Dr. Nuri NAKİPOĞLU .....**

ÖZET

METAL NANO PARÇACIK MODİFİYE EDİLMİŞ KARBON NANOTÜP VE POLİMER FİLM ELEKTROTLARIN HAZIRLANMASI, KARAKTERİZASYONU VE ANALİTİK UYGULAMALARI

BAKIR, Çağrı Ceylan

Yüksek Lisans Tezi, Kimya Bölümü
Tez Yöneticisi: Doç. Dr. Zekerya DURSUN
Temmuz, 2010, 119 sayfa

Son yıllarda nanoteknoloji ve nanobilimdeki gelişmeler ile fizik, kimya ve biyoloji konusunda bilgi sağlayan sensör çalışmaları da artmıştır. Geleneksel elektrotların kimi uygulamalardaki yetersizliği, analitlere karşı katalitik etkinliği ve seçimliliği yüksek, farklı yüzeylere ihtiyaç duyurmuştur. Bu amaca yönelik yüksek iletkenlik, geniş ve etkin yüzey alanlarına sahip karbon nanotüp ve iletken polimer filmlerin metal nanoparçacıklar ile birleştirilmesi önemli yeni elektrot malzemeleri olarak kullanılmaktadır.

İki bölümden oluşan bu tez çalışmasının ilk kısmında, metal nanoparçacıklar ile modifiye, koşullandırılmış çok duvarlı karbon nanotüp (MWCNT) kaplı elektrotlar hazırlanarak oksijenin elektrokatalitik indirgenmesine olan etkileri incelenmiştir. Oksijen ile doyurulmuş 0.1M NaOH çözeltisi içinde oksijen indirgenmesine karşı en yüksek katalitik etkinlik, bakır ve altın nano parçacıkların karbon nanotüp yüzeyinde birarada olduğu koşullarda gözlenmiştir (Cu-Au-MWCNT/GCE). Bimetalik nano parçacık modifiye karbon nanotüp kaplı elektrot camımsı karbon elektrot ile karşılaştırıldığında hem akımı 10 kat arttırmış hemde indirgenme pik potansiyelini 80 mV daha pozitife kaydırmıştır.

Diğer kısımda ise poli-4-aminofenol polimer film elektrotlar, askorbik asit (AA), epinefrin (EN) ve ürik asit (UA) moleküllerinin tek başlarına ve birarada olduğu koşullarda elektrokimyasal davranışlarının incelenmesinde kullanılmıştır. Polimer filmin mevcut iletkenlik özelliklerini arttırmak için aşırı yükseltgeme işlemi uygulanmış ve ardından yükseltgenmiş elektrot yüzeyinde elektrokimyasal yöntemle Pt nano parçacıklar oluşturulmuştur. Polimer film

elektrotta yalın camımsı karbon elektroda göre katalitik etkinin arttığı görülmüştür. Pt modifiye polimer film elektrot ile pik akımlarında artış gözlenmiş ve üç maddenin birarada bulunduğu koşullarda en iyi pik ayrımı gerçekleşmiştir.

AA, EN ve UA moleküllerinin tek tek ve birarada bulunduğu koşullardaki davranışları diferansiyel puls voltammetri ile çalışılmıştır. Belirtme sınırları Ox-PAP/GCE için AA, EN, UA in tek başlarına bulunduğu koşullarda sırasıyla $8x10^{-6}$M, $6.5x10^{-9}$ M, $6.4x10^{-8}$M olarak bulunmuştur. Bu analitlerinin ikisinin derişiminin sabit tutulup, diğer üçüncünün derişiminin incelendiği koşullarda ise belirtme sınırları AA, EN ve UA için sırasıyla $9.5x10^{-6}$ M, 9 $x10^{-8}$ M, $1.4x10^{-7}$ M dır. Ayrıca Pt-Ox-PAP/GCE için belirtme sınırları, AA, EN, UA in tek başlarına bulunduğu koşullarda sırasıyla $1.8x10^{-5}$M, $1.8x10^{-7}$ M, $2.2x10^{-6}$M olarak bulunmuştur. Bu analitlerinin ikisinin derişiminin sabit tutulup, diğer üçüncünün derişiminin incelendiği koşullarda ise belirtme sınırları AA, EN ve UA için sırasıyla $5x10^{-5}$ M, 3.6 $x10^{-7}$ M, 4.1 $x10^{-6}$ M dır.

Tüm polymer ve karbon nanotüp ile modifiye edilmiş elektrot yüzeyleri ve onların metal nano parçacık kaplı formları atomik kuvvet mikroskopu, taramalı elektron mikroskopu ve X-ışını fotoelektron spektroskopisi ile karakterize edilmiştir.

Anahtar sözcükler: metal nano parçacık, karbon nanotüp, poly-aminofenol, oksijen, askorbik asit, epinefrin, ürik asit, voltammetri, AFM, SEM, XPS.

ABSTRACT

PREPARATION AND CHARACTERIZATION OF METAL NANO PARTICLES MODIFIED CARBON NANOTUBE AND POLYMER FILM ELECTRODES AND THEIR ANALYTICAL APPLICATIONS

BAKIR, Çağrı Ceylan

MSc in Chemistry Deparment
Supervisor: Assoc. Prof. Dr. Zekerya DURSUN
July, 2010, 119 pages

In recent years, sensor studies that provide information on physic, chemistry and biology were increased with the progress on nanoscience and nanotechnology. The insufficient behaviour of conventional electrodes in some applications, cause the necessity of different active surfaces which were more selective and catalytically active towards analytes. The combination of metal nano particles with conductive polymers and carbon nanotubes which have high conductivity and wide active surface area was used as important new electrode materials.

In the first part of this thesis which consisted of two different sections, metal nano particles modified acid treated carbon nanotube covered electrodes were prepared and their effect on oxygen reduction reaction was investigated. The best catalytic activity towards oxygen reduction reaction in O_2 saturated 0.1 M NaOH solution was obtained for coexistence of Cu and Au nanoparticles on the carbon nanotube surface. Bimetallic nano particles modified carbon nanotube electrodes not only higher the peak current 10 times higher than the bare GCE but also shifted the reduction potential about 80 mV positive compared to the bare electrode.

In another part of this thesis, poly 4-aminophenol film modified electrodes were used for investigation of individual and simultaneous electrochemical behavior of ascorbic acid (AA), epinephrine (EN) and uric acid (UA). The over-oxidation process was applied to polymer film for increasing the conductive properties and then Pt nano particles were formed on

electrode surface by electrochemical method. It was observed that increasing catalytic activity for modified electrodes comparing bare glassy carbon electrode. The enhanced peak current and well-defined peak seperations in existence of all three molecules show that best catalytic activity was obtained using Pt nanoparticules modified Ox-PAP/GCE.

The individual and simultaneous determination of AA, EN and UA were studied by DP. The detection limits were calculated for individually ,AA, EN, UA $1.7x10^{-5}$M, $6.5x10^{-9}$ M, $1.8x10^{-7}$M and in simultaneously determination, limit of detection values were calculated for AA, EN, UA, $1x10^{-6}$ M, $9\ x10^{-8}$ M, $1.4x10^{-7}$ M, respectively at Ox-PAP/GCE. Also at Pt-Ox-PAP/GCE detection limits were calculated for individually, AA, EN and UA $1.8x10^{-5}$ M, $1.8x10^{-7}$ M, $2.2x10^{-6}$M and in simultaneously determination LODs were calculated for AA, EN, UA, $5x10^{-5}$ M, $3.6\ x10^{-7}$ M, $4.1x10^{-6}$ M, respectively

All polymer and carbon nanotube modified electrode surfaces were characterized by atomic force microscopy, X-Ray photoelectron spectroscopy and scanning electron microscopy.

Keywords: metal nano particles, carbon nanotube, poly-aminophenol, oxygen, ascorbic acid, epinephrine, uric acid, voltammetry, AFM, SEM, XPS.

ACKNOWLEDGEMENT

I would like to express my deep gratitude to my supervisor Associte. Prof. Dr. Zekerya DURSUN for his encouragement, patience and valuable guidance during the whole period of my research.

I also would like to express my sincere gratitutes to Dr. Süleyman KOÇAK for his encouragement and collaboration throughout the study.

I am very grateful to Res. Asst. Şükriye ULUBAY, M.Sc Chemist Buket GELMEZ and PhD Student Aydan ELÇİ BAŞARAN for their friendly assistance, collaboration and fellowships during my laboratory studies.

I wish to thank to Ege University Solar Energy Institute and IYTE MAM for AFM and SEM imaging studies.

Also I would like to thank EBİLTEM BAP and TUBITAK- Münir Birsel Foundation of Master Scholarships for their financial support.

Finally, I would like to thank my parents for immortal confidence, their support and encouragement for my education.

Çağrı Ceylan BAKIR

2010 İZMİR

LIST OF CONTENTS

	Pages
ÖZET	v
ABSTRACT	vii
ACKNOWLEDGEMENT	İX
LIST OF FIGURES	XXVİ
LIST OF TABLES	XXVİ
ABBREVIATIONS	XXVİİ
1. INTRODUCTION	1
1.1 The aim of The Thesis	3
1.2 Carbon Nanotubes	4
1.3 Types of CNTs and Their Synthesis.	7
1.4 Conductive Electroactive Polymers	13
1.4.1 Applications of Ceps	14
1.4.2 Studies at Polymer Modified Electrodes	15
1.5 Metal Nano Particles	17
1.6. Ascorbic Acid	19
1.6.1 Chemical Properties and Biological Importance of AA	19
1.6.2 Determination Methods for AA	21

LIST OF CONTENTS(continue)

1.7 Epinephrine	23
1.7.1 Chemical Properties and Biological Importance of EN	23
1.7.2. Determination Methods for EN	24
1.8 Uric Acid	27
1.8.1 Chemical Properties And Biological Importance of UA	27
1.8.2. Determination Methods for UA	28
1.9 Methods For Simultaneous Determination of, AA, EN and UA	30
1.10 Fundamentals of Voltammetric Techniques	33
1.10.1 Polarography	34
1.10.2 Pulse Voltammetry	34
1.10.1.1 Cyclic Voltammetry	36
1.11 Surface Characterization Techniques	39
1.11.1 Atomic Force Microscopy (AFM)	40
1.11.2 Scanning Electron Microscope (SEM)	41
1.11.3 X-Ray Photoelectron Spectroscopy (XPS)	43
2. EXPERIMENTAL	45
2.1 Instrumentation	45
2.2 Reagents And Solutions	45

LIST OF CONTENTS(continue)

2.3 Methods 47

2.3.1 Pre-Conditioning of GCE 47

2.3.2 Pre-Treatment of Multiwalled Carbon Nanotubes 47

2.3.3 Preparation of Mwcnt Modified GCE 47

2.3.4 Preparation of Polyaminophenol Film Modified GCE 47

2.3.5 Preparation of Pt, Au, Cu Metal Nanoparticles Modified MWCNT/ GCE and Ox-PAP/ GCE 48

2.3.6 Preparatin of EN Samples 48

3. RESULTS AND DISCUSSION 49

3.1 Voltammetric Behaviour of MWCNT /GC Electrode in the Presence of Cu^{2+}, Au^{3+} İons 49

3.2 Surface Characterization of CNT and Metal Nano Particules Modified CNT Film Electrodes 50

3.3 Voltammetric Behaviour of Oxygen at Bare and Modified Electrodes 52

3.4 Optimization Studies of Oxygen Reduction at Cu-Au-MWCNT/GCE. 53

3.4.1 Optimization of Sodium Hydroxide Concentration 53

3.4.2 The Influence of Nano Cu and Au Particles Amount on Oxygen Reduction 54

3.4.3 Electroreduction of Oxygen At GCE, MWCNT / GCE And $Cu_{(4cyc)}$ – $Au_{(6cyc)}$ - MWCNT / GCE 55

LIST OF CONTENTS(continue)

3.4.4. Scan Rate Study at $Cu_{(4cyc)} - Au_{(6cyc)}$ - MWCNT / GCE 56

3.4.5 Tafel Plots for Oxygen Reduction at Different Electrodes 56

3.5 Preparation of Polyaminophenol Film Modified GCE 57

3.6 Optimization Studies for AA, EN and UA Oxidation at PAP/GCE 58

3.6.1 Effect of Supporting Electrolyte pH on Cyclic Voltammetric Behaviour of AA, EN, UA and Their Mixture 58

3.6.2 Optimization of Aminophenol Cycle Number 64

3.6.3 Optimization of p-Aminophenol Concentration 66

3.7 Preparation of Oxidized Polyaminophenol Film Modified Gce 66

3.7.1 Optimization of Overoxidation Time of Polyaminophenol 67

3.8 Voltammetric Behaviour of Ox-PAP/GCE Electrode in the Presence of Cu^{2+}, Au^{3+}And Pt^{4+} İons 68

3.9 Surface Characterization of Ox-PAP/GCE and Metal Nano Particules Modified Ox-PAP/GCE 70

3.10 Electrochemical of Behaviour of AA, EN and UA Mixture At Metal Nano Particles Modified Ox-PAP/GCE 71

3.11 The Influence of Pt Nano Particles Amount on AA, EN and UA Oxidation. 73

3.12 Individual Electrocatalytic Oxidation of AA, EN and UA With GCE, Ox-PAP/GCE and Pt-Ox-PAP/GCE 74

3.13 Scan Rate Studies of AA, EN and UA at Different Electrodes 77

LIST OF CONTENTS(continue)

3.13.1 Scan Rate Studies of AA 77

3.13.2 Scan Rate Studies of EN 79

3.13.3 Scan Rate Studies of UA 81

3.14 Differential Pulse Voltammetric Determination of AA, EN and UA 83

3.17 Stability of Pt Nano Particles Modified Ox-PAP/GCE 105

3.18 Sample Analysis 106

4. GENERAL DISCUSSION AND CONCLUSION 108

REFERENCES 110

LIST OF FİGURES

Pages

Figure 1.1 Structure and geometry of different fullerene molecules. (a) The icosahedral C_{60} molecule, (b) C_{70} molecule, (c) a C_{80} molecule as an extended rugby ball-shaped molecule, (d) C_{80} molecule as in icosahedran 4

Figure 1.2 Different allotropes of the carbon element A) grafite B) diamond C) fullerene D) carbon nanotube. 5

Figure 1.3 A single walled carbon nanotube structure 6

Figure 1.4. Three basic geometric structure of carbon nanotubes (a) armchair, (b) zigzag, (c) chiral.....6

Figure 1.5 End sides of carbon nanotubes 7

Figure 1.6 Schematic diagram of (a) a single wall carbon nanotube (SWNT), (b) a multi-wall carbon nanotube (MWNT), (c) a double wall carbon nanotube (DWNT) and (d) a peapod nanotube consisting of a SWNT filled with fullerenes (e.g., C_{60}).....8

Figure 1.7 Images of SWCNT a) diameter and length b) Inner side of SWCNT. 9

Figure 1.8 Structure of p-aminophenol.....14

Figure 1.9 Scientific papers published on conducting polymers (1990-2000) catecorized into various topics. 15

Figure 1.10 Structure of Ascorbic Acid molecule 20

Figure 1.11 Dehydrogenation reaction of ascorbic acid.....20

Figure 1.12 Structure of epinephrine. 23

Figure 1.13 Oxidation reaction of Epinephrine to Epinephrinequinone.....24

LIST OF FIGURES(continue)

Figure 1.14 Structure of Uric Acid molecule 27

Figure 1.15 Oxidation reaction of Uric acid to Allantoin.....28

Figure 1.16 The schematic represantation of waveform of normal pulse voltammetry 35

Figure 1.17 Differential pulse voltammetry. (a) Scheme of application of potentials (sometimes superimposed on a ramp rather than a staircase); (b) Schematic I-E profile. 36

Figure 1.18 A) potential waveform B) current-potential representations. 37

Figure 1.19 Comparison of the imaging of many types 2D and 3D profiling and imaging instruments (Rosenauer, 2003). 39

Figure 1.20 Illustration of an AFM cantilever /probe used in an AFM sensor (Nanomanyetik Catalogue). 41

Figure 1.21 Schematic diagram of the layout of a SEM (Kelsall, 2005).....42

Figure 1.22 Schematic of the experimental setup for using X-ray photoelectron spectroscopy (XPS) to investigate the catalyst-electrode surface. (Vayenas, et al., 2002) 43

Figure 3.1 a) Cu deposition, b) Au deposition on MWCNT/GCE, c) Cu deposition on Au-MWCNT/GCE at 50 mV/s for 10 cycles in 1 Mm $CuSO_4$ and $HAuCl_4$ respectively. 50

Figure 3.2 EDX results and typical SEM images of a) bare MWCNT/GCE b)Au-MWCNT/GCE c) Cu-Au-MWCNT/GCE d) EDX results. 51

Figure 3.3 XPS spectra of Cu-Au-MWCNT/GCE a) represents the peaks of Au 4f7/2 and 4f5/2 b) represents the main peak of Cu 2p3/2.....52

LIST OF FIGURES(continue)

Figure 3.4 Cyclic Voltammetric behavior of GCE, MWCNT/GCE and different metal nano particles modified MWCNT/GC electrodes in O_2 saturated 0.1 M NaOH. 52

Figure 3,5 Cyclic voltammograms for oxygen reduction on Cu-Au-MWCNT/GC electrode at different NaOH concentrations. 53

Figure 3.6 Cyclic voltammogram for oxygen reduction at different cycle number of nano particle deposition 54

Figure 3.7 Cyclic voltammogram of oxygen reduction reaction on bare, MWCNT and $Cu_{(4cyc)} - Au_{(6cyc)}$ -MWCNT/GCE. 55

Figure 3.8 Cyclic voltammogram for oxygen reduction of $Cu_{(4cyc)} - Au_{(6cyc)}$ -MWCNT/GC electrode at different scan rates. (3, 10, 25, 50, 150, 500 mV/s). 56

Figure 3.9 Tafel slopes of oxygen reduction on different electrodes for 3 mV/s scan rate. 57

Figure 3.10 Cyclic voltammogram of p-AP electropolymerization in a 5.0 mM p-AP monomer/ 0.5 M $HClO_4$ solution on the surface of the glassy carbon electrode in the presence of 5.0 mM SDS at a scan rate of 100 mVs^{-1}. The arrows indicate the trends of current during CVs. 58

Figure 3.11 Cyclic Voltammograms of electrooxidation of AA at bare and PAP/GC electrode in various pH (3.76 to 10.2) at a scan rate of 50 mV/s. 59

Figure 3.12 Cyclic Voltammograms of electrooxidation of EN at bare and PAP/GC electrode in various pH (3.76 to 10.2) at a scan rate of 50 mV/s. 60

Figure 3.13 Cyclic Voltammograms of electrooxidation of UA at bare and PAP/GC electrode in various pH (3.76 to 10.2) at a scan rate of 50 mV/s. 61

LIST OF FIGURES(continue)

Figure 3.14 Cyclic Voltammograms of electrooxidation of AA, EN, UA (10^{-4}, $10^{-5,}$ 10^{-5} M), mixture at PAP/GC electrode in various pH (3.76 to 10.2) at a scan rate of 50 mV/s. 62

Figure 3.15 Influence of the pH on a) peak potential and b) peak current for AA, EN and UA on the PAP/GCE with cyclic voltammetry (pH: 3.76 - 10.2) 63

Figure 3.16 Cyclic voltammograms of PAP/GCE and bare electrode with and without AA+ EN+ UA (.10^{-4}, 10^{-5}, 10^{-5} M) 63

Figure 3.17 Cycle effect of aminophenol on AA, EN and UA. Inset: cycle number effect on oxidation currents of AA, EN and UA 64

Figure 3.18 Cycle number effect on oxidation peak potentials of AA, EN and UA. 65

Table 3.1 Cycle number effect on oxidation peak potentials of AA, EN, UA and peak seperation values of their mixture at PAP/GCE. 65

Figure 3.19 Effect of aminophenol concentration on AA, EN and UA. 66

Figure 3.20 Oxidation of polyaminophenol on GCE in 0.1 M NaOH solution.....67

Figure 3.22 Effect of over oxidation time of polyaminophenol film on peak potential seperations between AA-EN and EN-UA. 68

Figure 3.23 cyclic voltammograms of a) Cu, b) Au, c) Pt nano particles deposition on Ox-PAP/GCE. 69

Figure 3.24 AFM images of a) bare GCE, b)PAP/GCE, c) Pt nano particles modified Ox-PAP/GCE in three dimensional view. 70

Figure 3.25 SEM images of a) bare GCE, b) PAP/GCE, c) Oxidized PAP/GCE d) Pt nano particles modified Ox-PAP/GCE. 71

LIST OF FIGURES(continue)

Figure 3.26 Cyclic Voltammetric behavior of AA, EN, UA mixture at a) Au-Ox-PAP/GCE., b) Cu-Ox-PAP/GCE. and c) Pt-Ox-PAP/GCE compared with bare and Ox-PAP/GCE 72

Figure 3.27 Effect of cycle number of Pt deposition on Ox-PAP/GCE on simultaneous oxidation of AA, EN and UA in concentrations of $5x10^{-4}$ M, 10^{-5} M, 10^{-4} M, respectively. 73

Figure 3.28 Comperative voltammograms for individual oxidatios of a) AA, b) EN and c) UA at bare, Ox-PAP and Pt-Ox-PAP electrodes all in concent. of $5x\ 10^{-4}$ M 75

Figure 3.29 Cyclic voltammograms of AA oxidation at a) GCE, b) Ox-PAP/GCE, c) Pt- Ox-PAP/GCE with various scan rates (10-200 mV/s) 77

Figure 3.30 Dependence of scan rate on the a) peak current and b) peak potential of AA oxidation at bare GCE, Ox-PAP/GCE and Pt-Ox-PAP/GCE. 78

Figure 3.31 Cyclic voltammograms of EN oxidation at a) GCE, b) Ox-PAP/GCE, c) Pt-Ox-PAP/GCE with various scan rates (10-200 mV/s) 79

Figure 3.32 Dependence of scan rate on the a) peak current and b) peak potential of EN oxidation at bare GCE, Ox-PAP/GCE and Pt-Ox-PAP/GCE 80

Figure 3.33 Cyclic voltammograms of UA oxidation at a) GCE, b) Ox-PAP/GCE, c) Pt-Ox-PAP/GCE with various scan rates (10-200 mV/s) 81

Figure 3.34 Dependence of scan rate on the a)peak current and b) peak potential of UA oxidation at bare GCE, Ox-PAP/GCE and Pt-Ox-PAP/GCE. 82

LIST OF FIGURES(continue)

Figure 3.35 Differential pulse voltammograms at GCE for increasing concanterations of AA in 0.1 M pH 7.40 PBS with scan rate 10 mV/s and pulse amplitude 50 mV.(Inset: Corresponding calibration curve of increasing AA concentrations). AA concentrations (a-n) 0 M, $2x10^{-5}$ M, $8x10^{-5}$M, $1x10^{-4}$M, $1.5x10^{-4}$M, $2.0x10^{-4}$ M, $2.5x10^{-4}$ M, $3.0x10^{-4}$ M, $3.5x10^{-4}$M, $4.0x10^{-4}$M, $5x10^{-4}$ M, $6x10^{-4}$M, 8 $x10^{-4}$, 1 $x10^{-3}$ M. 84

Figure 3.36 Differential pulse voltammograms at Ox-PAP/GCE for increasing concanterations of AA in 0.1 M pH 7.40 PBS with scan rate 10 mV/s and pulse amplitude 50 mV.(Inset: Corresponding calibration curve of increasing AA concentrations). AA concentrations (a-0) 0 M, $2x10^{-5}$ M, $4x10^{-5}$M, $6x10^{-5}$M, $7x10^{-5}$M, $8x10^{-5}$ M, $1x10^{-4}$ M, $1.5x10^{-4}$ M, $2x10^{-4}$M, $2.5x10^{-4}$M, $3x10^{-4}$ M, $4x10^{-4}$M, 6 $x10^{-4}$, $8x10^{-4}$, 1 $x10^{-3}$ M. 85

Figure 3.37 Differential pulse voltammograms at Pt-Ox-PAP/GCE for increasing concanterations of AA in 0.1 M pH 7.40 PBS with scan rate 10 mV/s and pulse amplitude 50 mV.(Inset: Corresponding calibration curve of increasing AA concentrations). AA concentrations (a-j) 0 M, $4x10^{-5}$M, $7x10^{-5}$ M, $9x10^{-5}$ M, 2 $x10^{-4}$M, $3x10^{-4}$ M, $4x10^{-4}$M, 6 $x10^{-4}$, $8x10^{-4}$, 1 $x10^{-3}$ M. 86

Figure 3.38 Calibration curves for AA oxidation at bare, Ox-PAP/GCE and Pt-Ox-PAP/GCE for the same concentration ranges between 8 $x10^{-5}$- 10^{-3} M 87

Figure 3.39 Differential pulse voltammograms at GCE for increasing concanterations of EN in 0.1 M pH 7.40 PBS with scan rate 10 mV/s and pulse amplitude 50 mV.(Inset: Corresponding calibration curve of increasing EN concentrations). EN concentrations (a-g) 0 M, $1x10^{-5}$M, $2x10^{-5}$M, $3.0x10^{-5}$M, $5x10^{-5}$ M, $7x10^{-5}$M, 1 $x10^{-4}$ M. 88

LIST OF FIGURES(continue)

Figure 3.40 Differential pulse voltammograms at Ox-PAP/GCE in the presence of increasing concentration of Epinephrine 0.1 M pH 7.40 PBS with scan rate 10 mV/s, (a) 0 (b) $1.0x10^{-8}$, (c) $4.0x10^{-8}$, (d) $8.0x10^{-8}$, (e) $1.2x10^{-7}$, (f) $2.0x10^{-7}$, (g) $4.0x10^{-7}$, (h) $6.0x10^{-7}$, (i) $8.0x10^{-7}$, (j) $1.0x10^{-6}$, (k) $2.0x10^{-6}$, (l) $4.0x10^{-6}$, (m) $6.0x10^{-6}$, (n) $8.0x10^{-6}$, (o) $1.0x10^{-5}$, (p) $2.0x10^{-5}$, (r) $4.0x10^{-5}$, (s) $6.0x10^{-5}$, (t) $8.0x10^{-5}$ M.....89

Figure 3.41 Differential pulse voltammograms at Pt-Ox-PAP/GCE for increasing concanterations of EN in 0.1 M pH 7.40 PBS with scan rate 10 mV/s and pulse amplitude 50 mV.(Inset: Corresponding calibration curve of increasing EN concenrations.) EN concentrations (a-i) $4x10^{-6}$M, $5x10^{-6}$ M, $6x10^{-6}$ M, $8x10^{-6}$M, $1x10^{-5}$, $2x10^{-5}$ M, $4x10^{-5}$M, 6 $x10^{-5}$ M, $8x10^{-5}$M, 1 $x10^{-4}$ M. 90

Figure 3.42 Calibration curves for EN oxidation at bare, Ox-PAP/GCE and Pt-Ox-PAP/GCE for the same concentration ranges between 8 $x10^{-6}$- 10^{-4} M 91

Figure 3.43 Differential pulse voltammograms at GCE for increasing concanterations of UA in 0.1 M pH 7.40 PBS with scan rate 10 mV/s and pulse amplitude 50 mV.(Inset: Corresponding calibration curve of increasing UA concentrations). UA concentrations (a-n) 0 M, $4x10^{-6}$M, $6x10^{-6}$M, $7x10^{-6}$M, $8.0x10^{-6}$ M, $1x10^{-5}$ M, $2x10^{-5}$M, $4x10^{-5}$ M, $6x10^{-5}$M, $8x10^{-5}$M, $1.0x10^{-4}$M, $5x10^{-5}$ M, $7x10^{-5}$M, 1 $x10^{-4}$ M UA. 92

Figure 3.44 Differential pulse voltammograms at Ox-PAP/GCE in the presence of increasing concentration of Uric Acid in 0.1 M pH 7.40 PBS with scan rate 10 mV/s, (a) 0 (b) $1.0x10^{-7}$, (c) $2.0x10^{-7}$, (d) $4.0x10^{-7}$, (e) $6.0x10^{-7}$, (f) $8.0x10^{-7}$, (g) $1.0x10^{-6}$, (h) $2.0x10^{-6}$, (i) $4.0x10^{-6}$, (j) $8.0x10^{-6}$, (k) $1.0x10^{-5}$, (m) $2.0x10^{-5}$, (n) $4.0x10^{-5}$ M. (Inset: Corresponding calibration curve of increasing UA concentrations). 93

LIST OF FIGURES(continue)

Figure 3.45 Differential pulse voltammograms at Pt-Ox-PAP/GCE for increasing concanterations of UA in 0.1 M pH 7.40 PBS with scan rate 10 mV/s and pulse amplitude 50 mV.(Inset: Corresponding calibration curve of increasing UA concenrations.) UA concentrations (a-i) $4x10^{-6}$M, $6x10^{-6}$ M, $8x10^{-6}$ M, $1x10^{-5}$, $2x10^{-5}$ M, $4x10^{-5}$M, 6 $x10^{-5}$ M, $8x10^{-5}$M, 1 $x10^{-4}$ M.....94

Figure 3.46 Calibration curves for UA oxidation at bare, Ox-PAP/GCE and Pt-Ox-PAP/GCE for the same concentration ranges between 4 $x10^{-6}$- 10^{-4} M 95

Figure 3.47 Differential pulse voltammograms at Ox-PAP/GCE in the presence of EN ($2x10^{-5}$ M) and UA ($2x10^{-5}$ M) for increasing concanterations of AA in 0.1 M pH 7.40 PBS with scan rate 10 mV/s and pulse amplitude 50 mV.(Inset: Corresponding calibration curve of increasing AA concenrations). (a) 0 M AA, EN, UA, (b-j) $1x10^{-5}$M, $2x10^{-5}$ M, $4x10^{-5}$ M, $6x10^{-5}$, $8x10^{-5}$ M, $1x10^{-4}$M, 2.2 $x10^{-4}$ M, $4x10^{-4}$ M, $7x10^{-4}$ M AA. 96

Figure 3.48 Differential pulse voltammograms at Pt-Ox-PAP/GCE in the presence of EN ($2x10^{-5}$ M) and UA ($2x10^{-5}$ M) for increasing concanterations of AA in 0.1 M pH 7.40 PBS with scan rate 10 mV/s and pulse amplitude 50 mV. (Inset: Corresponding calibration curve of increasing AA concenrations). AA, EN, UA: (a-h) $8x10^{-5}$M, $1x10^{-4}$ M, $2x10^{-4}$ M, $3x10^{-5}$ M, $5x10^{-5}$ M, $6x10^{-5}$ M, $7x10^{-5}$ M, $1x10^{-3}$ M. 97

Figure 3.49 Differential pulse voltammograms at Ox-PAP/GCE in the presence of AA ($5x10^{-4}$ M) and UA ($5x10^{-5}$ M) for increasing concanterations of EN in 0.1 M pH 7.40 PBS with scan rate 10 mV/s and pulse amplitude 50 mV.(Inset: Corresponding calibration curve of increasing EN concenrations). (a) 0 M AA, EN, UA, (b-j) $6x10^{-7}$M, $8x10^{-7}$ M, $3x10^{-6}$ M, $6x10^{-6}$ M, $7x10^{-6}$, $8x10^{-6}$ M.....98

LIST OF FIGURES(continue)

Figure 3.50 Differential pulse voltammograms at Pt-Ox-PAP/GCE in the presence of AA ($5x10^{-4}$ M) and UA ($5x10^{-5}$ M) for increasing concanterations of EN in 0.1 M pH 7.40 PBS with scan rate 10 mV/s and pulse amplitude 50 mV.(Inset: Corresponding calibration curve of increasing EN concenrations). (a) 0 M AA, EN, UA, (b-j) $6x10^{-7}$M, $8x10^{-7}$ M, $2x10^{-6}$ M, $4x10^{-6}$ M, $6x10^{-6}$, $8x10^{-6}$ M, $1x10^{-5}$ M. 99

Figure 3.51 Differential pulse voltammograms at Ox-PAP/GCE in the presence of AA ($5x10^{-4}$ M) and EN ($2x10^{-5}$ M) for increasing concanterations of UA in 0.1 M pH 7.40 PBS with scan rate 10 mV/s and pulse amplitude 50 mV.(Inset: Corresponding calibration curve of increasing UA concentrations) (a) 0 M UA, $5x10^{-4}$ M AA, $2x10^{-5}$ M EN, (b-k) $4x10^{-7}$M, $2x10^{-6}$ M, $6x10^{-6}$ M, $1x10^{-5}$ M, $4x10^{-5}$, $6x10^{-5}$ M, $7x10^{-5}$ M, $8x10^{-5}$, $9x10^{-5}$ M, $1.5x10^{-4}$ M. 100

Figure 3.52 Differential pulse voltammograms at Pt-Ox-PAP/GCE in the presence of AA (5x10-4 M) and EN (2x10-5 M) for increasing concanterations of UA in 0.1 M pH 7.40 PBS with scan rate 10 mV/s and pulse amplitude 50 mV.(Inset: Corresponding calibration curve of increasing UA concenrations). (a-k) $1x10^{-5}$ M, $1.3x10^{-5}$ M, $1.5x10^{-5}$ M, $1.8x10^{-5}$ M $2x10^{-5}$ M, $4x10^{-5}$ M, $6x10^{-5}$, $8x10^{-5}$ M, $1x10^{-4}$ M, $1.25x10^{-4}$, $1.5x10^{-4}$ M UA. 101

Figure 3.53 A) Differential pulse voltammograms at Ox-PAP/GCE in the presence of increasing concentrations of AA, EN and UA in 0.1 M pH 7.40 PBS with scan rate 10 mV/s, analyte concentrations: (a) 0 (b) $4.0x10^{-6}$ AA, $1.2x10^{-7}$ M EN and UA, (c) $6.0x10^{-6}$ AA, $4x10^{-7}$ M EN and UA (d)$7.0x10^{-6}$ AA, $6x10^{-7}$ M EN and UA, (e) $1.0x10^{-5}$ AA, $1x10^{-6}$ M EN and UA (f) $2.0x10^{-5}$ AA, $2x10^{-6}$ M EN and UA (g) $4.0x10^{-5}$ AA, $4x10^{-6}$ M EN and UA (h) $6.0x10^{-5}$ AA, $6x10^{-6}$ M EN and UA (i) $7.0x10^{-5}$ AA, 8 $x10^{-6}$ M EN and UA. **B)** Calibration curves of AA, EN and UA. 102

LIST OF FIGURES(continue)

Figure 3.54 A) Differential pulse voltammograms at Pt-Ox-PAP/GCE in the presence of increasing concentrations of AA, EN and UA in 0.1 M pH 7.40 PBS with scan rate 10 mV/s, analyte concentrations: (a) 0 (b) $4.0x10^{-5}$ AA, $4x10^{-6}$ M EN, $4x10^{-6}$ M UA, (c) $1.0x10^{-4}$ AA, $6x10^{-6}$ M EN, $1x10^{-5}$ M UA, (d) $2.0x10^{-4}$ AA, $7x10^{-6}$ M EN, $2x10^{-5}$ M UA, (e) $4.0x10^{-4}$ AA, $1x10^{-5}$ M EN, $4x10^{-5}$ M UA, (f) $5.0x10^{-4}$ AA, $2x10^{-5}$ M EN, $6x10^{-5}$ M UA, (g) $6.0x10^{-4}$ AA, $3x10^{-5}$ M EN, $8x10^{-5}$ M UA, (h) $7.0x10^{-4}$ AA, $4x10^{-5}$ M EN, $1x10^{-4}$ M UA, (i) $1.0x10^{-3}$ AA, $6x10^{-5}$ M EN, $2.5x10^{-4}$ M UA,. (j) $1.5x10^{-3}$ AA, $8x10^{-5}$ M EN, $3x10^{-4}$ M UA, (k) $2.0x10^{-3}$ AA, $1x10^{-4}$ M EN, $4x10^{-4}$ M UA,, B**)** Calibration curves of AA,EN and UA 103

Figure 3.55 Variation of peak current for AA, EN, UA mixture during 3 days. 105

Figure 3.56 Differential pulse voltammograms at Ox-PAP/GCE **A)** (a) pH 7.40 phosfate buffer, (b) EN sample in pH 7.40 phosfate buffer, (c) $5x10^{-6}$, (d) $10x10^{-6}$, (e) $15x10^{-6}$, (f) $20x10^{-6}$, inset: standart addition curves. 106

Figure 3.57 Standart addition curves for EN sample in pH 7.40 phosfate buffers at Pt-Ox-PAP/GCE, EN standard solution ($5x10^{-6}$, $10x10^{-6}$, $15x10^{-6}$, $20x10^{-6}$ M). 107

LIST OF TABLES

Pages

Table 1 Comparison of chemical and electrochemical CP polymerization.....13

Table 3.2 Optimum conditions of Experimental parameters.....74

Table 3.3 The peak current and potential values of AA, EN and UA oxidation at different electrodes.....76

Table 3.4 Limit of detection (LOD) and linear concentration range of bare GCE, Ox-PAP/GCE and Pt-Ox-PAP/GCE for AA, EN, UA and their mixture in this thesis 104

Table 3.5. Peak current values of Pt nano particules modified Ox-PAP/GCE 105

ABBREVIATIONS

A	Electrode area
AA	Ascorbic Acid
AFM	Atomic force microscopy
C	Analyte concentration
CE	Capillary Electrophoresis
CFC	Carbon reinforced material
CFME	Carbon fibre micro electrophoresis
CL	Chemiluminescence
CNT	Carbon Nanotubes
C_{ox}	Concentration of oxidized form
C_{red}	Concentration of reduced form
CV	Cyclic Voltammetry
D	Diffussion coefficient
DA	Dopamine
DHAA	dehydro-l-ascorbic acid
DME	dropping mercury electrode
DPV	Differential Pulse Voltammetry
E^0	The standart potential
Ep	Peak potential
EN	Epinephrine
Epa	Anodic peak potential
Epc	Cathodic peak potential
Eq	Equation
FIA	Flow injection analysis
GCE	Glassy carbon electrode
i_l	Limiting current
i_{pa}	Anodic peak current
i_{pc}	Cathodic peak current
LOD	Limit of Detection
LR	Lineer range
MNP	Metal nano particle
MWCNT	Multiwalled Carbon Nanotubes
NPV	Normal pulse voltammetry

ORR	Oxygen reduction reaction
Ox	Oxidized form
PAP	Polyaminophenol
PBS	Phosphate buffer solution
Red	Reduced form
SAM	Self-assemblied monolayer
SEM	Scanning Electron Microscopy
SDS	Sodium dodecil sulphate
SPE	screen printed electrode
SWCNT	Single Walled Carbon Nanotubes
UA	Uric Acid
V	Scan rate

1. INTRODUCTION

In the last 20 years, researchers have been focused on a new interdisciplinary field which is known as ***nanoscience and nanotechnology***. The terminology starts with 'colloids' about 150 years ago let the scientists began to understand that objects in the nanometer size range have special properties and behavior.

There has been an explosive growth of nanoscience and technology in the last few years, primarily because of the availability of new strategies for the synthesis of nanomaterials and new tools for characterization and manipulation. Several methods of synthesizing nanoparticles, nanowires and nanotubes, and their assemblies, have been discovered (Cao, et al., 2004).

Carbon based materials plays a major role in nano-sciences. Fullerenes, nanotubes, carbon onions are typical representatives of nano-structured carbons. Carbon nanotubes (CNTs), have received increasing attention due to their unique properties such as high surface area, significant electrical conductivity, extremely high mechanical strength and good chemical stability. Carbon nanotubes have wide application field as sensitive electrodes for some analysts such as coenzymes, neurotransmitters, nucleic acids and also oxygen reduction reaction (Rivas, et al., 2007).

The oxygen reduction reaction is one of the most important reactions in chemistry due to its significant role in fuel cells, batteries, chlor/alkali production, electro-synthesis of hydrogen peroxide, metal corrosion, gas sensors.Renewable and clean power sources researches have been studied for several decades. In this way, fuel cells have been considered as a candidate to minimize fossil fuels usage and its poisonous emissions. Despite recent advances, several issues like limited oxygen reduction reaction due to its high over potential, still need to be developed. The main point for enhancing the performance of the electrode is to prepared appropriate catalyst for oxygen reduction (Aoun, et al., 2004).

The common nanomaterials generally include nanoparticles, nanowires, nanotubes, nanocapsules, nanostructured alloys and polymers, nanoporous solids. What is also noteworthy is that chemists have synthesized molecular entities of nanometric dimensions. nanometer-sized metal particles or metal

nano particles (MNP) are objects of great interest in modern chemical research due to their unique electrical, magnetic, optical and other properties, which are distinct from both those of the bulk metal and those of isolated atoms and molecules (Haudy, et al., 2006).

Electrochemical studies with nanosized particles require them to be accessible to the electrode surface where the potential can be controlled. This can be accomplished either by using the metallic colloid along with an inert and planar electrode or by attaching the nanoparticle onto a conducting matrix (Cheetham, et al., 2004).

Polymer films can be formed on an electrode surface via dip coating, spin coating, electrodeposition, and covalent attachment. From these methods, the electrochemically modified polymer film electrodes have received extensive interest in the detection of analytes because the electrochemical deposition offers a thin and uniform structure, homogeneity and strong adherence. Conducting polymers also offer a chemical stable film to electrode surface which offer a selective and sensitivite opportunity for the analyte determine many biologically and pharmaceutically importance molecules. Polymer film surface was also used as host material for the preparaton of homogeneously distrubuted metal nano particles modification for electrocatalytic electrode reactions (Biallozor and Kupniewska, 2005).

Epinephrine (EN) is an important catecholamine neurotransmitter in the mammalian central nervous system and biological body fluids. It has been used for the treatment of myocardial infarction, hypertension, bronchial asthma, cardiac arrest, and cardiac surgery in clinics. Many physiological phenomena are correlative to EN’s level in the body fluids. Therefore, a simple, fast, and sensitive method is necessary for its determination in both biological fluids and pharmaceutical preparations. Uric acid (UA) and ascorbic acid (AA) commonly coexist in such biological fluids as blood and urine. Extreme abnormalities of UA levels are symptoms of several diseases. Thus, the determination of EN concentration in human blood or urine is very important as warning of certain diseases, such as Lesch–Nyhan syndrome and gout. However, a major obstacle usually encountered in the detection of EN is the interference of UA and AA which is usually present at high concentrations and can be oxidized at a potential close to that of EN. Thus, their simultaneous determinations have always been considered as a serious challenge among

scientists. The electrochemical signal of EN was interfered with AA and UA using commen bare electrodes due to the homogeneously electron transfer. Therefore, their simultaneous determinations have always been considered as a serious challenge among scientists (Ensafi, et al., 2010).

1.1 The aim of the thesis

This thesis mainly comprises in two parts. In First part, multiwall carbon nanotube was purified and functionalized using pretreated procedure with concentrated HNO_3 and then glassy carbon electrode (GCE) surface was covered with the MWCNT. The MWCNT/GCE modified with different metal nano particles (Cu, Au and their bimetallic forms) by electrochemical deposition on MWCNT. The modified electrode surfaces were characterized with cyclic voltammetry and scanning electron microscopy with EDX detector. Finally, the metal nano particles modified electrodes were utilized as the catalytic surface for electrocatalytic reduction of oxygen in alkaline media and to compare the electrocatalytic activity of each MNP modified MWCNT/GCE with MWCNT/GCE and bare electrodes from their corresponding voltammetric curves.

The second part include that the preparation of polyaminophenol covered electrode and modified with different metal nano particles. The modified electrodes were used for the alone and simultaneous determination of ascorbic acid, epinephrine and uric acid.

The surface morphology of the bare GCE, MWCNT/GCE, PAP/GCE, Ox-PAP/GCE and their metal nano particles modified forms were characterized by cyclic voltammetry (CV), Atomic Force Microscopy (AFM), Scanning Electron Microscopy (SEM) and X-Ray Photoelectron Spectroscopy (XPS).

1.2 Carbon Nanotubes

Elemental carbon in its chemical allotropes of graphite and diamond occurs in a great variety of species and has been developed to a large number of highly specialised applications as structural and functional materials. The underlying reason for this unique manifold of species is twofold: The co-ordination chemistry of carbon is flexible in allowing continuos mixtures of C=C and C-C bonding in one structure. This leads to an infinite possibility of 3-dimensional structures and to continuous tunability of electronic properties from wide-gap semiconductor (diamond) to metallic (graphite). Carbon based materials plays a major role in nano-sciences. Fullerenes, nanotubes, carbon onions are typical representatives of nano-structured carbons to which all the above mentioned variables also apply in addition to the small scale of each object.

The new carbon meterials of fullerenes, are closedcage carbon molecules with three-coordinate carbon atoms tiling the spherical or nearly-spherical surfaces, the best known example is C_{60}, with a truncated icosahedral structure formed by twelve pentagonal rings and twenty hexagonal rings.

Examples of larger molecular weight fullerenes are C_{70}, C_{76}, C_{78}, C_{80} and higher mass fullerenes, which possess different geometric structure e.g. C_{70} has a rugby ball-shaped symmetry (Dresselhaus, et al.,1996).

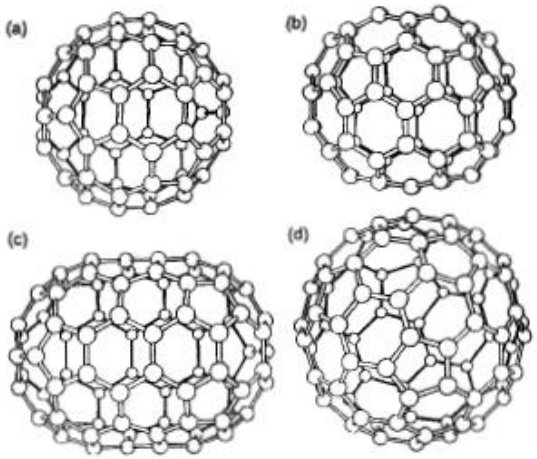

Figure 1.1 Structure and geometry of different fullerene molecules. (a) The icosahedral C_{60} molecule, (b) C_{70} molecule, (c) a C_{80} molecule as an extended rugby ball-shaped molecule, (d) C_{80} molecule as in icosahedran

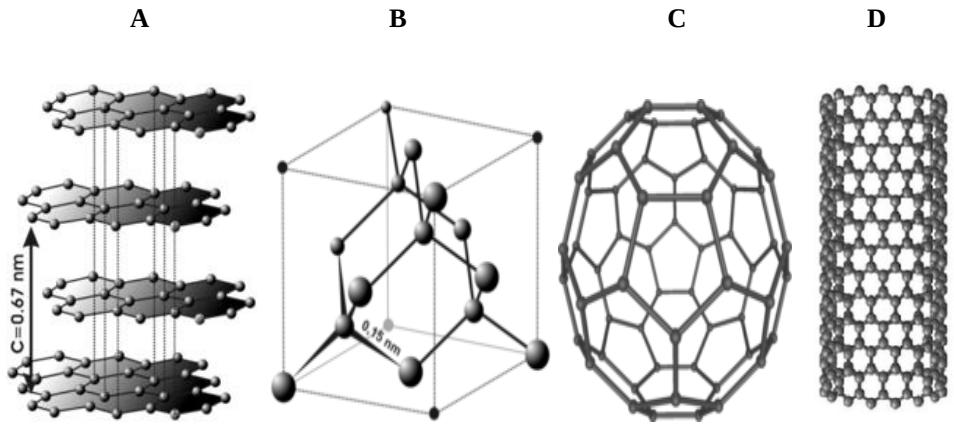

Figure 1.2 Different allotropes of the carbon element A) grafite B) diamond C) fullerene D) carbon nanotube.

Fullerenes were discovered by Kroto et al. in 1985 while investigating the nature of carbon present in interstellar space. The coordination at every carbon atom in fullerenes is not planar, but slightly pyramidalized, with some sp^3 character present in the essentially sp^2 carbons.

Carbon nanotubes were discovered by Iijima in 1991, observed that nanotubules of graphite were deposited on the negative electrode during the direct current arcing of graphite for the preparation of fullerenes.

The carbon nanotubes have been discovered using a transmission electron microscope to charecterized as a new carbon based material. Since that time, these long hollow cylindrical carbon molecules have revealed being remarkable nanostructures for several aspects. They are composed of just one element, Carbon, and are easily produced by several techniques. A carbon nanotube can bend easily but still is very robust. These nanotubes are concentric graphitic cylinders closed at either end due to the presence of five-membered rings (Iijima, 2002)

As described in Figure1.3 graphene sheets are rolled up in different directions to form different strutured carbon nanotubes. Figure describes that points O and A are crystallographically equivalent on the graphene sheet, where X-axis is placed parallel to one side of the honeycomb attice.

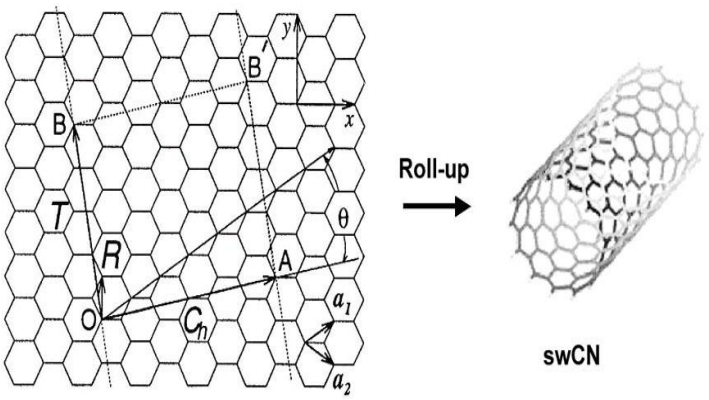

Figure 1.3 A single walled carbon nanotube structure

The points 0 and **A** can be connected by a vector $C_h = na1 + ma2$, where a_1 and a_2 are unit vectors for the honeycomb lattice of the graphene sheet. Next, can drawn normals to C *h* at points 0 and **A** to obtain lines OB and AB'. If it is known superimpose OB onto AB', obtain a cylinder of carbon atoms that constitutes a carbon nanotube when properly capped at both ends with half of a fullerene. Such a single-wall carbon nanotube is uniquely determined by the integers ***(n,m).*** However, from an experimental standpoint, it is more convenient to denote each carbon nanotube by its diameter ***dt*** = Ch/π and the chiral angle ϴ Depending on the chiral angle, a single-wall carbon nanotube can have three basic geometries; armchair with ϴ = 30", zigzag with ϴ = 0", and chiral with 0< ϴ <30", as shown in Figure 1.4.

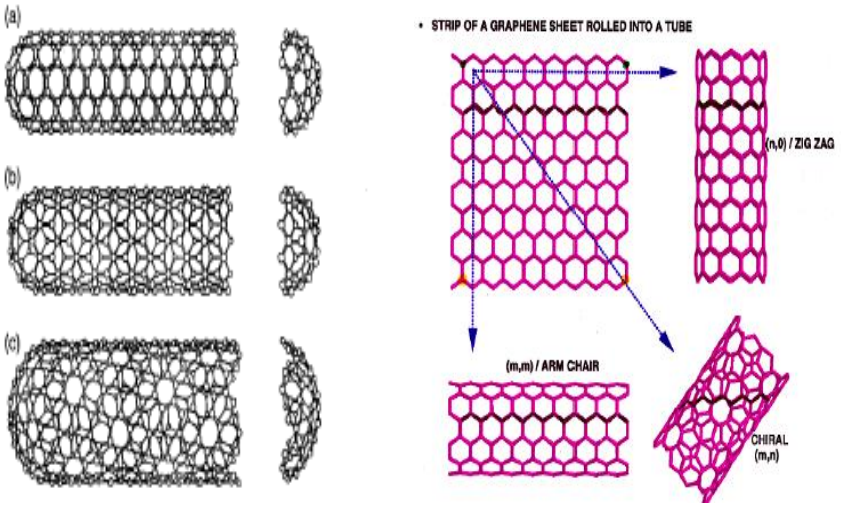

Figure 1.4. Three basic geometric structure of carbon nanotubes (a) armchair, (b) zigzag, (c) chiral

The structure of the nanotube influences its properties, including conductance, density and lattice structure. It is known that some nanotubes are conductors, that is, they are metallic, while some are semiconductors. The wider the diameters of the nanotube the more it behaves like graphite. The narrower the diameter the more its intrinsic properties depend on type (Cao, G., 2004).

In accordance with the mathematical laws of Euler, 12 pentagons are necessary at least to close the tube.

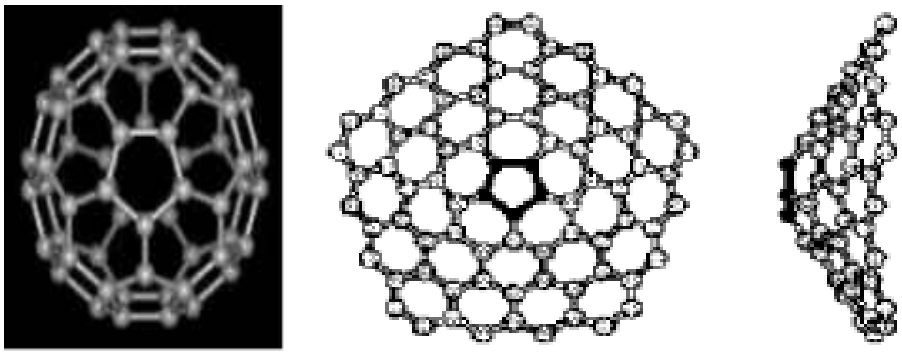

Figure 1.5 End sides of carbon nanotubes

1.3 Types of CNTs and their synthesis.

Carbon nanotubes were immediately studied by different group of researchers because of their relative simplicity, their unique properties, and their promise for practical applications.

In 1993, single-walled carbon nanotubes (SWNTs), new type of carbon nanotube in nanotube family, were reported by again Iijima. The report of this new type of carbon fiber triggered intense research focused on harnessing the unique properties of these nanostructures. This form was the pioneered fort he discovery of other special forms of carbon nanotubes. There are many kinds of carbon nanotubes, including single wall carbon nanotubes, double wall carbon nanotubes, multi-wall carbon nanotubes, intercalated nanotubes, and nanotubes filled with various species constituting internal nanowires including fullerenes and even fullerenes filled with metal species (endohedral fullerenes) (see Figure 1.6). (Dresselhausa, et al., 2003)

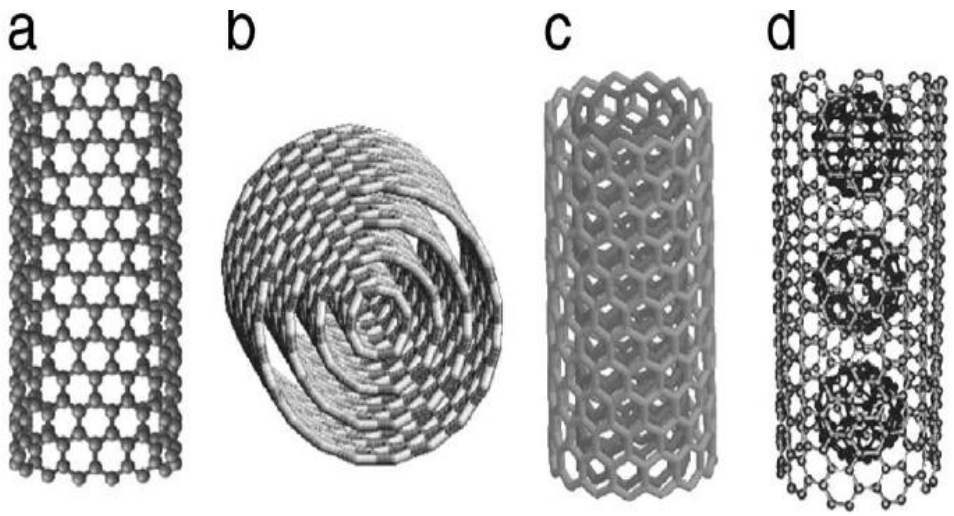

Figure 1.6 Schematic diagram of (a) a single wall carbon nanotube (SWNT), (b) a multi-wall carbon nanotube (MWNT), (c) a double wall carbon nanotube (DWNT) and (d) a peapod nanotube consisting of a SWNT filled with fullerenes (e.g., C_{60}).

Multi-wall carbon nanotube (MWCNT) is formed from composed of a mixture of cylindrical tubes having different or no hecility, thereby resembling turbostratic graphite. The arrangement of the carbon atoms in the hexagonal network of the multi-wall carbon nanotube is often helicoidal, resulting in the formation of chiral tubes.

MWCNT was originally discovered as a by-product of synthesis of C_{60} **.** The yield of MWCNT is 30 - 50 % in the electric a arcdischarge method using pure carbon. MWCNT is still attractive besides SWCNTs due to their sufficient ability for industrial application utilising its high chemical stability and high mechanical strength.

For instance, MWCNT has intrinsic properties suitable for field emitters in the form of a sharp tip with nanometer-scale radius of curvature, high mechanical stiffness, chemical inertness and high electrical conductivity. In addition to these well-known properties it also has the unique coaxial shape, which will afford good possibilities to be applied to various fields of industry (Tanaka, et al., 1999).

Typical dimensions of multi-wall carbon nanotube are outer diameter: 2-20 nm, inner diameter: 1-3 nm, and length: 1-100 nm. The intertubular distance is 0.340nm, which is slightly larger than the interplanar distance in graphite.

There are several ways or methods on preparing them have been developed. Carbon nanotubes are readily prepared in that;

i. by using plasma arc-jets and in large quantities, optimizing the quenching process in an arc between a graphite anode and a cooled copper electrode,

ii. by carrying out electrolysis in molten halide salts with carbon electrodes in an argon atmosphere,

iii. by striking an arc between graphite electrodes in 2/3 atm (~500 torr) of helium, considerably higher than the pressure of helium used in the production of fullerene soot. The arcing process can be optimized such that the major portion of the carbon anode is deposited on the cathode in the form of carbon nanotubes and graphitic nanoparticles.,

iv. MWNTs with well-ordered graphitic structures have been synthesized under hydrothermal conditions using a polyethylene and water mixture in the presence of nickel catalyst at around 800 ˚C under 60–100 MPa pressure,

v. Besides the conventional arc-evaporation technique, carbon nanotubes are produced by the decomposition of hydrocarbons such as C_2H_2 under inert conditions at around 700 ˚C, over Fe/ graphite, Co/graphite or Fe/silica catalysts.

The presence of transition metal particles is essential for the formation of nanotubes by the pyrolysis process, and the diameter of the nanotube is determined by the size of the metal particles (Cheetham, et al., 2004)

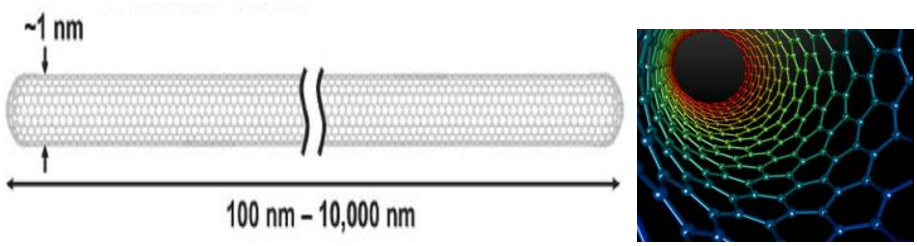

Figure 1.7 Images of SWCNT a) diameter and length b) Inner side of SWCNT.

Single-walled carbon nanotubes (SWCNT) are unique molecules with perfect structure that formed as a polymer by the pure form of carbon. The structure of SWCNT consists of an enrolled graphene to form a tube without seam. The length and diameter depend on the kinds of the metal catalyst used in the synthesis. The maximum length is several pm and the diameter varies from 1 to 3 nm (Figure 1.7). The thinnest diameter is about the same as that of C_{60} (~ 0.7 nm). The structure and characteristics of SWCNT are apparently different from those of MWCNT and rather near to fullerenes. Hence novel physical properties of SWCNT as the one-dimensional material between molecule and bulk are expected (Tanaka, et al., 1999).

SWCNTs have extraordinary properties such as;

- Their strenght were nearly 100 times higher than steel
- Electrical conductivity of SWCNT was 6 times higher than copper
- Termal conductivity nearly 3 times higher than diamond.
- They easily functionalized.

SWNTs were prepared using various oxides Y_2O_3, La_2O_3, CeO_2 as catalysts. The arc discharge technique, though cheap and easy to implement, gives low yields of SWNTs. It can be produced in more than 70% yield by the condensation of a laser-vaporized C–Ni–Co mixture at 1200 ˚C. The product is nearly uniform in diameter and self-assamble into ropes which consist of 100 to 500 tubes in a 2D triangular lattice. Under controlled conditions of pyrolysis, dilute hydrocarbon-organometallic mixtures also yield SWNT.

SWNTs are also prepared using metal- catalyzed dc arcing of graphite rods in a He atmosphere. The graphite anode incorporated with metal powders (Fe, Co or Ni) and the pure graphite cathode was used to produce the SWCNT. SWNTs generally occur in the web-like material deposited behind the cathode.

However CNT walls are not reactive, their tips are known to be more reactive, so end functionalization of CNTs is used relatively often to generate functional groups (e.g., -COOH, -OH, or -C=O) By differing the functionalization a number of potential applications obtained by CNTs,

including electronic devices, reinforced materials, hydrogen storage, sensor application or field emission materials.

Large number of applications can be found that CNTs as electrode materials or modifiers of conventional working electrodes in analytical voltammetry. The advantages of CNTs in electrochemical measurements, such as the large active surface at electrodes of small dimensions, the enhanced electron transfer or the often indicated electrocatalytic properties (Trojanowicz, 2006)

The number of literatures reports the use of carbon nanotubes as sensitive electrodes for some analysts such as coenzymes, neurotransmitters, nucleic acids and also oxygen reduction reaction. For instance, Dursun et al., was modified glassy carbon electrode with multiwall carbon nanotube and then they obtained Pt nano particles on the surface of CNT by electrochemically deposition technique..A higher catalytic activity was obtained to electrocatalytic oxidation of ascorbic acid, dopamine, and uric acid due to the enhanced peak current and well-defined peak separations compared with both, bare and MWCNT/GCE. The detection limits were individually calculated for ascorbic acid, dopamine, and uric acid as being 1.9×10^{-5} M, 2.78×10^{-8} M, and 3.2×10^{-8} M, respectively. In simultaneous determination, LODs were calculated for AA, DA, and UA, as of 2×10^{-5} M, 4.83×10^{-8} M, and 3.5×10^{-7} M, respectively obtained from DP results (Dursun, et al., 2010)

In other study CNTs modified GCE was used for enhancing the sensitivity of electrochemical measurements of enzimaticaly generated thiocoline. Under the optimal batch conditions the detection limit of $5x10^{-6}$ mol/L was obtained with a good precision. The high sensitive electrochemical detection of enzimatically generated thiocoline with CNT sensing platforms holds great promise to prepare acetycholinesterase biosensor for monitoring organophosphate pesticides and nerve agents (Lin, et al., 2005).

The catalytic oxygen reduction reaction (ORR) has attracted increasing attention due to its technological importance in electrochemical devices such as fuel cells as well as in industrial electrolysis processes. In fuel cell research, the ORR has been extensively studied in acidic or alkaline medium since fuel cells were in the focus over the last decade

Although the ORR is much faster in alkaline media, the commercial viability of fuel cells is still hindered by poor kinetics and large-scale synthesis due to high costs and low abundance of noble metal catalysts. The search for a low-cost, stable and more active electrocatalyst for the ORR in alkaline medium is thus of great importance.

Alexeyeva et al., studied oxygen reduction reaction with carbon naotubes in 0.5 M H_2SO_4 using the rotating disk electrode (RDE) method. They prepare the modified electrode AuNP/MWCNT catalysts by chemical deposition of AuNPs onto MWCNTs spontaneously grafted with 4-nitrophenyl groups. The oxygen reduction behaviour of the electrodes was compared with that of a bulk gold electrode. The AuNP/MWCNT catalyst showed a pronounced electrocatalytic activity towards O_2 reduction in acid media. The half-wave potential of O_2 reduction on the AuNP/MWCNT catalyst shifted *ca* 80 mV to more positive potentials as compared to that of a polished Au electrode. (Alexeyeva, et al., 2010),

The thermally treated CNTs were then oxidized via a HNO_3 vapor treatment in the gas phase at 200 C for 48 h. After cooling, the CNTs were dried at 60 C overnight. In order to introduce The N functionalize CNTs were then obtained by heating under ammonia into a tubular quartz reactor with a total flow rate of 25 sccm at different centigrates for 6 h. They studied in conditions of oxygen saturated 0.1M NaOH. Modified electrode exhibits a favourable positive onset potential for ORR, increased reduction currents, and a good stability. In view of its non-metallic nature, particularly free from noble metals, cost effectiveness makes NCNT-800 a very promising cathode catalyst for reactions in alkaline medium (Nagaiah, et al., 2010),

Another work was studied by the helping of double walled carbon nanotubes for investigation of oxygen reduction in both acidic and alkaline mediaTo obtain a uniform layer of DWCNTs onto GC surface, the electrodes were modified with nanotubes using aqueous suspensions ($1 mg ml^{-1}$) containing 0.3 % Triton X-100 or 0.5% Nafion. All the suspensions were sonicated for 1h. Then a 20µl aliquot of a DWCNT suspension was pipetted onto GC surface and the solvent was allowed to evaporate in air. The RDE results indicated that the DWCNT modified GC electrodes are active catalysts for oxygen reduction in alkaline solution. In acid media DWCNT/GC electrodes possess poor electrocatalytic properties for O_2 reduction which

indicates lack of metal catalyst impurities in the DWCNT material studied (Kruusenberg, et al., 2010).

1.4 Conductive Electroactive Polymers

However conducting electroactive polymers (CEPs) were discovered in the mid-1970s, their impact was recognized in 2000 by the awarding of the Nobel Prize for Chemistry to the three discovers of conducting polymers: Alan MacDiarmid, Alan Heeger, and Hideki Shirakawa. CEPs provide a wide searching area for many researchers. The industrial development of conducting polymer products and has provided the fundamental understanding of the chemistry, physics, and material science of these materials (Wallace, et al., 2009).

CEPs can be classified in two categories which are electron-conducting polymers and proton (ion)-conducting polymers. Much of current understanding of conjugated polymers is based on the two-band model, such as that appropriate for the π-electronic structure of polyacetylene. Studies on the two-band model system have led to a rather detailed understanding of the electronic structure, including the effects of π-bond alteration and electron–electron interactions on the photophysics. (Inzelt, 2008).

CPs can be synthesized either chemically or electrochemically, with each having advantages and disadvantages as summarized in Table 1.

Table 1 Comparison of chemical and electrochemical CP polymerization

Polymerization approach	Advantages	Disadvantages
Chemical polymerization	• Larger-scale production Possible • Post-covalent modification of bulk CP possible • More options to modify CP backbone covalently	• Can not make thin films • Synthesis more complicated
Electrochemical polymerization	• Thin film synthesis possible • Ease of synthesis • Entrapment of molecules in CP Doping is simultaneous	• Difficult to remove film from electrode surface • Post-covalent modification of bulk CP is difficult

Among all conductive polymers poly aminophenol, polythiophene, polypyrrole and polyaniline has an attractive place. Aminophenols are interesting members of the class of substituted anilines which gave a surface film of interesting electrochemical and electrochromic properties when their's electropolymerized in acidic solution. As in the many organic molecules, the electropolymerization reaction of PAP is initiated by oxidizing the respective monomer to a radical cation (Wallace, et al., 2009).

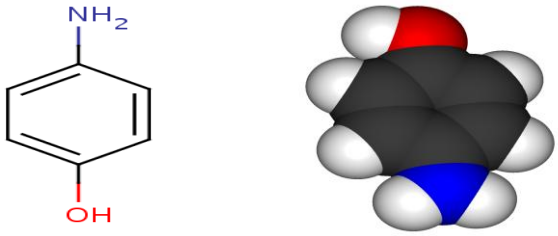

Figure 1.8 Structure of p-aminophenol.

1.4.1 Applications of CEPs

Conducting polymers are keys to technology due to their wide range application in sensors, actuators, batteries, molecular devices and modified electrodes. They have been studied increasigly after 1980 and Figure 1.9 shows the main areas of interest for papers published on CEPs that listed below. A further breakdown of the areas of application of CEPs are greatly used in this fields such as; batteries, sensors, membrans, and polymer light-emitting diodes (PLEDs). There has been a distinct move in recent years toward biological/biomedical applications of CEPs.

a) Energy storage/convertion

b) Polymer Photovoltaics

c) Display Technologies

d) Electrochromics

e) Electromechanical Actuators

f) Seperation Technologies

g) Corrosion Protecion

h) Chemical Sensors

i) Biomedical Applications

j) Communication and Characterization Tools

k) Electrochemical Methods

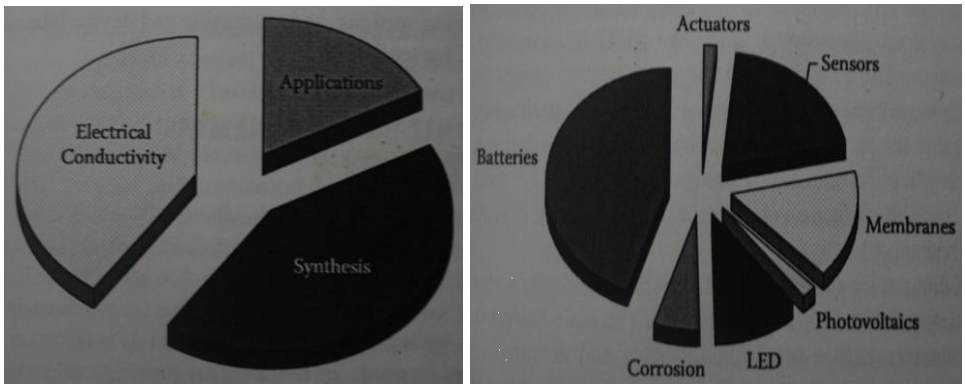

Figure 1.9 Scientific papers published on conducting polymers (1990-2000) categorized into various topics.

1.4.2 Studies at polymer modified electrodes

Polymer films obtained by different methods such as vapor deposition, dip coating, and spin-coating that all of them required toxic solvents and special equipments. Besides these methods electrochemical techniques are simple methods that provide a uniform, strongly adherent conducting polymer films with better conducting properties at the electrode surfaces without any expensive equipments (MacDiarmid, 1997).

Polypyrrole has attracted considerable interest due to long-term stability of its conductivity as well as ease in synthesis by anodic oxidation of the monomer in either aqueous or non-aqueous medium and Ulubay et al., studied with purified pyrrole modified electrode for sensitive determination of UA in coexistance of DA. When the pyrrole is oxidized and polymerized simultaneously during electrochemical synthesis, the obtained polymer possesses positive charge which is electroneutralized by the incorporation of

dopant anions. The electrocatalytic oxidation currents of UA and DA were found linearly related to concentration over the range 1×10^{-9} to 1×10^{-5}M for UA and 1×10^{-9} to 1×10^{-7}M for DA using DPVs method. The detection limits were determined as 8×10^{-10} M (s/n = 3) for UA and 8.5×10^{-10}M (s/n = 3) for DA at this electrode. (Ulubay, et al., 2010)

Li-Ping, L. et al., 2010, was studied the determination of L-cysteine.at electrochemically polimerized poly (o-aminophenol) (POAP) film. Then modified electrode was decorated with platinum again by electrochemical method. The resultant nano-Pt/POAP/GCE was showed excellent electrochemical response to L-cysteine at low oxidative potential in BR buffer solution (pH=3.0), with good stability and sensitivity. The detection limit (0.08 μM, S/N=3) and wide linear range (0.4 μM–6.3 mM). (Liu, et al., 2010),

Another study was again the investigation of POAP film in the presence of different counter ions. The POAP films were deposited on graphite electrode by cyclic voltammetry. The deposited films were characterized by EIS in wide frequency range. Mott-Schottky plot of the polymer capacitance describes the reduced polymer as a p-type semiconductor with a flat band potential of about 200mV vs. SCE. The results were showed that the nature of the anion plays a major role on the electrochemical behavior of the polymer. (Mahjani, et al., 2010)

Morover the electrochemical behaviour of 2-(2-nitrophenyl)-1H-benzimidazole (NB) was investigated by CV and SWV at 1-naphtylamine (1-NAP) polymer film modified GCE. Poly-1-NAP films were obtained from a solution of 6×10^{-4}M 1-NAP in 0.1 M $HClO_4$ aqueous solution by cycling between 0.0 and 0.8V at a v=0.050 Vs^{-1} during five cycles. Then the chemically modified electrode was rinsed with water and cyclic voltammograms were performed in the mixture 10% ethanol +90% buffer solution of pH 2. A well-defined quasi-reversible redox couple in the potential range from 0.50 to −1.0 V. over-oxidation process was applied this chemically modified electrode in 0.2 M NaOH alkaline medium to obtain a certain degree of perm selectivity by cycling the potential between 0.0 and 0.9 V at a v=0.025 Vs^{-1}. The presence of hydroxyl groups in poly-1-NAPox has previously been confirmed by the polymer FTIR spectra. The NB detection limit was calculated 5×10^{-7}.within the linear range of 2×10^{-6} to 5×10^{-5}M (Fabiana, et al., 2010).

1.5 Metal Nano Particles

Nanometer-sized metal particles or metal nano particles (MNP) are objects of great interest in modern chemical research due to their unique electrical, magnetic, optical and other properties, which are distinct from both those of the bulk metal and those of isolated atoms and molecules. They improve the catalytic activity of the surfaces where thay attached (Haudy, et al., 2006).

However metal nanoparticles play a significant role in many applications such as sensors, catalysts, field-emitters, they can be so fragile and unstable that if their surfaces touch, they will fuse together, losing their special shape and properties.

The stabilization of MNP is required for a number of reasons:

1) to prevent the uncontrollable growth of particles, but also

2) to prevent particle aggregation;

3) to control the particles growth rate;

4) to control particle size, and finally

5) to allow particle solubility in various solvents (Muraviev, 2005).

The stabilizing agent can be either some ligands, capping agents and passivating agents or surfactants, carbon nanotubes and polymers. Among this materials, conducting polymers and carbon nanotubes as the support for catalytic active metal particles provide good electron-ion conductivity and in some cases also good proton conductivity. The porous structure of conducting polymer and the functionalized tip sides of carbon nanotubes allows dispersing the metal nano particles easily.

Metal particles can be divided into three following groups:

1) Nanometric or ultradispersed: from 1 to 30–50nm;

2) Submicrometric or highly dispersed: from 30–50 to 100-500nm, and

3) Micrometric: from 100–500 to 1000 nm (Muraviev, 2005).

Chemistry plays a particularly important role in the synthesis and characterization of nanosized metarials of metals/oxides and semiconductors, nanoparticles and composites involving ceramics, carbon nanotubes (Cheetham et al., 2004).

Metal nano particles can be synthesized with different techniques. These methods can be divided in to four main groups.

1. Synthesis of semiconductor nanoparticles in solutions of he corresponding salts by controlled addition of anions (cations) or by hydrolysis.

2. Preparation of nanoparticles as a result of phase transformations

3. The synthesis of nanoparticles in aerosol

4. The synthesis of nanoparticles with electrochemical methods.

In above methods, the electrochemically synthesis of metal nanoparticles is one of the most reliable uniformly dispersed nano particle preparation techniqe on the stabilized conducting material covered electrode surface. The advantage of electrodeposition method offer low cost, taken short time, a high purity of the particles, more easily control the nano particules dimensions, lower particle size distribution compare to chemical and physical methods. In addition to other advantages of the electrodeposition method includes the ability to uniformly coat non-planar substrates, to plate over wide areas, and to deposit a nanocomposite to an overall thickness much larger than can be generally achieved with vacuum deposition methods (Heflin, et al., 2004).

Metal nano particules modified electrodes have been used in modern chemical research due to their unique electrical, magnetic, optical and other properties to improve catalytic activity and the analytical sensitivity and selectivity.

In other study, the electrochemical reduction of oxygen was investigated on gold nanoparticle/ MWCNT modified GCE in acidic media. Gold nanoparticles were prepared with the chemically reduction of $HAuCl_4$ by $NaBH_4$ in MWCNT solution and the aqueous dispersion was assembled onto GCE by physical adsorption. The electrode shows a remarkable electrocatalytic activity towards oxygen reduction reaction (ORR) (Tammevski, et al., 2006).

The electrochemical detection of ammonia in drinking water was carried out on MWCNT-copper nanoparticle composite paste electrodes. The optimized electrodes showed significantly better performance than simple CNT or Cu paste electrodes, in terms of linear range of concentrations (3-100 μM), lower detection limit(3,47μM), higher sensitivity. The sensorswere applied to the determination of ammonnia in real samples of tap water (Valentini, et al., 2007).

Noble metal nano-structures like Au, Pt and Pd have attracted tremendous attention in recent decades, due to their excellent optical, electrochemical and electronic properties, which are different from those of bulk metal materials.

1.6. Ascorbic Acid

1.6.1 Chemical Properties and Biological Importance of AA

Ascorbic acid (vitamin C, AA), a water soluble vitamin, is widely) present in both animal and plant kingdoms, is a vital component in human diet and in multivitamin preparations. AA is commonly used to supplement inadequate dietary intake and as anti-oxidant. (Thiagarajan, et al., 2007)

Ascorbic acid is a derivative of monosaccharid like glucose and the other six carbon monosaccharides. Molecular formula of AA is $C_6H_8O_6$ (Ma, 176.12 $gmol^{-1}$) and known as the enol form of the 2-oxo-L-gulofuranolactone as seen in Figure 1.5. The acidic enolic hydroxyl on ring carbon-3 has acidity constant

(pKa) of 4.20. The ascorbic acid is white crystalline solid which is soluble in water (33g/100mL).

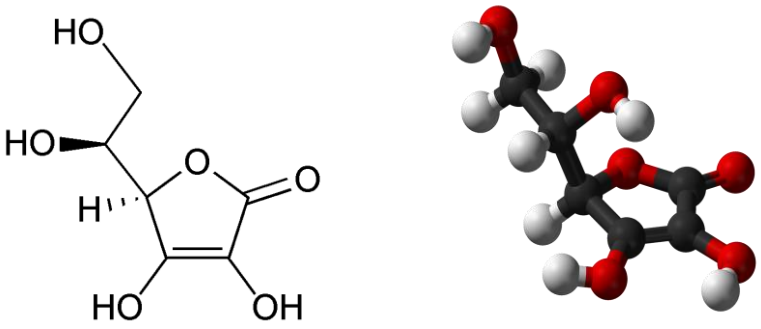

Figure 1.10 Structure of Ascorbic Acid molecule

Ascorbic acid is a relatively strong reductant with an E_0' (pH 7.40) of +0.58 volt. It is reversibly oxidized to dehydroascorbic acid, also shown in Figure1.6 this deprotonated form is an enolate and more labile than enol form.

It can be prepared by synthesis from glucose, or extracted from plant sources such as rose hips, blackcurrants or citrus fruits.

Plants and most animals possess the ability to synthesize the ascorbic acid from D-glucose via the lactones of d-glucuronic and L-gulonic acids; however, some mammals, including the human, lack L-glulonolactone oxidase, the enzyme that catalyses the formation of 2-keto-L-gulonolactone, which spontaneously tautomerizes to L-ascorbic acid (Tietz, 1987).

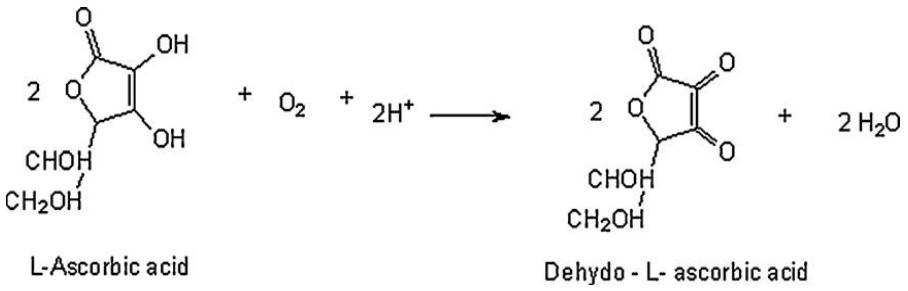

Figure 1.11 Dehydrogenation reaction of ascorbic acid

The most clearly and critical roles in human body is that, ascorbic acid is essential for the formation of collagen and intercellular material, bone and teeth and for the healing of wounds. It helps maintain elasticity of the skin, aids the absorption of iron and improves resistance to infection.

AA deficiency leads to the development of a well known syndrome called scurvy. Inability to form enough intercellular substance in connective tissue is reflected in swollen, often bleeding or bruised areas at joints and in other areas where structally weakened tissue can not withstand stres. It is administered in the treatment of many disorders, including Alzheimer's disease, atherosclerosis, cancer, infertility and in some clinical manifestations of HIV infections. Due to its importance, many modified electrodes have been developed and reported for the electrochemical determination of this compound.

1.6.2 Determination Methods of AA

Different AA determination methods have been developed İnclude colorimetry, titrimetry, voltammetry, fluorometry, potentiometry, kinetic-based luminescence, flow injection analyses and chromatography. However, each method has its limitations. For example, titrimetric methods, including official method, require a large amount of sample (generally 5 mL), what can be a problem when only small amounts of sample are available.

Traditional procedures for AA determination are generally based on enzymatic methods, on titration with oxidizing agent, like iodine or 2,6-dichlorophenolindophenol (Kumar, et al., 2008).

AA can be determined by thermoelectrochemically. The thermoelectrochemistry of ascorbic acid (AA) at a disposable screen-printed carbon electrode (SPE) was studied and found that the response of AA is greatly suppressed at higher temperatures when the electrolyte solution containing AA is directly heated. It is interesting that the heated SPE electrode is capable of increasing the detection sensitivity without decomposing the substrates. It is further applied for flow injection analysis (FIA) of AA by using a specifically designed electrochemical cell coupled with the disposable SPE. Applicability in real sample shows in good agreement with the quoted value as well as the results observed by other methods (Zen, et al., 2008).

AA can be determined by spectrophotometry. In this method, AA reduces methyl viologen to form a stable blue coloured free radical ion. This method has a sensitivity and lower limit detection of 0.1 $\mu g ml^{-1}$ of ascorbic acid (0.1 ppm) which is comparable to the flow injection techniques. Beer's

law is obeyed over the concentration range of 1.0–10 μgml^{-1} of ascorbic acid per 10 ml of the final solution (0.1–1.0 μgml^{-1}) at 600 nm. The molar absorptivity was found to be 1.5×10^5 ±100l mol^{-1} cm^{-1}. The method has been applied to the determination of ascorbic acid in food, pharmaceuticals and biological samples (Janghel, et al., 2007).

Moreover, determination of total AA (vitamin C) in foods has been studied with HPLC. The method requires less time than the traditional methodologies and uses a radical oxidation of *l*-ascorbic acid (AA) to obtain dehydro-*l*-ascorbic acid (DHAA) by means of a peroxyl radical generated *in situ* by thermal decomposition of an azo-compound, 2,2′-azobis(2-amidinopropane) dihydrochloride (AAPH). The dehydro-*l*-ascorbic acid is condensed with benzene-1,2-diamine (*o*-phenylenediamine, OPDA) to form its highly fluorescent quinoxaline derivative, 3-(1,2-dihydroxyethyl)furo[3,4-b]quinoxaline-1-one (DFQ), then separated on a C18 column eluted with a mobile phase of 80mM phosphate buffer and methanol at pH = 7.8 and detected fluorometrically at λex = 355 nm and λem = 425 nm. The reaction conditions for the complete conversion of AA to DFQ were 56 ◦C, 36 min and a μmol AAPH/AA ratio of 60. The sample, extracted with an aqueous metaphosphoric acid solution, was analyzed after being filtered through a 0.45 μm membrane. The method has shown good repeatability, sensitivity and accuracy compared to the results obtained with the reference method. The response of the detection system was linear within a range of 0.5–8.0 μg/mL with a correlation coefficient of 0.9997. The LOD was 0.27 μg/mL and the LOQ was 0.83 μg/mL (Buruni, 2007).

In other study, this time a multilayer thin film composed of poly (allyaminehydrocloride) PAH and carboxymethly cellulose (CMC) have been prepared on the surface of a gold disc electrode by a layer -by- layer deposition of PAH and CMC and ferricyanide ions ($[Fe(CN)_6]^{3-}$) were confined in the film. Electrocatalytic determination of AA in the concentration range of 1-50 nM (Anzai, et al, 2007).

A simple selective method for determination of AA using polymerized direct blue 71 (DB71) is described Chen et. al. DB71 was polymerized on GCE surface electrochemically in 0.1 M H_2SO_4. Poly (DB71) modified GCE showed excellent electrocatalytic activity towards AA in neutral pH. Using amperometric methods, linear range (10^{-6}–$2x10^{-3}$ M), and detection limit (10^{-6}

M, S/N=3) were estimated. Major interferences such as DA and UA are tested at this modified electrode and found that selective detection of AA can be achived (Kumar, et al., 2008).

1.7 Epinephrine

1.7.1 Chemical Properties and Biological Importance of EN

Epinephrine (EN), commonly called adrenaline, is a hormone in the catecholamine family which is secreted by the suprarenal gland along with norepinephrine. It was first isolated in 1901 by Takamine and Aldrich, and was synthesized in 1904 by Stolz and Dalkin (Hernández, et al.. 1998)

Adrenaline [1-(3,4-dihydroxyphenyl)-2-methyloaminoethanol] has molecule formula of $C_9H_{13}NO_3$. (Ma: 183.204 g/mol), a hormone exists as an organic cation in the nervous tissue and biological body fluid. Many diseases are related to the changes of its concentration in the body fluid.

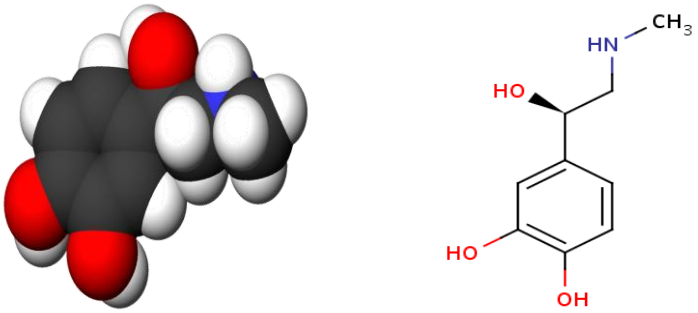

Figure 1.12 Structure of epinephrine.

Epinephrine is synthesized naturally in the body from L-tyrosine by the action of different enzymes. Almost 50% of the secreted hormone appears in urine as free and conjugated, 3% as vanilmandelic acid, (VAM), the most abundant metabolite in urine. Only small amounts of free epinephrine are excreted. (Hernández, et al. 1998)

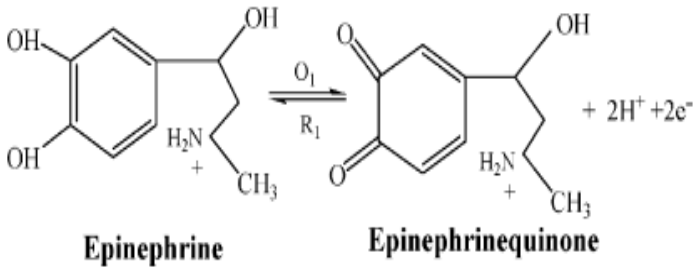

Figure 1.13 Oxidation reaction of Epinephrine to Epinephrinequinone.

EN is one of the important catecholamine neurotransmitters in the mammalian central nervous system and plays a very important role in the function of central nervous, renal, hormonal, and cardiovascular systems.

Epinephrine has been used for the treatment of myocardial infarction, hypertension, bronchial asthma, cardiac arrest, and cardiac surgery in clinics. Many physiological phenomena are correlative to EN's level in the body fluids (Ensafi, et al., 2010). Therefore, a simple, fast, and sensitive method is necessary for its determination in both biological fluids and pharmaceutical preparations

1.7.2. Determination Methods for EN

Many phenomena are related to the concentration of EN in blood as well as in urine. Therefore, it is very important to develop sensitive and selective analytical methods for the detection of EN in biological fluids. All methods for determining catecholamines in urine require careful purification of the sample due to the many related amines and catecholes in urine.

The oldest methods for epinephrine analysis are based on the native fluorescence of original amines. Norepinephrine and epinephrine are isolated from urine by absorption on aluminum oxide and subsequently eluted with diluted acid. The amines are then converted by oxidation to their trihydroxyindole derivatives, which give a high and specific fluorescence. 5 ml of 0.2 N EDTA was added to the urine sample. The pH of the 50 ml of 24-h urine collection was adjusted to pH 8.4. Then the catecholamines (CA) were adsorbed on 1 g aluminium oxide (Brockmann type) with stirring. Then 0.2 N EDTA was add to the urine and the eluate to prevent the formation of a gelatinous calcium–magnesium–phosphate precipitate in the final reaction

mixture which interferes with subsequent fluorescence (Tzontcheva, et al. 2000).

Another method is based on the development of a red colour with sodium bismuthate, as a sensitive chromogenic reagent, in aqueous medium at pH 3. Oxidation of these catecholamines produces aminochrome derivatives which can be measured spectrophotometrically at 486.0 nm. Calibration graphs are linear in the range 4.8–800 (μmol l^{-1}) for epinephrine bitartarate with detection limits of 0.26 (μmol l^{-1}) for epinephrine. The method also has been applied to determination of these catecholamines in pharmaceutical preparations (Sorouraddin, 1998)

3,4-Dihydroxybenzylamine (DHBA) is commonly used as the internal standard in HPLC catecholamine assays. In his study researchers have developed sensitive HPLC-ED method with alumina extraction for measurement of catecholamines in sheep plasma using deoxyepinephrine (epinine) as the internal standard. Separation was performed on a p~Bondapak C,~ column (300×3.9 mm, 10 p~m) with a mobile phase containing 2% acetonitrile and 98% buffer (0.05% sodium acetatL'-0.02% EDTA-0.013% sodium heptanesulfonate),pH 3.25.. The R^2 of regression curves (n=51 of epinephrine (El (25.82 pg/ml-l.03 ng/ml), epinine was used as internal standard were greater than 0.99. The technique described has the advantage that it allows the simultaneous determination of both endogenous and epinephrine in sheep plasma using a sensitive and reproducible. (Huaibing, at al, 1997)

Moreover, catecholamines in human urine samples can be quantitatively determined by utilizing capillary electrophoresis coupled with amperometric detection. The detector employs a parallel-opposed dual-electrode scheme assembled with an on-capillary electrode and a disk electrode and takes advantage of the redox cycling of analytes between the two working electrodes to improve the limit of detection. The matrix effect of urine samples significantly decreases the detection sensitivity from that obtained in standard solutions. A method of standard addition and internal standard was used in this study. The results suggest that isoproterenol is a good internal standard to facilitate the measurements of dopamine, epinephrine, and norepinephrine in human urine samples (Chen, et al. 2001).

Raw apple juice exhibits the activity of polyphenol oxidase which can be employed for the determination of mono-, di- and polyhydric phenols. The chemiluminescence detection in the two-channel manifold was used for determination of epinephrine. Epinephrine can be determined by this method in pharmaceutical preparations in concentration ranges 1.0–10.0 and 10.0–25.0 mg L^{-1}, with a detection limit of 0.2 mg L^{-1}. Good selectivity against typical antioxidants and other coexisting substances was achieved. Relatively slow loss of the enzyme activity was observed during 1 week. Fresh juice solution from one apple was prepared in 10 min and used for at least 8 h with goog precision. Consumption of luminol solution was 0.15 mL min^{-1}. The throughput was 20 samples per hour (Michałowski, 2001).

Also electrochemical detection of EN was studied with various modified electrodes; A carbon paste electrode was modified with electropolymerized films of isonicotinic acid. The modified electrode was used toward the oxidation of both dopamine (DA) and epinephrine (EP). Separation of the reduction peak potentials for dopamine and epinephrine was about 357 mV in pH 5.3 phosphate buffer solution (PBS) and the character was used for the detection DA and EP simultaneously. The peak currents increase linearly with DA and EP concentration over the range of 8.0×10^{-5} to 7.0×10^{-4} mol/L and 5.0×10^{-6} to 1.0×10^{-4} mol/L with detection limits of 2×10^{-5} and 1×10^{-6} mol/L, respectively. The modified electrode was showed selectivity in the presence of large excess of interferent ascorbic acid (Zhou et al, 2009).

Flow injection amperometric quantification of AA, dopamine (DA), EN and dipyrone (DI) in mixtures (in the μg g^{-1} range) was studied by matos et al., by using an array of microelectrodes with units modified by the electrodeposition of different noble metals, together with multivariate calibration analysis. The four groups of microelectrodes utilized included a pure gold electrode and electrodes modified by electrodeposition of platinum, palladium or a mixture of platinum + palladium. The array of microelectrodes was inserted in a flow cell and the amperometric data acquisition was performed with a four-channel potentiostat. The analysis of the resulting signals was carried out by a multivariate calibration method, using a group of 16 standard mixtures selected by a two-level factorial design. The average absolute errors (in μg g^{-1}) calculated for each analyte were 0.3, 0.2, 0.4 and 0.4 for AA, DA, EN and DI, respectively. (Matos, at al, 2000)

1.8 Uric Acid

1.8.1 Chemical Properties and Biological Importance of UA

Uric acid is essential for human; because of that UA is the main final product of purine metabolism, being present in biological fluids, especially blood and urine. UA is chemically known as 2,6,8-trioxypurine and the molecular formula is $C_5H_4N_4O_3$(Ma 168 $gmol^{-1}$) ,as seen figure 1.14. Uric acid is a white crystalline compund structurally and its first pKa of UA is 5.75; above this pH, uric acid exists generally as urate ion, which is more soluble than uric acid (Tietz, 1987).

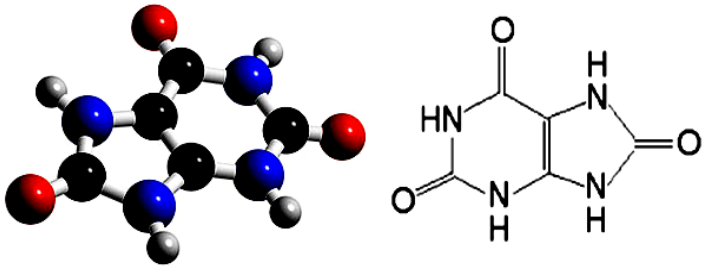

Figure 1.14 Structure of Uric Acid molecule.

Purines from catabolism of dietary nucleic acid reconverted to uric acid directly. Catabolism of the nucleotides begins with removal of their ribose-linked phosphate, forms hypoxanhine and guanine, both of which are converted to xanthine. Xanthine is converted to uric acid through the action of xanthine oxidase.

Electroactive UA can be quasi-reversibly oxidized in aqueous solution and the major product is allantoin. This oxidation reaction of UA was illustrated schematically in Figure 1.8

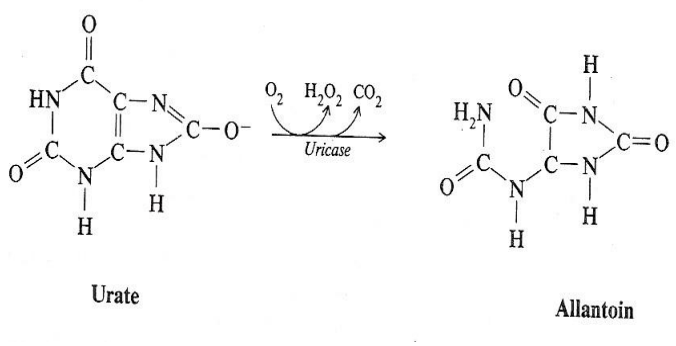

Figure 1.15 Oxidation reaction of Uric acid to Allantoin

Abnormal UA level in human body could be caused by several diseases, including gout, the Lesch-Nyhan syndrome, cardiovascular, chronic renal disease and hyperuricemia. Causes of high uric acid levels in human blood (hyperuricemia) include obesity, excessive alcohol use, diets high in purines. Certain medications, including low-dose aspirin, diuretics and some high blood pressure drugs also causes high uric acid levels in human blood (Zang, et al., 2008).

Uric acid is excreted via the kidneys. Owing to its relatively low solubility, an increase in serum uric acid levels often triggers the formation and precipitation of uric acid crystals, typically resulting in conditions such as gout or urate stones in the urinary tract. Significantly elevated serum uric acid concentrations can also be associated with rapidly proliferating cancers or, in particular, with onset of chemotherapy. On the other hand lower serum values of uric acid have been associated with Multiple sclerosis. In this regard determination of uric acid is crucial in biological fluids (Walsh, 2007).

1.8.2. Determination Methods for UA

Determination of UA can be done by several methods such as electroanalytical, spectroscopic and chromatographic methods are developed to determine UA in blood and urine. The advantages of electrochemical technique for determining UA are its high sensitivity, low cost and less time consumption (Liu, et al., 2006).

Analytical techniques based on enzymatic reaction combined with spectroscopy or electrochemically oxidized on proper electrodes are the most widely used for this purpose. However, UA could be selectively determined by

enzymatic methods which are one of the expensive method compare to others. In addition to this, enzymatic methods are affected by the high absorbance of the matrix itself and by the possibility of enzymatic inhibition caused by purines which are present in the sample (Lima, et al., 2004)

High performance liquid chromatography (HPLC) is one of the techniques to establishing a highly sensitive method for the determination of uric acid (UA) in human saliva. For this aim, reversed-phase high-performance liquid chromatography with electrochemical detection (HPLC–ED) was employed. UA was obtained bu solid phase extraction of human saliva. To quantify UA, the ED efficiencies of an amperometric ED Ampero-ED) with a single electrode and a coulometric ED (Coulo-ED) with a multiple electrode array were compared. The results showed that the detection limits (S/N=3) were 3 nM for Ampero-ED and 6 nM for Coulo-ED, and the linearity of the calibration curves of 60–6000 nM had correlation coefficients exceeding 0.999. The recoveries of UA spiked at 0.6 and 3 mM in saliva were above 95% with a relative standard deviation (RSD) of less than 15% (Nakazawa, et al., 2008).

A method for the fluorometric determination of uric acid in blood serum was devoloped by its reaction with uricase (UOx). The sample was excited at 287 nm and the emission is measured at 330 nm. The signal measurements was based on the changes in fluorescence intensity that take place during the enzymatic reaction of UOx with uric acid. Analytical characteristics of this method were found as linear response range (3×10^{-5}–6×10^{-4} M) and reproducibility (4%, n=7) (Galban, et al., 2001).

In another study determination of UA in human urine and serum was carried out by capillary electrophresis with chemiluminescence detection. The sensitive detection was based on the enhancement effect of UA on the chemiluminescence (CL) reaction between luminol and potassium ferricyanide ($K_3[Fe(CN)_6]$) in alkaline solution. A laboratory-built reaction flow cell and a photon counter were deployed for the CL detection. The proposed CE–CL assay showed good repeatability (relative standard deviation [RSD] = 3.5%, n = 11) and a detection limit of 3.5 x 10^{-7} M UA (signal/noise ratio [S/N] = 3). A linear calibration curve ranging from 6.0 x 10^{-7} to 3.0 x 10-5 M UA was obtained. The method was evaluated by quantifying UA in human urine and serum samples with satisfactory assay results (Zhoa, et al., 2008).

Determination of UA by electrochemical method using ultrasonic situmulating has been studied. Optimal conditions such as sonication time, sonication powder, pH, temperature have been examined. The calibration curve for determination of UA at GCE by sono-linear sweep voltammetry was linear over a range of $8x10^{-6}$–$5x10^{-4}$ M and the LOD was $6.5x\ 10^{-6}$ M (Bae and Cho, 2001).

With the same aim gold nanotubule membranes were prepared by using electrodless deposition of gold within the pores and surfaces of polycarbonate track-etched membranes. And the gold nanotubule membrane was used as an electrode for determination of uric acid in urine samples for the first time. In pH 4.56, uric acid exhibited well-defined differential pulse voltammograms. And the interference between coexistent ascorbic acid and uric acid was overcome owing to the attractive ability of the gold nanotubule electrode to yield a large anodic peak difference ca. 0.404 V (vs. SCE). The proposed method was then applied to the determination of uric acid in urine without any pretreatment (Hu, et al., 2007).

1.9 Methods for Simultaneous Determination of, AA, EN and UA

Electroanalytical methods have been used during the past three decades to investigate the role of neurotransmitters in human body due to their electroactive nature. AA, adrenaline (EN) and UA are playing important roles in various biological processes. In that the chemically modified electrodes have been widely used as sensitive and favorable analytical methods. Simultaneous detection of AA, EN and UA is a problem of critical importance not only in the field of biomedical chemistry and neurochemistry but also for diagnostic and pathological research. For overcomethis problem many researchers study in this field such as;

A carbon-paste electrode (CPE) modified with iron (II) phthalocyanine was used for voltammetric determination of epinephrine EN. AA and UA were investigated by cyclic and differential pulse voltammetry. The results show an efficient catalytic activity of the electrode for the electro-oxidation of EN, which leads to improvement of reversibility of the electrode response and lowering its overpotential by more than 100 mV. The modified electrode exhibits an efficient electron mediating behavior together with well-separated

oxidation peaks for EN, AA and UA. Under the optimum pH of 4.0 in 0.1M acetate buffer solution, the DPV anodic peak current showed a linear relation versus EN concentration in the range of 1–300μM, with a correlation coefficient of 0.998 and a detection limit of 0.5 μM for under coexistance of AA and UA (Shahrokhiana, at al, 2009)

A biosensor was fabricated by electrochemical deposition of gold nanoclusters on ultrathin overoxidized polypyrrole (PPyox) film, formed a nano-Au/PPyox composite on glassy carbon electrode (nano-Au/PPyox/GCE).. The nano-Au/PPyox/GCE had strongly catalytic activity toward the oxidation of AA, EN and UA and resolved the overlapping voltammetric response of them into three well-defined peaks with a large anodic peak difference. The peak currents increased linearly with increasing EN and UA concentrations in the range of 3.0×10^{-7} to 2.1×10^{-5} M and 5.0×10^{-8} to 2.8×10^{-5}M with a detection limit of 3.0×10^{-8} and 1.2×10^{-8}M (*s*/*n* = 3), respectively. The nano-Au/PPyox/GCE has also been applied to determination of EN in epinephrine hydrochloride injection and UA in urine samples (Li, et al., 2007)

In another study, multi-wall carbon nanotubes (MWCNT) are evaluated as an immobilization matrix for the construction of a modified electrode based on hematoxylin electrodeposited on MWCNT immobilized on the surface of a glassy carbon electrode, GCE. The reversibility of hematoxylin is significantly improved at a MWCNT modified GCE in comparison with GCE alone. Hematoxylin MWCNT modified GCE (HMWCNT-GCE) shows a good activity for adrenaline oxidation, with a diminution of the electrode overpotential of about 395 mV. The detection limit of 0.024μM and two linear calibration ranges of 0.2–78.3μM and 78.3–319.7μM are obtained for EN determination at HMWCNT-GCE surface using a differential pulse voltammetric method. This modified electrode is found quite effective not only in detection of AA, EN, and UA, but also in simultaneous determination of each component in a mixture. Also in this study HMWCNT-GCE has been applied to determination of EN in an adrenaline injection and of UA in a human urine sample (Zare, et al, 2010)

Mercaptopropionic acid (MPA), gold nanoparticles (Au-NPs) and cystamine (CA) modified gold bare electrodes have been applied in voltammetric sensors for simultaneous detection of AA, EN and UA. Modification of the electrode surface by self-assembled layers (SAMs)

improves the reactivity of a gold electrode for EN oxidation remarkably. A linear relationship between the epinephrine concentration and the current response is obtained in the range of 0.1–700μMwith the detection limit ≥0.042μM for the electrodes modified at 2D template and in the range of 0.1–800μM with the detection limit ≥0.040μM for the electrodes modified at 3D template. The results have shown that the overlapping voltammetric response of epinephrine, ascorbic and uric acids is well resolved at modified electrodes. The modified SAMs electrodes show high selectivity, sensitivity, reproducibility and stability (Łuczak, 2009)

1.10 Fundamentals of Voltammetric Techniques

Voltammetry represents a wide range of electrochemical techniques those can be used to study the solution composition through current-potential relationships in an electrochemical cell and with the current time response of a microelectrode at a controlled potential.

The advantages of voltammetry quickly demonstrate that it is a potent analytical tool. The foremost advantage is sensitivity. Voltammetry ranks among the most sensitive analytical techniques available; it is routinely used for the determination of electroactive substances in the sub-parts per million range. Analysis times of seconds are possible. The simultaneous determination of several analytes by a single scan is often possible with a voltammetric procedure. Voltammetric techniques have a unique capability to distinguish between oxidation states that may affect a substance's reactivity and toxicology. The theory of voltammetry is well developed, and reasonable estimates of unknown parameters can be made (Willard, et al., 1988).

The existence of polarized electrodes was recognized and utilized in a practical way. All voltammograms are recorded with a three-electrode system consisting of a reference, counter and the working electrode. The aim of the technique is accomplished by monitoring the transfer of electron during the redox process onto surface electrode of analyte:

$$O + ne^{-} \rightarrow R$$

where, O and R are the oxidized and reduced forms, respectively. This is achieved by monitoring the transfer of electrons thermodynamically or kinetically throughout redox process of the analyte. The potential of electrode can be used to establish the concentration of the electroactive species at the electrode surface at 25^0C according to the Nernst equation:

$$E = E^{o} + \frac{0.059}{n} \log \frac{C_O}{C_R}$$

where, C_O and C_R are the concentrations of the oxidized and reduced forms of the electroactive species at the electrode surface. E^0 is the standart electrode potential for redox reaction.

1.10.1 Polarography

Polarography is a subclass of voltammetry in which the working electrode is dropping mercury. Because of the special properties of this electrode, is wide cathodic range. Polarography has been widely used for the determination of many important reducible species.

This classical technique was invented by J. Heyrovsky in Czechoslovakia in 1922. The excitation signal used in conventional (DC) polarography is a linearly increasing potential ramp. We can obtain the Ilkovic equation for the limiting diffusion current:

$$(i_d)_l = 708nD^{1/2}m^{2/3}t^{1/6}C$$

Here, $(I_d)_l$ will have microamperes (μA), when D is in cm^2/s, m is in mg/s, t in second, C is mmol/L. In equal, the current can be taken 607 instead of 708 when taking mean of oscillations. When all the device parameters are kept constant, this equation becomes as given below; and this equation is used in quantitative analysis

$$i_d = KC$$

The relationship between current and potential is derived by the Nernst equation (Wang, 2001).

$$E = E_{1/2} + \frac{0.059}{n}\log\frac{i_d - i}{i}$$

1.10.2 Pulse Voltammetry

The potential step is the basis of pulse voltammetry. Pulse techniques were initially developed for the dropping mercury electrode, the objective being to synchronize the pulses with drop growth and reduce the capacitive current contribution by current sampling at the end of drop life. After applying a pulse of potential, the capacitive current dies away faster than the faradaic current; thus the current is measured at the end of the pulse (Bard and Faulkner, 2001).

Normal pulse voltammetry uses a series of potential pulses of increasing amplitude. Between the pulses the electrode is kept at a constant potential at which no reaction of the analytes occurs. The amplitude of the pulse increases linearly with each drop. The current is measured about 40 ms after the pulse is applied, at which time the contribution of the charging current is nearly zero. In addition, because of the short pulse duration, the diffusion layer is thinner than that of DC polarography and hence the faradaic current is increased and normal-pulse polarography will be 5–10 times more sensitive than DC polarography. The limit of detection is about 10^{-7} to 10^{-8} (mol/L) for NPV technique. NPV is also a very good technique for determining diffusion coefficient.

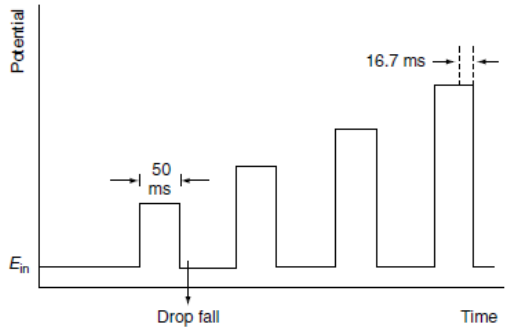

Figure 1.16 The schematic represantation of waveform of normal pulse voltammetry

Differential pulse voltammetry (DPV) is an extremely useful technique for measuring trace levels of organic and inorganic species. DPV is similar to NPV but with two important differences: The base potential is incremented between pulses, these increments being equal and the current is measured immediately before pulse application and at the end of the pulse: the difference between the two currents is registered.

Two current samples are taken during each drop's life time. One is taken immediately before applying the potential pulse, and the second the drop is dislodged. For each cycle the first current difference value is instrumentally subtracted from the second. A plot of this current difference versus applied (dc ramp) potential produces a stepped peak-shaped incremental derivative voltammogram (Figure 1.16).

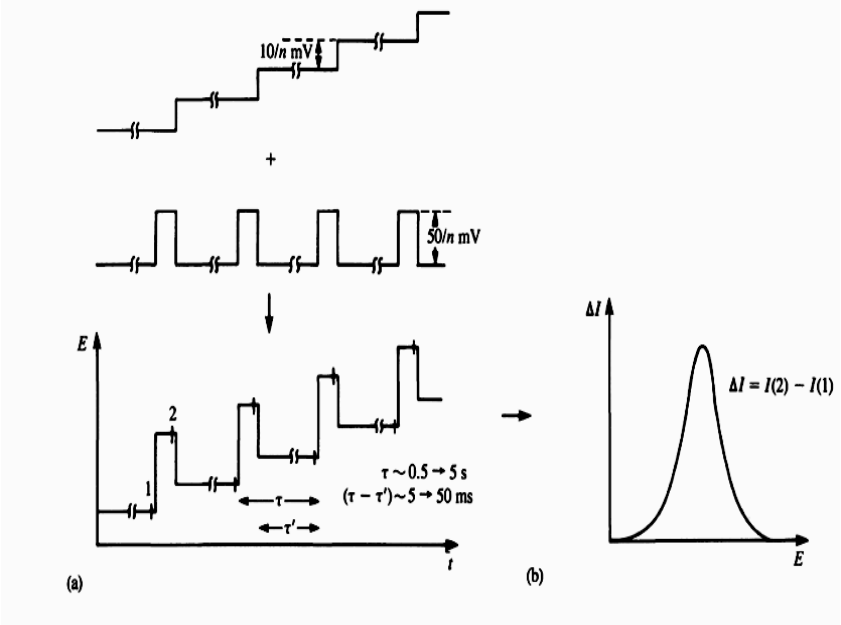

Figure 1.17 Differential pulse voltammetry. (a) Scheme of application of potentials (sometimes superimposed on a ramp rather than a staircase), (b) Schematic I-E profile.

1.10.1.1 Cyclic Voltammetry

Cyclic voltammetry is the most widely used technique for acquiring qualitative information about electrochemical reactions. The power of cyclic voltammetry results from its ability to rapidly provide considerable information on the thermodynamics of redox processes and the kinetics of heterogeneous electron transfer reactions and on coupled chemical reactions or adsorption processes.

This technique is based on varying the applied potential at a working electrode in both forward and reverse directions (at some scan rate) while monitoring the current. Cyclic voltammetry consists of scanning linearly the potential of a stationary working electrode (in an unstirred solution), using a triangular potential waveform (Figure. 1.18) (Wang et al., 2006).

The important parameters in a cyclic voltammogram are the peak potentials (Ep_c, Ep_a) and peak currents (ip_c, ip_a) of the cathodic and anodic peaks, respectively.

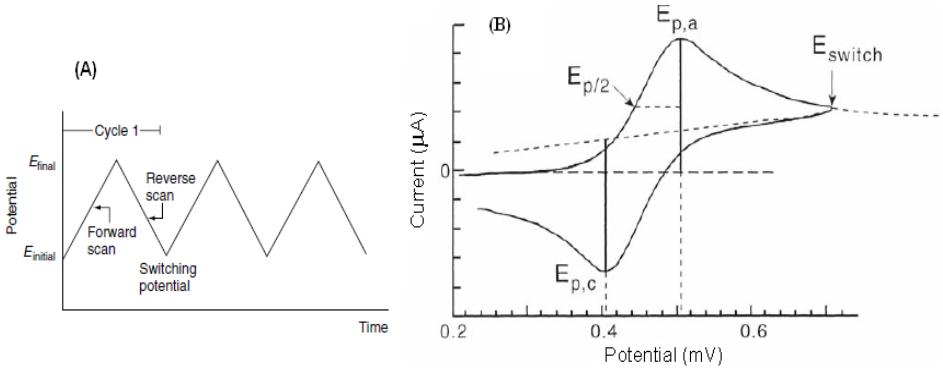

Figure 1.18 A) potential waveform B) current-potential representations.

If the electron transfer process is fast compared with other processes (such as diffusion), the reaction is said to be electrochemically reversible, and the peak separation is

$$\Delta Ep = Epa - Epc = 2.303\ RT/nF$$

Thus, for a reversible redox reaction at 25 °C with n electrons ΔEp should be $0.0592/n$ V or about 60 mV for one electron. In practice this value is difficult to attain because of such factors as cell resistance. Irreversibility due to a slow electron transfer rate results in $\Delta Ep > 0.0592/n$ V, than 70 mV for a one-electron reaction. The formal reduction potential (Eo) for a reversible couple is given by

$$E^o = \frac{Epc + Epa}{2}$$

For a reversible reaction, the concentration is related to peak current by the Randles–Sevcik expression (at 25 °C):

$$i_p = (2.69 \times 10^5)\ n^{3/2}\ A\ C\ D^{1/2}\ v^{1/2}$$

where i_p is the peak current in amper, A is the electrode area (cm^2), D is the diffusion coefficient ($cm^2 s^{-1}$), C_0 is the concentration in $molcm^{-3}$, and ν is the scan rate in $V\ s^{-1}$.

For irreversible processes (those with sluggish electron exchange), the individual peaks are reduced in size and widely separated totally irreversible

systems are characterized by a shift of the peak potential with the scan rate (Wang et al.,2006).

For quasi-reversible systems the kinetics of the oxidation and reduction reactions have to be considered simultaneously. As a general conclusion, the extent of irreversibility increases with increase in sweep rate, while at the same time there is a decrease in the peak current relative to the reversible case and an increasing separation between anodic and cathodic peaks (Gosser, 1993).

1.11 Surface Characterization Techniques

In the micro- and nano- science studies have led to increased demand for analytical and characterization methods for these materials and systems. All interactions with a finite body of matter must take place through its surface. The relation between the properties of a surface and the process history of the material must be understood since control of the surface properties is critical in many technological processes. Surface analysis is a necessary tool for determination of desired surface properties such as optical, electrical, chemical, mechanical or visual. The analysis of the surface composition and surface geometry has been increasingly important role in a wide range of industries and science studies. Generally, scanning electron microscopy (SEM), transmission electron microscopy (TEM), scanning tunnelling microscopy (STM) and atomic force microscopy(AFM) have been useful for imaging electrode surfaces directly (under potential control), and have thus dramatically improved the understanding of electrode reactions.

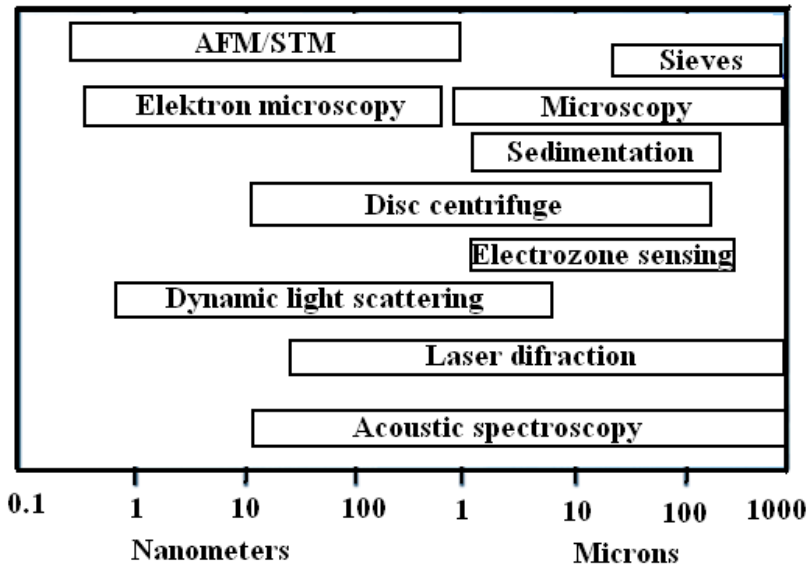

Figure 1.19 Comparison of the imaging of many types 2D and 3D profiling and imaging instruments (Rosenauer, 2003).

1.11.1 Atomic Force Microscopy (AFM)

AFM has become a standard technique to image with high resolution the topography of surfaces. AFM is a mechanical imaging instrument that measures the three dimensional topography as well as physical properties of a surface with a sharpened probe. This powerful probe microscopy operates by measuring the force between the probe and the samples.

Unlike traditional microscopes, the AFM does not rely on electromagnetic radiation, such as photon or electron beams, to create an image. The probe consists of a sharp tip (made of silicon or silicon nitride) attached to a force-sensitive cantilever (Figure 1.20).

AFM is the visualisation of surface microtopography from atomic structures to features of tens of microns. AFM uses a sharp tip, about 2 mm long and down to a minimum of 20 nm in diameter, which is scanned closely over the specimen surface, but in AFM the magnitudes of atomic forces rather than tunnelling currents are monitored as a function of the probe position on the sample surface.

AFM probe is very sharp; typically less than 50 nanometers in diameter and the areas scanned by the probe are less than 100 μm. In practice the heights of surface features scanned with an AFM are less than 20 μm. Scan times can range from a fraction of a second to many tens of minutes depending on the size of the scan and the height of the topographic features on a surface. Magnifications of the AFM may be between 100X and 100,000,000X in the horizontal (x-y) and vertical axis. The tip scans across the surface (by a piezoelectric scanner), and the cantilever deflects in response to force interactions between the tip and the substrate. Such deflection is monitored by bouncing a laser beam off it onto a photodetector.

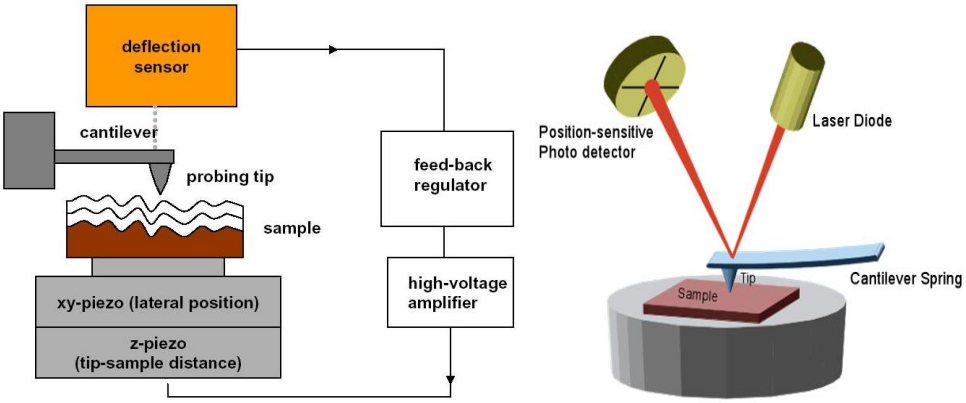

Figure 1.20 Illustration of an AFM cantilever /probe used in an AFM sensor (Nanomanyetik Catalogue).

The measured force is attributed to repulsion generated by the overlap of the electron cloud at the probe tip with the electron cloud of surface atoms. It partly depends on the nature of the electrode, the distance between the electrode and the tip, any surface contamination, and the tip geometry. An image is created as the probe is translated across the surface, while sensing the interaction of the force fields by the cantilever beam. An AFM could be used with not only conductive surface and substrate, but also it is used for insulating materials. AFM is capable of resolving features in three dimensions of a few nanometers with scan ranges up to a hundred microns. The surface structure of a wide range of materials can thus be explored. The technique is very useful for observing changes in electrode surfaces caused by adsorption, etching or underpotential deposition.

1.11.2 Scanning Electron Microscope (SEM)

The SEM consists a source of electrons; lenses for focusing them to a fine beam; facilities for sweeping the beam in a raster; arrangements for detecting electrons (and possibly other signals) emitted by the specimen; and an image-display system (Figure 1.21). Secondary-electron (SE) images, which show topographic features of the specimen, are the most commonly used type. Backscattered-electron (BSE) images are principally used to reveal compositional variations (Reed, 2005).

The magnification of a scanning image is equal to the ratio of the size of the image as viewed by the user to that of the raster scanned by the beam on the specimen. The minimum magnification is determined by the maximum

angle through which the beam can be deflected, and depends on the working distance, being least when this is greatest. The typical minimum magnification is about 10, with a scanned area of the order of 1 cm^2. Magnification can be increased by reducing the amplitude of the scanning waveform.

Resolution, defined as the size of the smallest detail clearly visible in the image, is limited not only by the diameter of the electron beam but also by the interaction between the electrons and the specimen. Therefore, correct focus setting is achieved by adjusting the control to obtain the sharpest possible image of fine detail in the specimen, preferably with the magnification set to a high value.

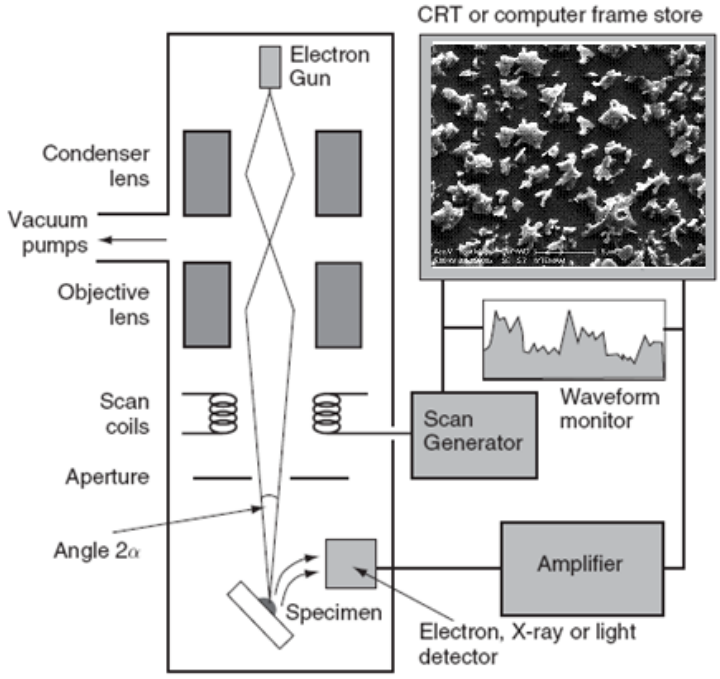

Figure 1.21 Schematic diagram of the layout of a SEM (Kelsall, 2005)

Secondary electrons (SE) are emitted from very near the surface of the sample, with energies of a few electron volts. The SE yield increases with decreasing angle between beam and specimen surface. ***Backscattered electrons (BSEs)*** have very high energies and low yields compared to secondary electrons. The ET detector may be used to collect only BSEs by making the grid bias slightly negative so as to exclude secondary electrons. However, only those electrons travelling in line-of-sight towards the detector will contribute to the relatively low signal and therefore images will show very strong shadowing contrast and a low signal-to-noise ratio (Kelsall, 2005).

1.11.3 X-Ray Photoelectron Spectroscopy (XPS)

XPS, one of the most frequently used methods, is based on the determination of the kinetic energy of the electrons emitted from the core levels in a photoelectric process. The energy of the core levels is assessed with the help of the kinetic energy of the photoelectrons. The basic principle is shown schematically in Fig. 1.22. XPS is based on the photoelectric effect. When a sample is irradiated with monochromatic X-rays, such as the K_α lines of Mg (1253.6 eV) or Al (1486.6 eV), core-level electrons from the inner shells of atoms in the sample will be ejected from the sample to the surrounding vacuum. The kinetic energy, E_K, of the emitted photoelectron is given by;

$$E_K = h\nu - E_B - e\phi_{sp}$$

where $h\nu$ is the energy of the incident X-ray photon, E_B is the binding energy of the core electron, and $e\phi_{sp}$ is the spectrometer work function. The binding energy increases with atomic number Z.

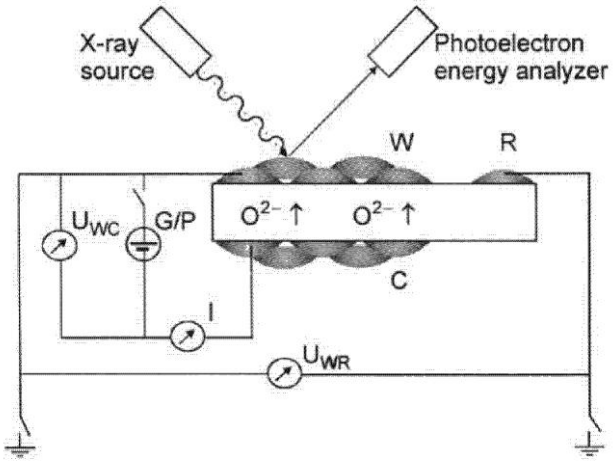

Figure 1.22 Schematic of the experimental setup for using X-ray photoelectron spectroscopy (XPS) to investigate the catalyst-electrode surface. (Vayenas, et al., 2002)

These energies unambiguously characterize the given atom. The measurement is quite precise and thus not only can elemental analysis be carried out but also fine changes in the core level energies produced by changes in the electron densities due to the formation of chemical bonds, i.e. chemical shifts, can be studied. Photoelectron spectroscopy can indicate, for

example, various oxidation states of a metal in oxide films on the electrode; it is widely used in the study of chemically modified electrodes and substances adsorbed on electrodes. It is important to do this type of work by comparison of E_B values of standard reference compounds. The XPS method yields information on several monolayers of atoms in the surface (Bagotsky, 2006)

There are several factors affecting these core level shifts and both initial state and final state effects play a role. Yet the dominant factor affecting such "chemical" shifts is the oxidation state of the element under consideration. A negative charge on an element (e.g. O) will in general cause a decrease in the binding energy of core level electrons (such as for example the Ols core level electrons) while a positive charge on an element (e.g. Na) will cause an increase in the binding energy of core level electrons (e.g. the Na Is core level electrons). Thus the observed (up to ±2 eV) chemical shifts can provide useful information on the oxidation state of an element in its local environment. (Vayenas, et al. 2002)

2. EXPERIMENTAL

2.1 Instrumentation

Voltammetric measurements were carried out using Bass 100B Electrochemical Analyser and Ivium Stat Electrochemical Interface Equipped with a three electrode system consisted of a working electrode (GCE, MWCNT-GCE, MNP-MWCNT-GCE PAP/GCE, Ox-PAP/GCE, MNP-Ox-PAP/GCE), an auxilary a platinum electrode and an Ag/AgCl (sat.KCl) used as reference electrode. Cyclic and differential pulse (dp) mode and time base mode were used throughout the electroanalytical studies. The pH measurements were made with WTW handheld 330i ion analyzer meter pH. Ambios Q-Scope Atomic force Microscopy and Philips XL30 SFEG and Micro Tech Polar 10 Spatter Coater Scanning Electron Microscopy were used for the charecterization of bare and modified elecrode surfaces. Bandelin Sonorex model ultrasonic bath was used for preparation of solutions and cleaning the electrodes.

2.2 Reagents and Solutions

All reagents were of analytical reagent grade. 4-Aminopheol (Fluka), Acetic acid (CH_3COOH) (Merck), sodium acetate (CH_3COONa) (Merck), sodium dihydrogen phosphate (NaH_2PO_4) (Merck), disodium monohydrogen phosphate (Na_2HPO_4) (Merck), boric acid (H_3BO_3) (Merck), sodium meta borate ($NaBO_2$) (Merck), sodium hydroxide(NaOH) (Riedel de Haen), ethanol (C_2H_5OH) (Merck), copper sulphate ($Cu(SO_4)_2.3H_2O$) (Merck), chloroplatinic acid (H_2PtCl_6)(Sigma–Aldrich), chloroauric acid (H_2AuCl_6), alimuna (Al_2O_3) (Baikowski), sodium dodecil sulphate ($C_{12}H_{25}NaO_4S$) (SDS), *N*,*N*-dimethylformamide (DMF) (Merck), uric acid ($C_5H_4N_4O_3$) (Fluka), Epinephrine ($C_9H_{13}NO_3$) (Alfa Aesar), ascorbic acid ($C_6H_8O_6$) (Alfa Aesar) were used in experimental studies. MWCNT was supplied from Aldrich (diam: 110-170 nm, lenght: 5-9 micron).

Stock standart solutions of EN, UA and AA (0.01 mol/L) were freshly prepared by dissolving the required amount of reagent in 0.1 M $HClO_4$, 0.1 M NaOH and ultrapure water [Millipore Milli Q system (18.2 MΩ)], respectively. Standart solutions were also prepared by dilution shortly before use.

Buffer solutions were prepared from acetic acid/sodium acetate, sodium dihydrogen phosphate/disodium monohydrogen phosphate, boric acid / sodium meta borate ($NaBO_2$) in the pH range from 3.76 to 10.02. Ionic strength was kept nearly constant for each buffer solution as 0.1 M. All buffer solution was prepared from analytical grade reagents and in ultrapure water Millipore Milli Q system (18.2 MΩ).

All experiments were carried out at ambient temperature and high purity nitrogen kept flowing over the solution during electrochemical experiments.

In the experiments of oxygen reduction, supporting electrolyte was kept under high purity oxygen until the saturation of solution.

2.3 Methods

2.3.1 Pre-conditioning of GCE

GCE was activated by polishing with different grade of Al_2O_3 slurry (0.05-3 micron) on a synthetic cloth then rinsing with pure water and ultrasonicated for 3 minutes in ethanol and ultra pure water mixture. GCE was also electrochemically cleaned by keeping 10 minutes at constant potential at 1.0 V.

2.3.2 Pre-treatment of Multiwalled Carbon Nanotubes

Multiwalled carbon nanotube which as received, is pretreated with concentrated HNO_3. 0.1g. MWCNT was boiled in approximately 4 mL concantrated HNO_3 and then washed many times with ultrapure water. The asit-treated MWCNT was dispersed in DMF to get a black suspension after 30 minutes ultrasonicataion.

2.3.3 Preparation of MWCNT modified GCE

A 10 μL of MWCNT suspension was injected on the pre-conditioned bare GCE surface. The solvent (DMF) of the suspension on the GCE surface was evaporated at 60˚C for more then one hour.

2.3.4 Preparation of Polyaminophenol Film Modified GCE

Electrochemical polymerization of p-aminophenol was carried out in 0.5 M $HClO_4$ solution containing 5mM SDS and 5mM p-aminophenol by CV. The polymerization voltammograms were obtained by repetitive 20 potential cycles from -0.6 to 2 V vs. Ag / AgCl (sat. KCl) at a scan rate of 100 mV/s. This electrode donated as PAP/GCE and transferred into 0.1 M NaOH solution for electrochemical oxidation of the conductive PAP film at +1.0 V for 300 sec. The obtained electrode was wash with ultra pure water and denoted as Ox-PAP/GCE.

2.3.5 Preparation of Pt, Au, Cu metal nanoparticles modified MWCNT/GCE and Ox-PAP/GCE

The metal nanoparticles were electrochemically deposited on the MWCNT/GCE and Ox-PAP/GCE by cyclic voltammetry (CV). For MWCNT/GCE modification, Au nano particles deposited by CV scanning between 0.6 to -0.9 V in $HAuCl_4$ with a scan rate of 50 mV/s for 10 cycles and Cu nano particles were deposited by CV scanning between -1.1 V and 0.0 V in 1 mM $CuSO_4$ at the same condition. Bimetallic nano particles modified MWCNT/GC electrodes were obtained by applying the same prosedure consecutively that mentioned above. The obtained metal nano particles modified MWCNT/GCE electrodes were ready for use after the final wash with ultra pure water and denoted as Cu-Au-MWCNT/GCE and Au-Cu-MWCNT/GCE.

For Ox-PAP/GCE modification, with metal nano particles, Pt nano particles were deposited by CV scanning between 0.8 V and -1.0 V with a scan rate of 50 mV/s for 10 cycles in 0.1 M H_2SO_4 containing 1 mM K_2PtCl_6. Au nano particles deposited by CV scanning between 0.6 to -0.7 V in $HAuCl_4$ + 0.1 M HCl and Cu nano particles were deposited by CV scanning between -0.5 V and 0.5 V in 1 mM $CuSO_4$ + 0.1 M H_2SO_4 solution at the same condition.

2.3.6 Preparatin of EN Samples

The EN samples were purchased from pharmach in an injection solution (0.25 mg EN/mL). 294 μL samples were completed to 1 mL with ultrapure water. Total concentration of EN was calculated $4x10^{-4}$ M. 1 mL of this EN sample was transfered into the voltammetric cell that contains 10 mL pH 7 PBS.

3. RESULTS AND DISCUSSION

The main goal of this study is firstly the qualitative analysis of oxygen at more positive potentials with higher current density than bare electrodes to simplify the cathode reaction for maximize the yield at fuel cells.

Another important point of this thesis is to simultaneous determination of AA, EN and UA which have nearly similar oxidation potentials. So coming through of this aim many experimental studies were carrying out. All of the experiments were established the optimum conditions for simultaneous determination of AA, EN, UA.

3.1 Voltammetric behaviour of MWCNT/GC electrode in the presence of Cu^{2+}, Au^{3+} ions.

Voltammetric behaviour of MWCNT-GCE was studied in the presence of $CuSO_4$+0.1 M H_2SO_4 and $HAuCl_4$ + 0.1 M HCl and the mixture of $CuSO_4$+ $HAuCl_4$ + 0.1M H_2SO_4 in Figure 3.1. The growth of Cu nano particles on the MWCNT/GCE surface corresponds to a reduction peak at -0.73 V and an oxidation peak at -0.58 V in Figure 3.1 a A stable peak currents were observed for both reduction and oxidation on the electrode reaction after the 10 CV cycles.

Deposition of Au nano particles on the MWCNT/GCE electrodes in $HAuCl_4$ solution was studied and after 10 CV cycles a stable voltammogram was obtained in the potential range between 0.8 to-0.8V. Figure 3.1 b CV showed that, Au nano particles obtained by Au (III) ions reduction at 0.05 V and oxidation at 0.20 V. These data are well aggrement with previous study (Gelmez, 2009).

Figure 3 c shows deposition of Cu nano particles on Au-MWCNT/GCE. The characteristic oxidation and reduction peak potentials of Cu shifted to more positive potentials by the existance of Au molecules on MWCNT surface. Two reduction peaks were observed at +0.07 V and –0.02 V supposed that correspond with Au and Cu respectively. Oxidation peak was observed at 0.1 V. The increasing of the reduction peaks depending on cycle number showed that electrodeposition of metal nano particles were carried out on the MWCNT-GCE surfaces.

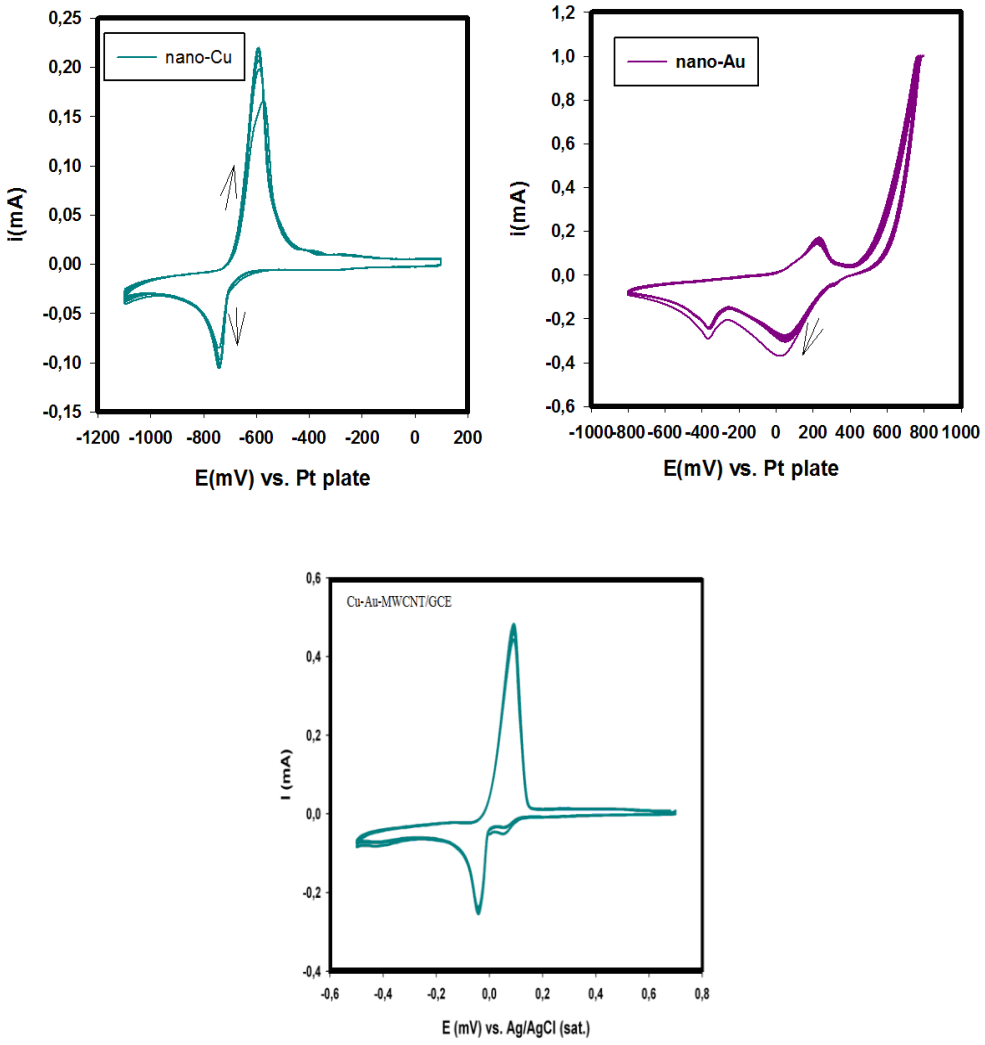

Figure 3.1 a) Cu deposition, b) Au deposition on MWCNT/GCE, c) Cu deposition on Au-MWCNT/GCE at 50 mV/s for 10 cycles in 1 Mm $CuSO_4$ and $HAuCl_4$ respectively.

3.2 Surface Characterization of CNT and Metal Nano Particules Modified CNT Film Electrodes

Figure 3.2 shows the SEM micrographs of MWCNT/GC electrodes modified with different nano particles. Figure 3.2 a shows loosely grown of MWCNTs which allow easily electrodeposited Au and Cu nano particles on the sidewalls. In Figure 3.31 b Nano Au particles were formed as bright round-shaped which homogeneously dispersed particles decorating on the electrode surface. It can be seen that nano Au particles decorated on the sidewalls of the MWCNT/GCE. Figure 3.31 c shows co-deposition of Au and Cu nano particles. In backscattered image, Au nano particles have seen brighter than Cu

nano particles due to its higher moleculer weight. Energy dispersive X-ray spectroscopy study confirmed the presence of nano Au and Cu particles decorating MWCNT/GCE. The weight gain of the MWCNTs due to the Au and Cu loading was about 4.7% and 1.3% (Figure 3.31 d).

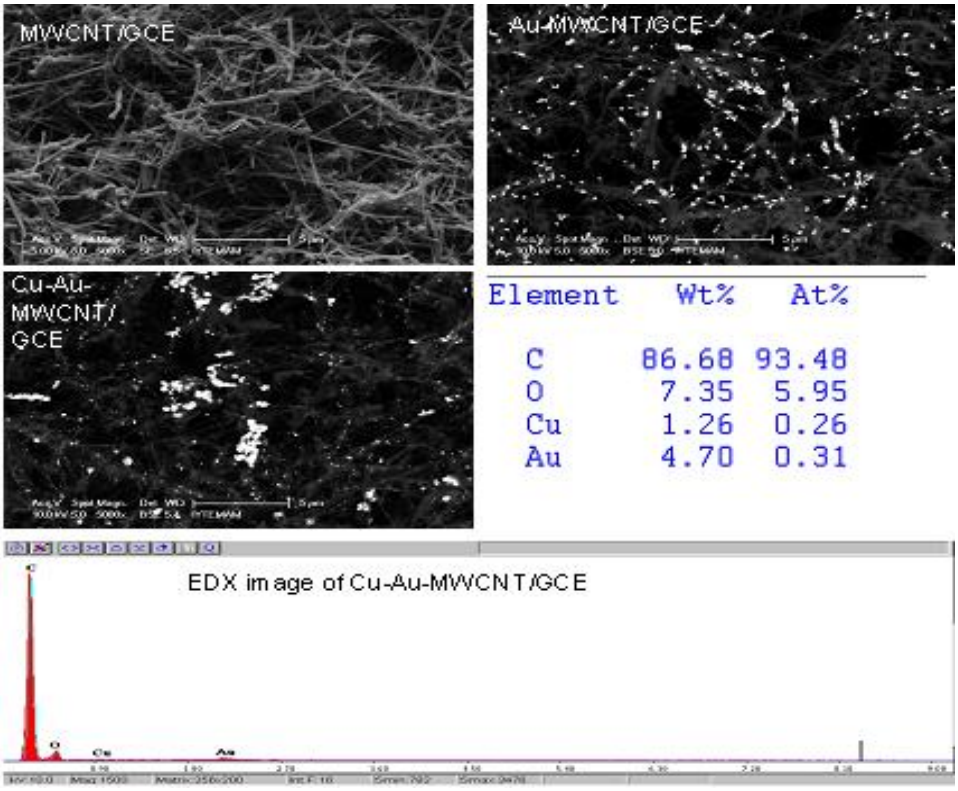

Figure 3.2 EDX results and typical SEM images of a) bare MWCNT/GCE b)Au-MWCNT/GCE c) Cu-Au-MWCNT/GCE d) EDX results.

Cu-Au MNPs modified MWCNT/GCE surface was also investigated by X-ray photoelectron spectroscopy (XPS) (Figure 3.3). The Au 4f spectrum consists of two peaks located at 84.6 and 88.1 eV, corresponding to the Au 4f7/2 and Au 4f5/2 components, respectively (Figure 3.32 a). The Au 4f7/2 photoelectronic peak is located at 84.6 eV and this value is typical of pure metallic Au species. Also the the binding energy of Cu 2p that obtained from XPS analysis was 935 eV (Figure 3.3 b), which were typically characteristic of Au^0 and Cu^0. Finally, it can be claimed that, a uniformly covered layer of Cu and Au nano particles modified MWCNT on the GCE could be easily prepared with the present technique depending on XPS and SEM images.

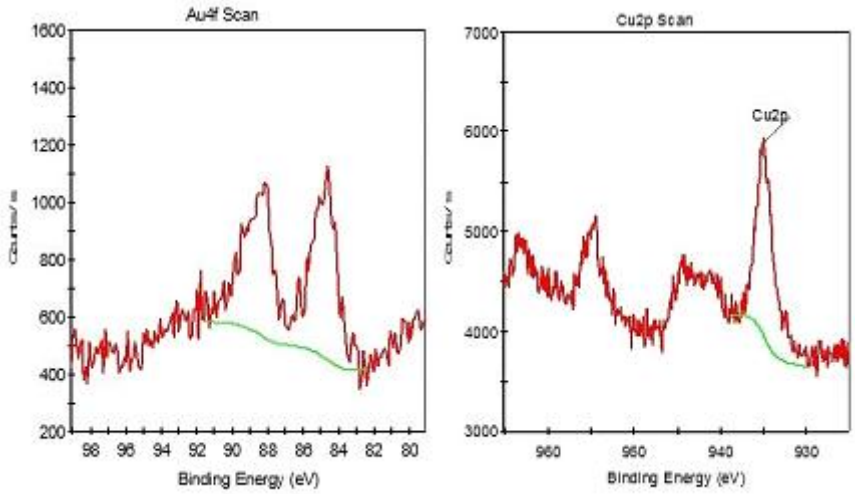

Figure 3.3 XPS spectra of Cu-Au-MWCNT/GCE a) represents the peaks of Au 4f7/2 and 4f5/2 b) represents the main peak of Cu 2p3/2

3.3 Voltammetric Behaviour of Oxygen at Bare and Modified Electrodes

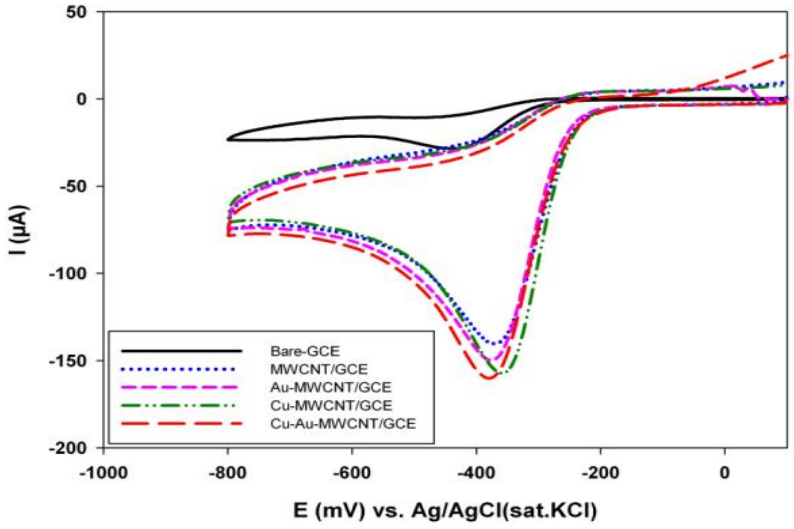

Figure 3.4 Cyclic Voltammetric behavior of GCE, MWCNT/GCE and different metal nano particles modified MWCNT/GC electrodes in O_2 saturated 0.1 M NaOH.

Figure 3.2 shows the cyclic voltammograms of bare GCE, and MWCNT-GCE and MNP/ MWCNT-GCEs in 0.1 M NaOH solution in the absence and presence of oxygen. An irreversible electrochemical behaviour was observed at all electrodes for oxygen reduction. However, the reduction of oxygen was take

placed at -0.44 V at bare GCE, but the peak potential was shifted to -0.38 V at MWCNT/GCE and MNP modified /MWCNT/GCE. On the other hand, a well-defined reduction peak with obviously increased current response was obtained in both MWCNT/GCE and MNPs modified MWCNT/GCE compare with bare GCE. The best catalytic activity was observed on bimetalic Cu-Au MNP modified MWCNT/GCE. The remarkably enhanced signal of oxygen reduction at all modified electrodes can be attributed increasing the effective surface area and improve the conductivity of the modified electrodes surfaces which can be played important role to accelerate the electron transfer.

3.4 Optimization studies of oxygen reduction at Cu-Au-MWCNT/GCE.

3.4.1 Optimization of Sodium Hydroxide Concentration

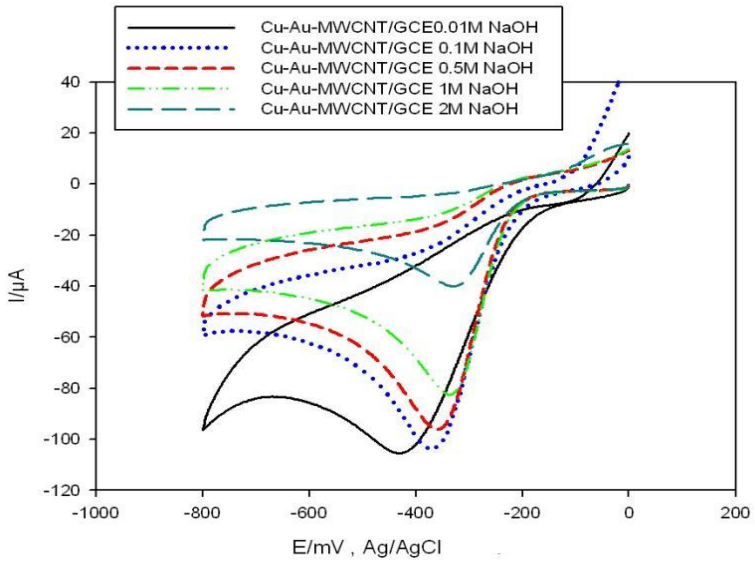

Figure 3,5 Cyclic voltammograms for oxygen reduction on Cu-Au-MWCNT/GC electrode at different NaOH concentrations.

The effect of NaOH concentrations on the oxygen reduction reaction was investigated in the concentration range of 0.01-2.0 M at bimetalic Cu-Au MNP modified MWCNT/GCE. As shown at Figure 3.5 the peak potential was observed at -0.420 V at negatively potentail in 0.01 M NaOH. The modified electrode exhibited a substantial negative shift to -0.38 V of the reduction peak potential and gradually decreased the current signal with increasing the NaOH concentration. The best catalytic activity was observed at at bimetalic Cu-Au MNP modified MWCNT/GCE in 0.1 M NaOH solution.

3.4.2 The Influence of nano Cu and Au Particles Amount on oxygen reduction

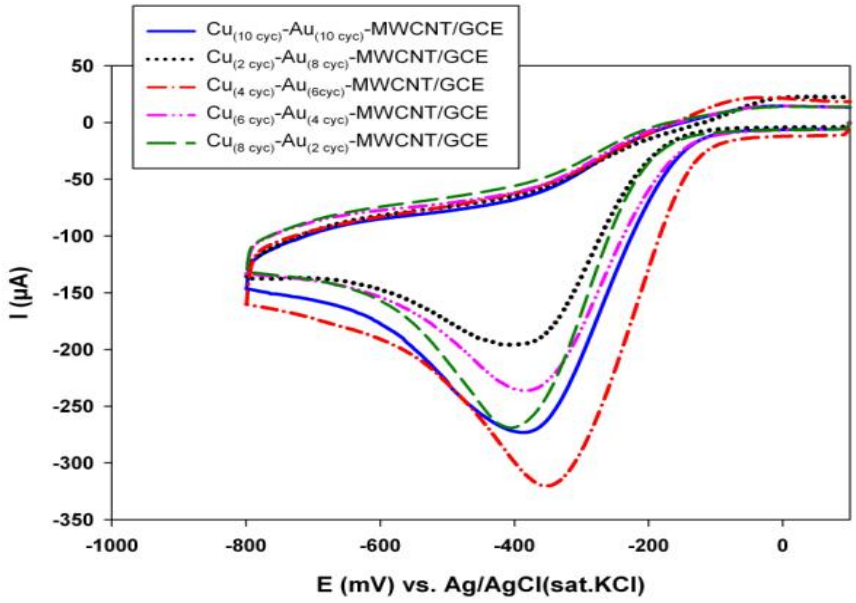

Figure 3.6 Cyclic voltammogram for oxygen reduction at different cycle number of nano particle deposition

Copper and gold modified MWCNT/GC electrodes prepared with different coverage depending on the cycle number of CV that was examined by changing the cycle numbers both for gold and copper deposition to obtain most appropriate surface towards oxygen reduction. When the CV of oxygen reduction was compared for modified elecetrodes, which obtained under the same experimental conditions, 4 cycles copper deposition after 6 cycles of gold deposition on MWCNT/GCE surface obviously provide the desirable change in peak characteristics in terms of peak current and peak potential (Figure 3.6). Overall results have prove that bimetallic nano particles modified MWCNT/GC electrodes have offer a satisfactory enhancement in peak characteristics related to the oxygen reduction.

3.4.3 Electroreduction of oxygen at GCE, MWCNT/GCE and $Cu_{(4cyc)} - Au_{(6cyc)}$ -MWCNT/GCE

Figure 3.7 clearly demonstrates the distinction in the performances of the modified and bare electrodes for oxygen reduction in alkaline media. The oxygen reduction peak has appeared as a broad peak at the bare GC electrode as the electron transfer process was slow-moving in alkaline media. On the other hand, a distinct peak was observed at -0,37 V for MWCNT/GC electrode indicating a fast electron transfer. The performance of Cu-Au bimetallic nanoparticles modified MWCNT/GC electrode towards oxygen reduction found very effective compared with the bare GCE, MWCT/GCE and all MNPs modified MWCNT/GCE, Significant current enhancement as a increase peak signal about 10 times than bare GCE and 2 times than MWCNT/GCE was observed while the peak potential has shifted about 80 and 20 mV in positive directions, respectively.

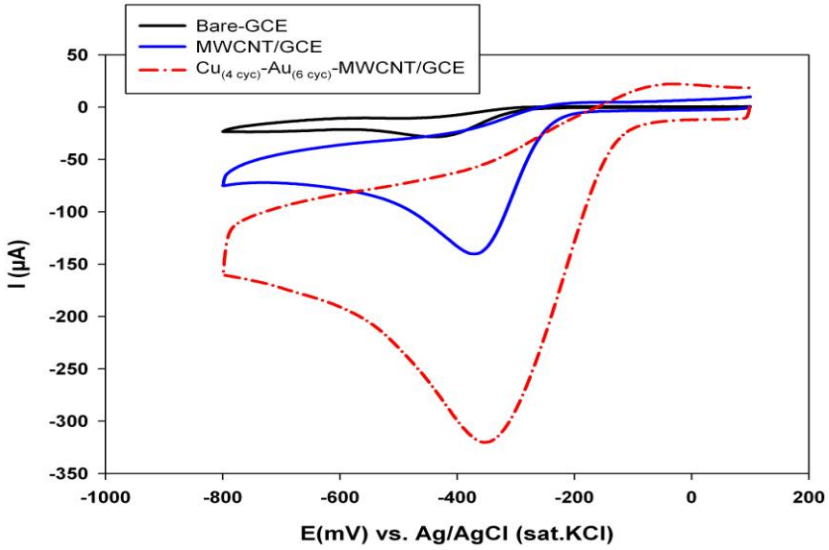

Figure 3.7 Cyclic voltammogram of oxygen reduction reaction on bare, MWCNT and $Cu_{(4cyc)} - Au_{(6cyc)}$ -MWCNT/GCE.

3.4.4. Scan rate study at $Cu_{(4cyc)} - Au_{(6cyc)}$ -MWCNT/GCE

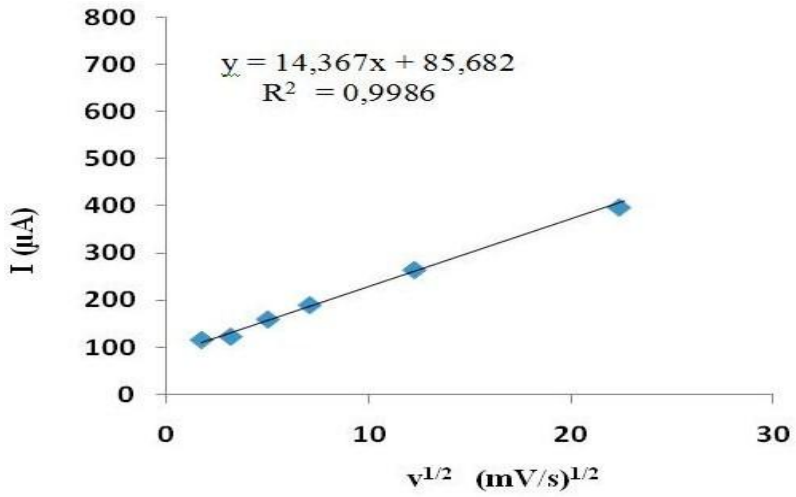

Figure 3.8 Cyclic voltammogram for oxygen reduction of $Cu_{(4cyc)}$ –$Au_{(6cyc)}$ -MWCNT/GC electrode at different scan rates. (3, 10, 25, 50, 150, 500 mV/s).

In order to confirm the electrode behaviour on the reduction of oxygen, a series of cyclic volatmmograms were recorded at bimetalic Cu-Au MNPs modified MWCNT/GCE by varying potential scan rate. The reduction peak current increased linearly with the square root of the scan rate (Figure 3.6), suggesting that oxygen reduction reaction at this modified electrode was controlled by diffusion. The reduction peak potential of oxygen shifted negative values with increasing the scan rate, indicating that the electron transfer was irreversible.

3.4.5 Tafel plots for oxygen reduction at different electrodes

Tafel behavior was studied in the mixed kinetic diffusion control region with 3 mVs^{-1} scan rate at Cu-Au-MWCNT/GCE (Figure 3.7). Tafel slopes at low and high current regions have 59.07 and 142.8 mV gradient values, respectively. This result can attribute to the change from Temkin to Langmiur conditions for changing coverage of surface by adsorbed oxygen species.

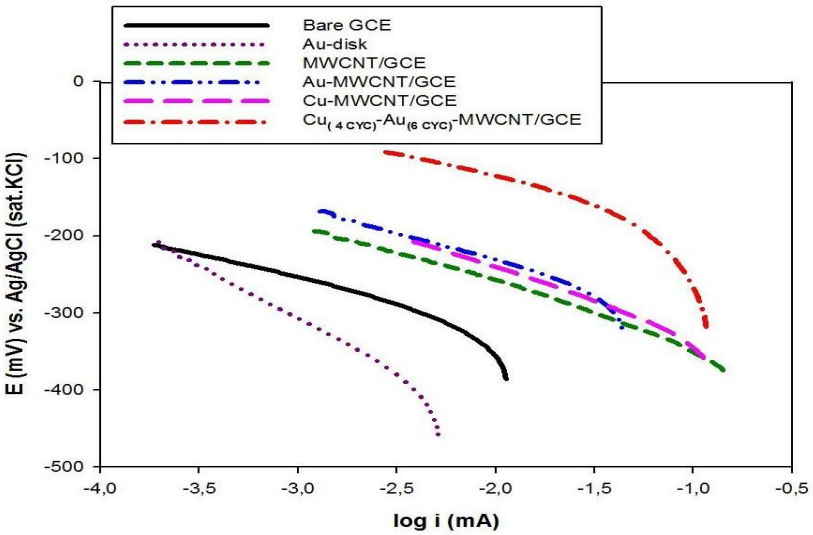

Figure 3.9 Tafel slopes of oxygen reduction on different electrodes for 3 mV/s scan rate.

3.5 Preparation of Polyaminophenol Film Modified GCE

Figure 3.10 shows multisweep cyclic voltammograms of p-amoniphenol electropolymerization on GCE surface in 0.5 M $HClO_4$ solution containing 5mM SDS and 5mM p-aminophenol by cycling the potential from -0.5 to 2 V vs. Ag / AgCl (sat. KCl) at a scan rate of 100 mV /s for 20 cycles.

In the presence of SDS, the oxidation of p-aminophenol can be easily occurred on the electrode surface in the presence of SDS which is leading more monocation radicals formation on the electrode surface. The conductivity of PAP was increased due to the SDS behave as an anionic dopant of the polymer.

An irreversible oxidation peak was observed at 1.55 V for p-AP without the corresponding cathodic processes in the reverse scan. After the second current potential CV scan, a single cathodic at -0.1 V and reversible oxidation and reduction peaks were seen at around +0.55 and +0.50 V respectively. The generation of the peaks might be attributed to the intermediate species during the oxidation process of the AP (Ojani, 2009) .The peak current increasing with cycles of CV showed that, an electropolymerization takes place and increase the content of polymer on the GCE surface. Increasing of the oxidation current indicated the increasing of polymer content on the surface of the electrode with the increasing of the potential cycling times showing electropolymerization takes place on the GCE surface. The AFM and SEM images were also

supported the content of the polymer on the GCE surface (can be seen on the electrode characterization

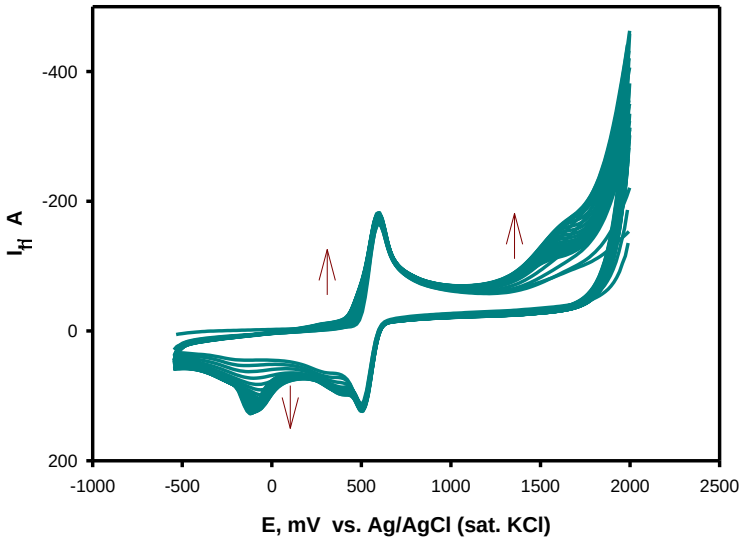

Figure 3.10 Cyclic voltammogram of p-AP electropolymerization in a 5.0 mM p-AP monomer/ 0.5 M $HClO_4$ solution on the surface of the glassy carbon electrode in the presence of 5.0 mM SDS at a scan rate of 100 mVs^{-1}. The arrows indicate the trends of current during CVs.

3.6 Optimization studies for AA, EN and UA Oxidation at PAP/GCE

3.6.1 Effect of supporting electrolyte pH on cyclic voltammetric behaviour of AA, EN, UA and their mixture

The effect of pH on the peak currents and peak potentials of the electrocatalytic oxidation of AA, EN, UA were investigated for $5x10^{-4}$ M AA, EN and UA at bare and PAP/GCE (Figure 3.11-3.13) by CV techniques in the pH range of 3.76-10.02.

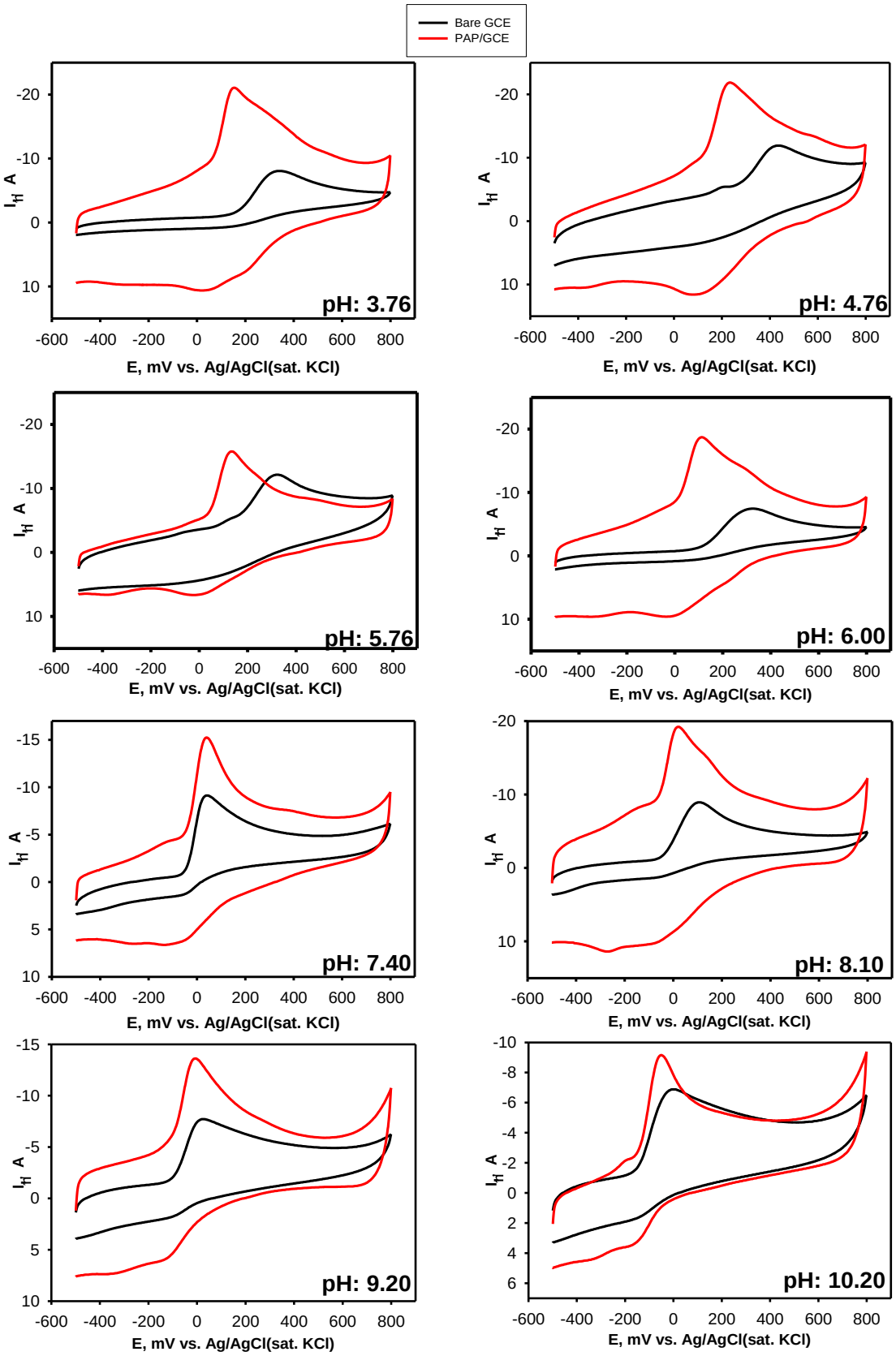

Figure 3.11 Cyclic Voltammograms of electrooxidation of AA at bare and PAP/GC electrode in various pH (3.76 to 10.2) at a scan rate of 50 mV/s.

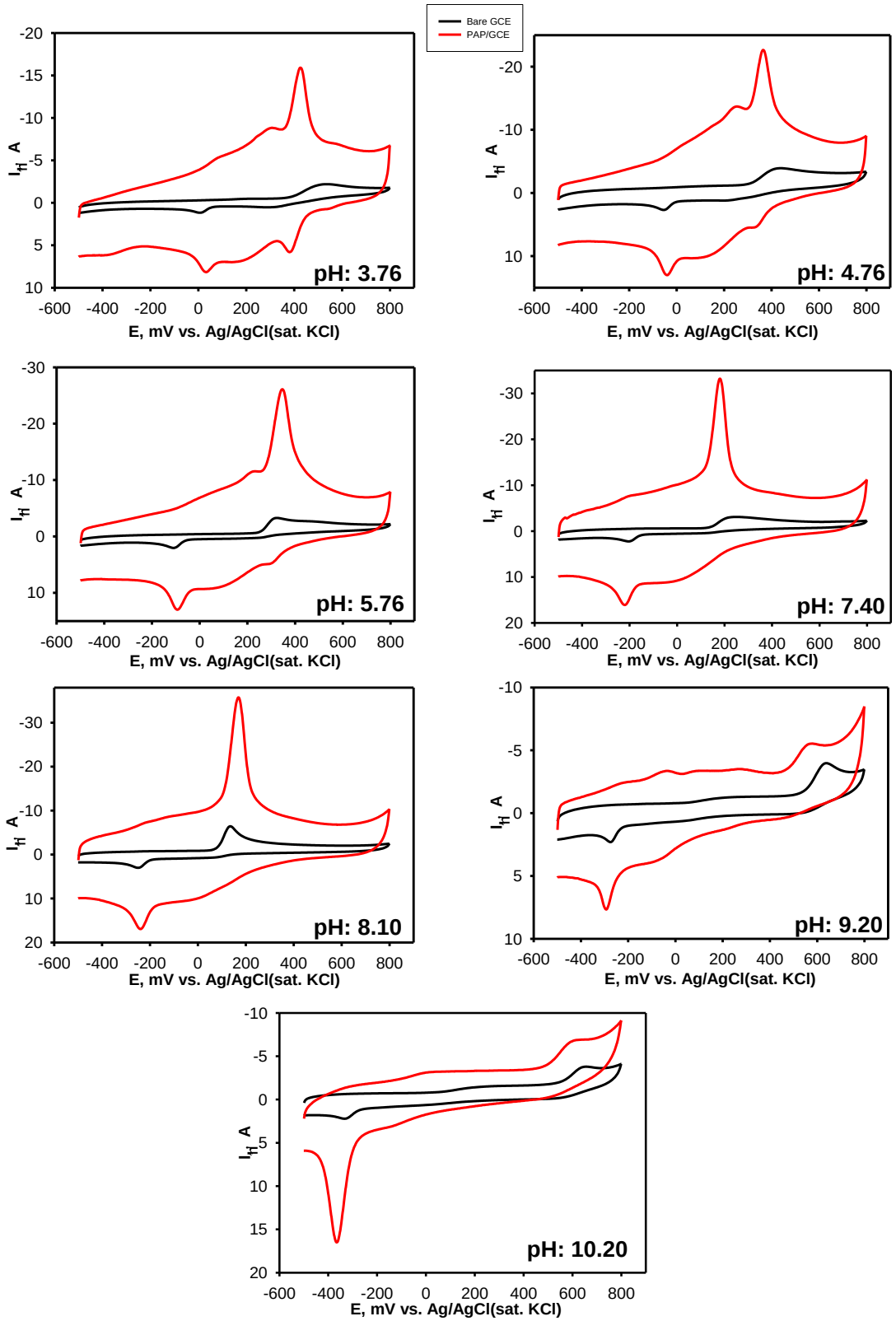

Figure 3.12 Cyclic Voltammograms of electrooxidation of EN at bare and PAP/GC electrode in various pH (3.76 to 10.2) at a scan rate of 50 mV/s.

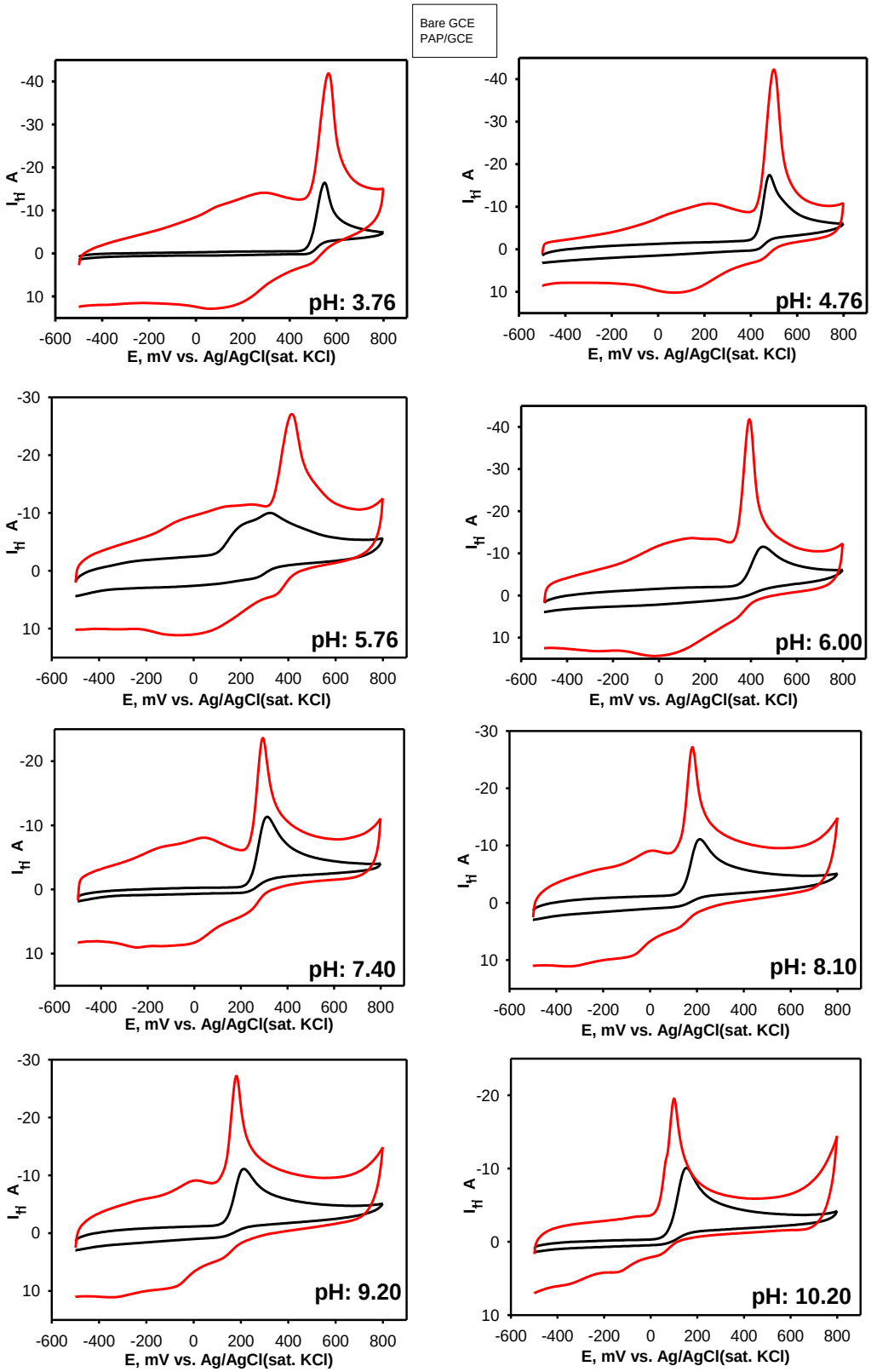

Figure 3.13 Cyclic Voltammograms of electrooxidation of UA at bare and PAP/GC electrode in various pH (3.76 to 10.2) at a scan rate of 50 mV/s.

The peak potentials for AA, EN and UA showed same trend and shift almost linearly towards negative potentials when pH was increased in the range of 3.00 – 7.70, indicating that proton ions were directly involved in the rate determination step of the oxidation of the analytes.

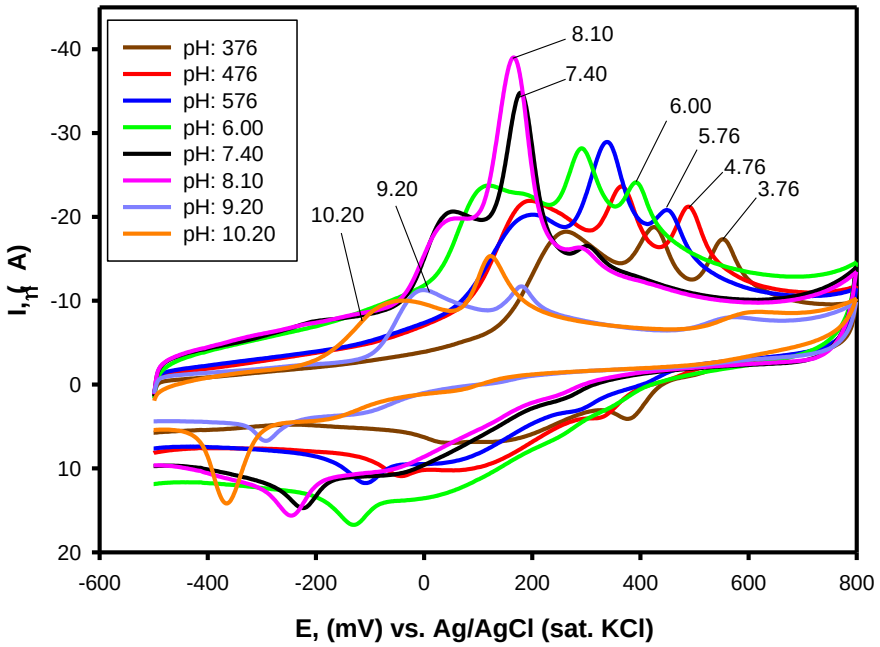

Figure 3.14 Cyclic Voltammograms of electrooxidation of AA, EN, UA (10^{-4}, 10^{-5}, 10^{-5} M), mixture at PAP/GC electrode in various pH (3.76 to 10.2) at a scan rate of 50 mV/s.

The effect of pH on the 10^{-5} M EN, UA and $5x10^{-4}$ M AA mixture responds at PAP/GC electrode was found almost same compare with in the case of alone AA, EN and alone UA at same concentration in the 0.1 M acetate, phosphate and borate buffer systems corresponds the pH range of 3.76-10.02 (Figure 3.14). As the given at Figure 3.15 a the peak potentials of AA, EN and UA oxidations that investigated from their mixture showed a linear variation with the value of pH and shifted to more negative potentials with slopes of about -65 mV, 62 mV, 56 mV, respectively. The slopes indicate that the uptake of electrons is accompanied by an equal number of protons for AA, EN and UA.

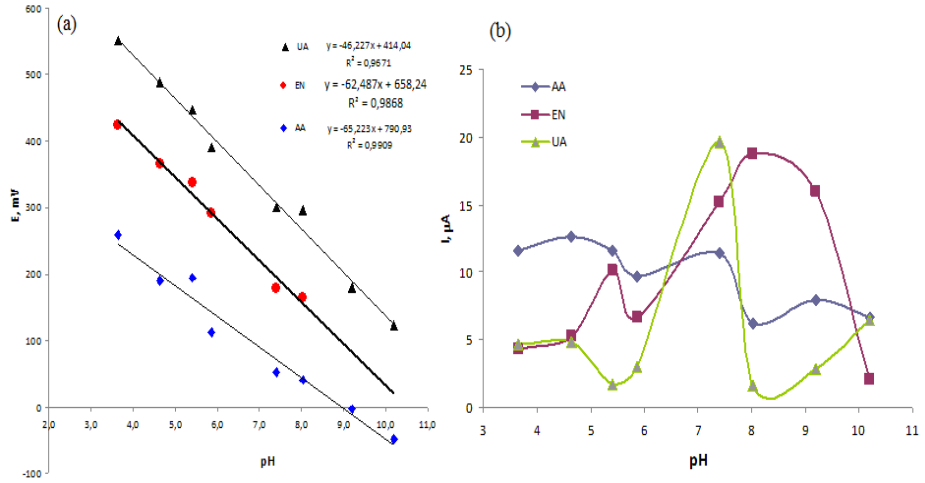

Figure 3.15 Influence of the pH on a) peak potential and b) peak current for AA, EN and UA on the PAP/GCE with cyclic voltammetry (pH: 3.76 - 10.2)

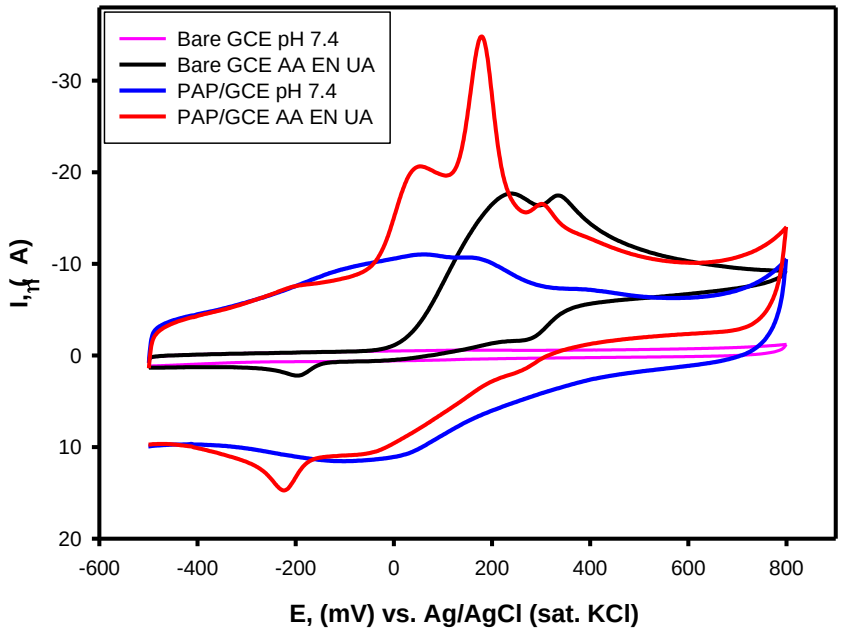

Figure 3.16 Cyclic voltammograms of PAP/GCE and bare electrode with and without AA+ EN+ UA (.10^{-4}, 10^{-5}, 10^{-5} M)

Another important point of the pH study was that the highest oxidation peak currents were observed in pH 7.40 PBS for uric acid and ascorbic acid in the mixture and their individual form. Different values were observed for EN oxidation (Figure 3.15 b). The peak current increased with pH values increasing from 3.76 to 8.0 and reached a maximum at pH 8.0, then decreased quickly, which is in agreement with the litherature (Jin, et al., 2002). However,

pH 7.40 was selected in the subsequent experiments due to the similar environment to the human body and obtained maximum peak seperation for AA, EN and UA. Figure 3.16 shows the voltammograms of simultaneous oxidation of AA, EN, UA at bare and PAP/GC electrode at optimum pH 7.40. It was clearly seen that PAP/GCE succesfully carry out the simultaneous oxidation of AA, EN and UA while homogene electrone transphere was seen at bare GCE.

3.6.2 Optimization of Aminophenol Cycle Number

Figure 3.17 demostrated the effect of aminophenol cycle number on the response of on UA, EN ($5x10^{-5}$ M) and ($5x10^{-4}$ M) AA mixture at pH 7.40 of PBS. Figure 3.17 inset shows the oxidation peak currents for all AA, UA and especially EN increased sharply from 10 to 20 cycles of aminophenol and then suddenly decreased for higher cycle numbers. This decrease can be explained to increase the electrode resistance and capacitance by increasing the polymer content on the GCE surface.

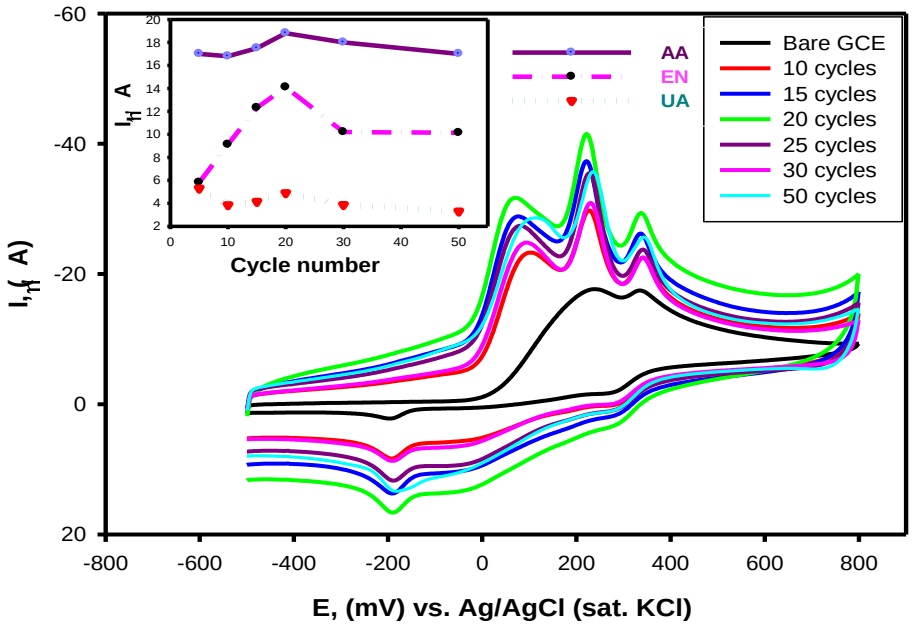

Figure 3.17 Cycle effect of aminophenol on AA, EN and UA. Inset: cycle number effect on oxidation currents of AA, EN and UA

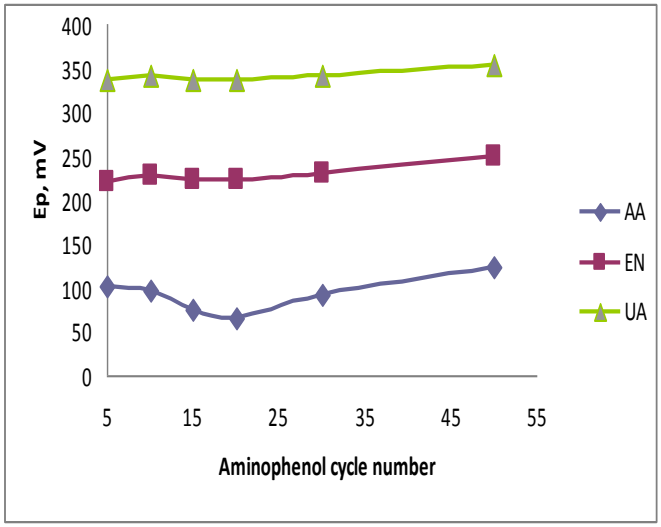

Figure 3.18 Cycle number effect on oxidation peak potentials of AA, EN and UA.

As can be seen clearly in Figure 3.18 and Table 3.1 maximum peak potential seperations between AA-EN and EN-UA were obtained for 20 cycles with the value of 156 mV and 115 mV, respectively. Oxidation peak potentials of AA, EN and UA were became closer by the incerasing cycle numbers more then 20 cycles. Therefore, the optimum cycle number was distinguished as 20 for preparation of polyaminophenol film modified GCE.

Table 3.1 Cycle number effect on oxidation peak potentials of AA, EN, UA and peak seperation values of their mixture at PAP/GCE.

Cycle Number	**AA. (mV)**	**EN (mV)**	**UA (mV)**	**ΔE(AA-EN) (mV)**	**ΔE(EN-UA) (mV)**
5	102	220	336	118	116
10	98	227	341	129	114
15	74	222	336	148	114
20	**66**	**222**	**337**	**156**	**115**
30	92	230	341	138	111
50	123	250	355	127	105

3.6.3 Optimization of p-Aminophenol Concentration

Figure 3.19 shows the effect of aminophenol concentration on the response of 10^{-4} M AA, 10^{-5} M UA and EN mixture at pH 7.40 of PBS. Variation of aminophenol concentration didn't cause an desirable change on peak current of AA, EN and UA however the maximum peak potential sepertion observed for $5x10^{-3}$ M that it was chosen for further studies.

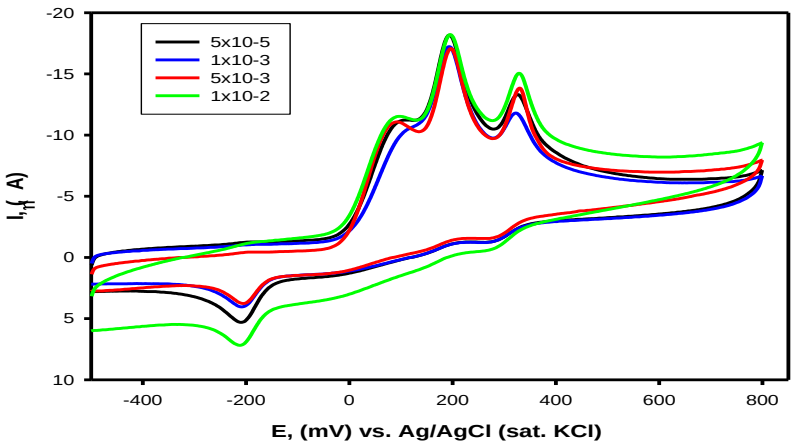

Figure 3.19 Effect of aminophenol concentration on AA, EN and UA.

3.7 Preparation of Oxidized Polyaminophenol Film Modified GCE

Some conducting polymers can be overoxidized at high positive potential for porous surface and gained to higher the catalytic activity toward analytes due to the superior selectivity and sensitivity (Jing, at al, 2007). To obtained a better conductive and more porous PAP film on the GCE surface the PAP film electrode was overoxidized at +1.0 V for 300 s in 0.1 M NaOH solution (Figure 3.20).

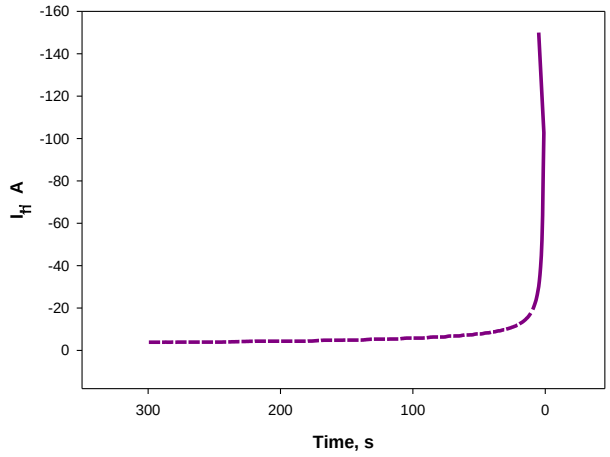

Figure 3.20 Oxidation of polyaminophenol on GCE in 0.1 M NaOH solution.

3.7.1 Optimization of overoxidation time of polyaminophenol

The overoxidation time of polyaminophenol film on the electrode surface was studied in 0.1 M NaOH solution and the modified electrodes were used the simultaneous electrocatalytic oxidation of AA, EN and UA. It was clearly seen in Figure 3.21 that oxidation of polymer film made a desirable change in the oxidation response of AA, EN and UA. Peak current value of UA 4 times higher than the PAP/GCE however EN oxidation current was in a small decrease.

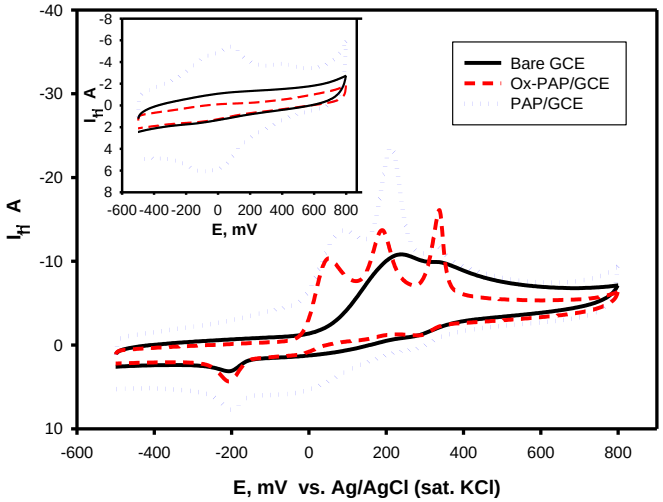

Figure 3.21 Cylic voltammograms of AA ($5x10^{-4}$ M), EN (10-4 M) and UA (10^{-4} M), oxidation at bare, PAP/GCE and Ox-PAP/GCE.

Another advantage of the oxidation prosedure was the increase in the peak potential difference between AA-EN and EN-UA compared to unoxidized aminophenol film modified GCE. The maximum peak potential seperation for AA, EN and UA were observed at 300 seconds overoxidized polyaminophenol modified GCE (Figure 3.22).Therefore, the reasonable overoxidation time of polyaminophenol on the GCE surface was 300 second for future experiments.

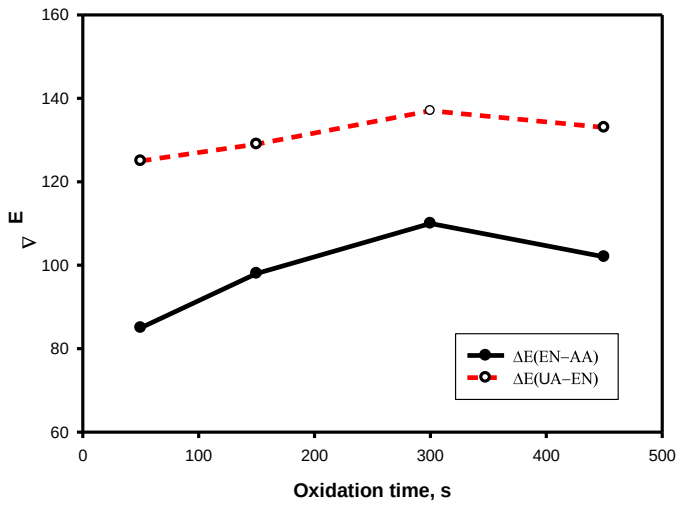

Figure 3.22 Effect of over oxidation time of polyaminophenol film on peak potential seperations between AA-EN and EN-UA.

3.8 Voltammetric behaviour of Ox-PAP/GC electrode in the presence of Cu^{2+}, $Au^{3+}$and Pt^{4+} ions

Ox-PAP was improved the catalytic activity of GCE toward the AA, EN and UA. It is well known that, metal nano particles modified polymer film electrodes exhibited higher catalytic activity for electrochemical reaction of many organic compounds.

Therefore, Ox-PAP/GCE surface was modified with different metal nanoparticles such as Cu, Au and Pt for electrocatalytic oxidation of AA, EN and UA. Figure 3.10 shows the voltammetric behaviour of Ox-PAP/GCE in the presence of Cu^{2+}, Au^{3+}, Pt^{4+} ions in acidic electrolytes. The growth of Cu nano particles on the Ox-PAP/GCE surface corresponds to two reduction peaks at 0.15 V and – 0.19 V also two oxidation peaks at 0.0 and 0.19 V (Figure 3.23 a). A gradually increasing of reduction peak currents depending on current

potential cycles of CV showed that metal nano particles was formed on the ox-PAP/GCE surface after the 10 CV cycles.

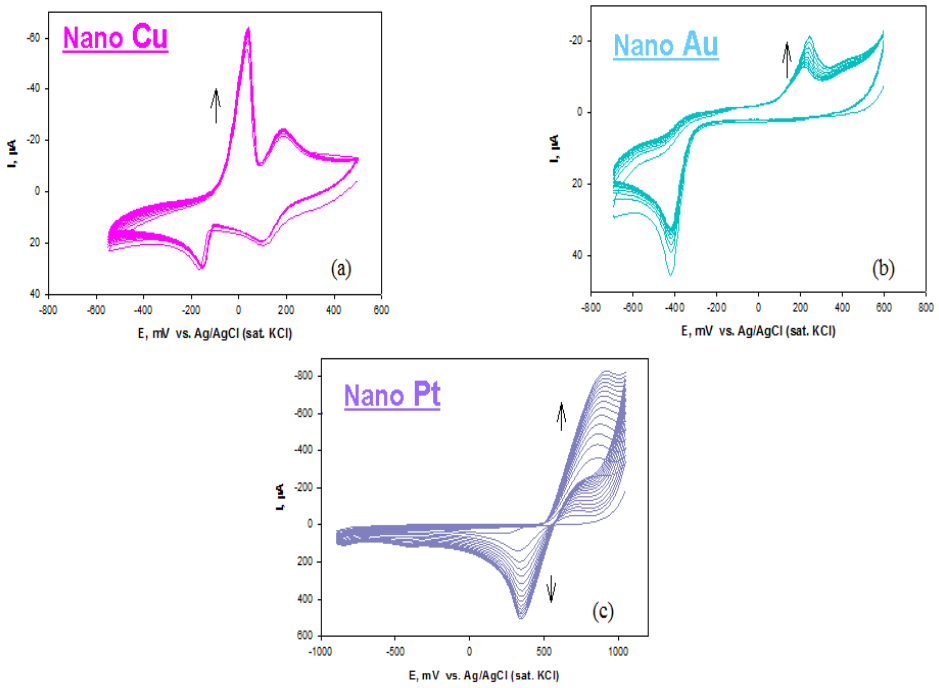

Figure 3.23 cyclic voltammograms of a) Cu, b) Au, c) Pt nano particles deposition on Ox-PAP/GCE.

Deposition of Au nano particles on the Ox-PAP/GCE electrodes in $HAuCl_4$ solution was studied and after 10 CV cycles, voltammogram was obtained in the potential range between 0.6 to -0.7V. Figure 3.23 b CV showed that, Au nano particles formed with Au (III) ions reduction at -0.41 V and oxidation at 0.22 V. Increasing of both reduction and oxidation peaks by increasing the cycle numbers of current potential cycling showed that nano Au particles were formed on the electrode surface. Figure 3.23 c demonstrates a pair well-defined redox peaks appeared at 0.4V for reduction of Pt (IV) ions and at 0.9 V for oxidation of Pt nano particles and the peak current increasing demostrated the Pt nano particles attached on the ox-PAP/GCE surface. The results showed that all metal nano particles was deposited on the Ox-PAP/GCE surface and the modified electrodes could be used for the simultaneously electrocatalytic oxidation of AA, EN and UA by heterogeneous electron transfer.

3.9 Surface Characterization of Ox-PAP/GCE and Metal Nano Particules Modified Ox-PAP/GCE

The surface morfology of bare GCE and modified GCE were characterized by AFM and SEM. The three dimensional AFM images showed that the bare GCE surface was partially rough in Figure 3.24 a. Figure 3.24 b shows image of polymer film modified GCE. Polymer film can be observed clearly on the surface with 39.1 nm of height that offering rougher surface than bare electrode and shaped as irregular round islands. When the polymer film was modified with Pt nano particules, the surface structure was extremely different with the height of 333 nm suggested that Pt nano particules deposited top sides of polymer islands (Figure 3.24 c).

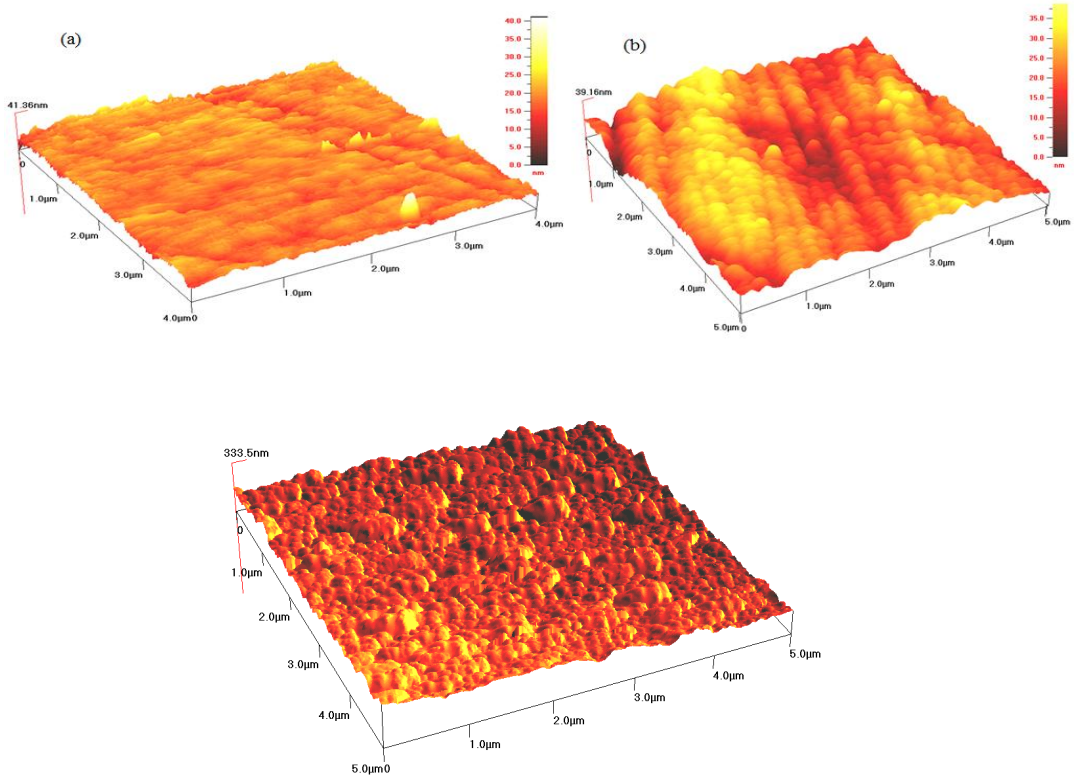

Figure 3.24 AFM images of a) bare GCE, b) PAP/GCE, c) Pt nano particles modified Ox-PAP/GCE in three dimensional views.

Figure 3.25 shows the SEM images of GCE, polymer film modified GCE and Pt nano particles modified polymer film covered GCE. Comparison Figure 3.25 a and b which were corresponding to a smooth electrode surface obtained at bare GCE, and almost homogeneosly distributed porous PAP/GCE surface. Figure 3.25 c shows the swollen like surface of oxidized polymer film that was

clearly different from un-oxidized so this was help to clarifying the different catalytic properties of these electrodes. Nano Pt particles were formed as bright round-shaped which homogeneously dispersed particles decorating on the electrode surface were seen in Figure 3.25 d. Energy dispersive X-ray spectroscopy study confirmed the presence of nano Pt particles decorating Ox-PAP/GCE. The weight gain of the polymer film due to the Pt loading was about 12 %.

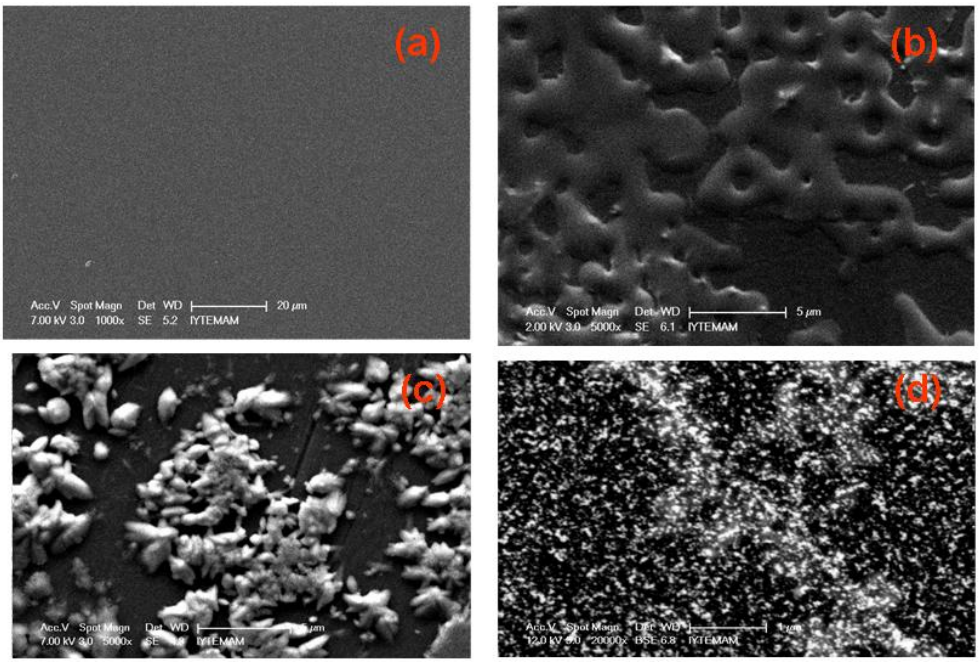

Figure 3.25 SEM images of a) bare GCE, b) PAP/GCE, c) Oxidized PAP/GCE d) Pt nano particles modified Ox-PAP/GCE.

Depending on all of AFM and SEM images it can be said that uniformly covered layer of Pt nano particles modified polymer film could be easily prepared with eletrodeposition technique described previously.

3.10 Electrochemical of behaviour of AA, EN and UA mixture at metal nano particles modified Ox-PAP/GCEs

Typical voltammetric response of bare GCE, Ox-PAP/GCE and Cu, Au and Pt nano particles modified Ox-PAP/GCEs in pH 7.40 phosphate buffer solution at the scan rate of 50 mV/s are shown in Figure 3.26. Metal nano particles modified GCEs were prepared as mentioned previously in experimental section 2.3.5.The electrocatalytic activity of all modified electrodes were used in the presence of AA, EN and UA mixture.

In Figure 3.26.a peak potential values obtained from Au-Ox-PAP/GCE were 104, 201 and 330 mV and current values 7, 6.5 and 3 µA for AA, EN and UA, respectively. At Cu-Ox-PAP/GCE the peak potential and oxidation current values were obtained for AA, EN and UA; 104, 201 and 331 mV and 8.8, 6.2 and 2.8 µA respectively. Also the results calculated for Pt-Ox-PAP/GCE the peak potential and oxidation current values were obtained for AA, EN and UA; 80, 201 and 338 mV and 9, 9.2 and 6.2 µA respectively. The results obtained for unmodified Ox-PAP/GCE was 110, 198 and 331 mV and 7.7, 5.9 and 1.7 µA for AA, EN and UA respectively.

When the catalytic activity of metal nano particles was compared to the results of AA, EN and UA, the maximum peak seperation and peak currents were found to be with Pt metal nano particles deposited Ox-PAP film modified GCE in pH 7.40 (Figure 3.26 c). However, higher current values also observed at Cu nano-particles modified Ox-PAP/GCE, the electrode signal was unstable due to the decreasing peak current with sequential current-potential scans (Figure 3.26 b). Voltammetric responce of Ox-PAP/GCE towards AA, EN and UA oxidation was decreased in the presence of Au nano particles modified Ox-PAP/GCE (Figure 3.26 b). Therefore Pt/MWCNT/GCE was prefered as working electrode for future studies

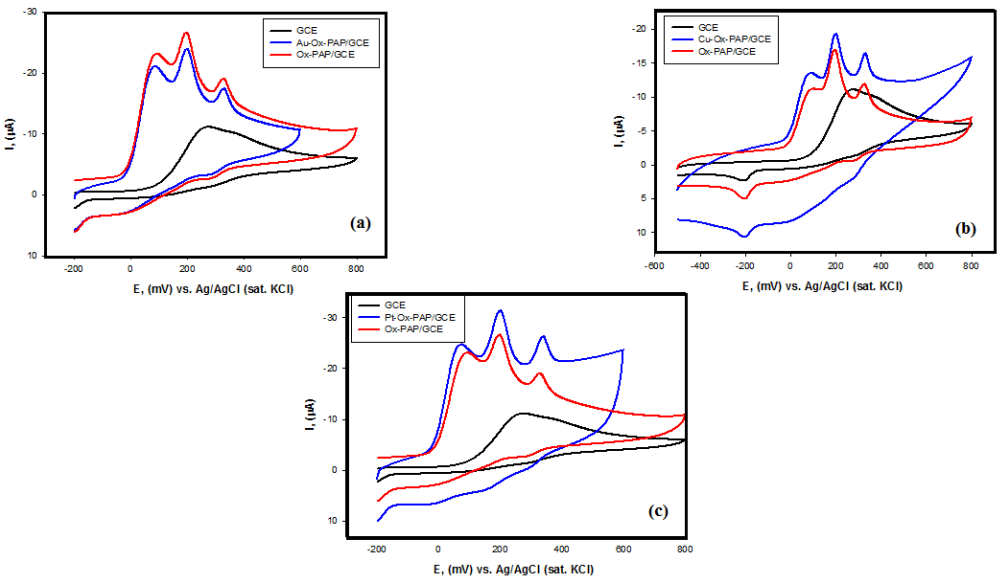

Figure 3.26 Cyclic Voltammetric behaviors of AA, EN, UA mixture at a) Au-Ox-PAP/GCE, b) Cu-Ox-PAP/GCE and c) Pt-Ox-PAP/GCE compared with bare and Ox-PAP/GCE

3.11 The Influence of Pt Nano Particles Amount on AA, EN and UA oxidation.

For the optimization of Pt deposition on the Ox-PAP/GCE surface, the cycle number effect on the simultaneous electrochemical oxidation of AA, EN and UA was also investigated. The amount and the size of the deposited Pt nano particles were controlled by changing the cycle number in electrodeposition process. It was clearly seen in Figure 3.27 that the peak potential of each analytes was not changed whereas the maximum peak current was obtained for AA, EN and UA at 15 consecutive scans deposition procedure of Pt nano particles modified -Ox-PAP/GCE.

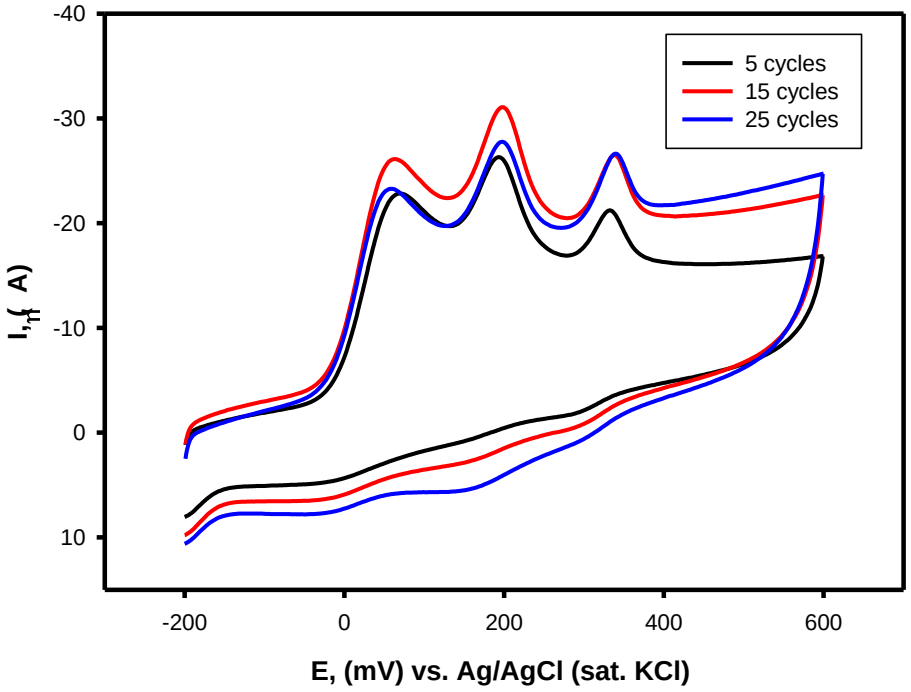

Figure 3.27 Effect of cycle number of Pt deposition on Ox-PAP/GCE on simultaneous oxidation of AA, EN and UA in concentrations of $5x10^{-4}$ M, 10^{-5} M, 10^{-4} M, respectively.

As a result, optimum conditions of experimental parameters was summarized at Table 3.2

Table 3.2 Optimum conditions of experimental parameters

Experimental parameter	Optimum Conditions
pH of supporting electrolyte	pH 7.40 PBS
p-Aminophenol concentration	5 mmol.L^{-1}
Cycle number of p-Aminophenol	20 cycles
NaOH concentration	0.1 mol.L^{-1}
Overoxidation time of polyaminophenol	300 second
Kind of metal nano-particles	Pt nano-particles
Cycle number of Pt nano-particles	15 cycles

3.12 Individual Electrocatalytic Oxidation of EN, AA and UA with GCE, Ox-PAP-GCE and Pt- Ox-PAP-GCE

Voltammetric studies were classification according to the electrodes used. The electrochemical behaviour of bare GCE, Ox-PAP-GCE and Pt- Ox-PAP-GCE in presence of electroactive species were investigated by cyclic voltammetry. Figure 3.28 demonstrates the cyclic voltammograms of $5x10^{-4}$ M AA, EN UA in pH 7.40 phosphate buffer solution (PBS) on bare GCE, Ox-PAP/GCE and nano- Pt Ox-PAP/GCE with a scan rate 50 mV/s.

An irreversible oxidation electrode reaction was obtained for AA at all electrodes. At the GC, Ox-PAP/GC and Pt- Ox-PAP/GC electrodes (Figure 3.28 a), the peak was broad at 100 mV, 50 mV and 40 mV respectively. A, 60 mV negative shift was at Pt-Ox-PAP/GCE compare to bare GCE while there was no desirable increasing observed in peak currents between Pt- Ox-

PAP/GCE and Ox-PAP/GCE. The results indicated that, Pt nano particles and overoxidized polimer film has an important role to accelerate the electron transfer kinetic and increased the electrocatalytic activity of the bare GCE towards the oxidation of AA.

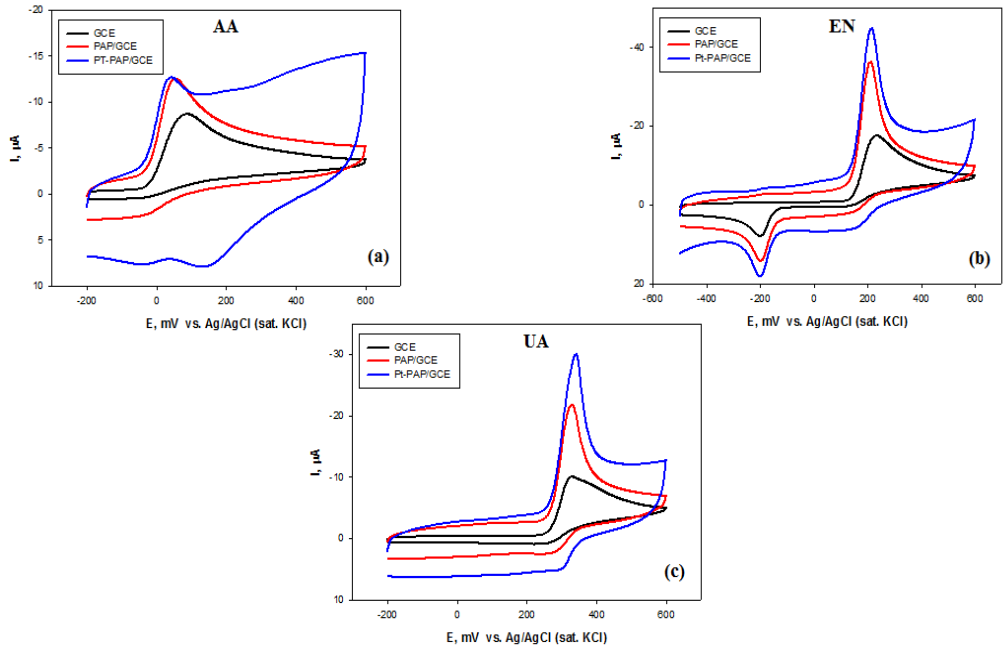

Figure 3.28 Comperative voltammograms for individual oxidatios of a) AA, b) EN and c) UA at bare, Ox-PAP and Pt- Ox-PAP electrodes all in concent. of 5x 10^{-4} M

Figure 3.28 b shows the cyclic voltammograms of EN at bare, Ox-PAP/GC and Pt- Ox-PAP/GC electrodes in pH 7.40. As can be seen at bare GCE, voltammetric behaviour of EN shows a quasi-reversible electrode reaction with a sluggish and small peaks response. The anodic and cathodic peak potentials were 232 mV and -200 mV respectively. The separation of redox peak potentials (ΔEp) was 432 mV, indicating a quasi-reversible electrode reaction. After coating with Ox-PAP and modified Pt nano particles, the anodic peak potential shifted negatively to 210 mV and the cathodic peak potential shifted positively to -198 mV for both electrodes In addition to these results substantial increases in the peak currents were also observed due to the positive synergistic catalytic effet of polymer and metal nano particles. 2.5 and 2 times higher peak current enhancement observed for Pt- Ox-PAP/GCE and Ox-PAP/GCE, respectively.

The electrocatalytic oxidation of UA was studied at bare, Pt- Ox-PAP/GCE and Ox-PAP/GCE (Figure 3.28 c). A poor quasi-reversible electrode reaction for UA observed at all electrode surfaces. The anodic peak was appeared at 350 mV at all 3 electrodes with a small cathodic peak at about 280 mV, showing that the electron transfer for reduction process was too sluggish.In addition that a well-defined sharp oxidation peak with obviously increased current response was obtained in both Ox-PAP/GCE and Pt- Ox-PAP/GCE compare with bare GCE, but the best catalytic activity was observed at Pt-Ox-PAP/GCE. The modifier plays important role to accelerate the electron transfer and increase the peak current.

The results were summarized at Table 3.3 for individual oxidations of AA, EN and UA at all three electrodes.

Table 3.3 The peak current and potential values of AA, EN and UA oxidation at different electrodes.

Analyte	Electrodes	i_{peak} (µA)	E_{peak} (mV)
AA	**Bare GCE**	9.04	100
	Ox-PAP/GCE	12.57	50
	Pt-Ox-PAP/GCE	11.51	40
EN	**Bare GCE**	16.8	232
	Ox-PAP/GCE	32.2	210
	Pt-Ox-PAP/GCE	39.4	210
UA	**Bare GCE**	9.70	357
	Ox-PAP/GCE	19.2	350
	Pt-Ox-PAP/GCE	25.7	350

3.13 Scan Rate Studies of AA, EN and UA at different electrodes

3.13.1 Scan Rate Studies of AA

In order to research bare and modified electrodes behaviour on the oxidation of AA, a series of cyclic voltammograms were recorded at varying potential scan rate (Figure 3.29).

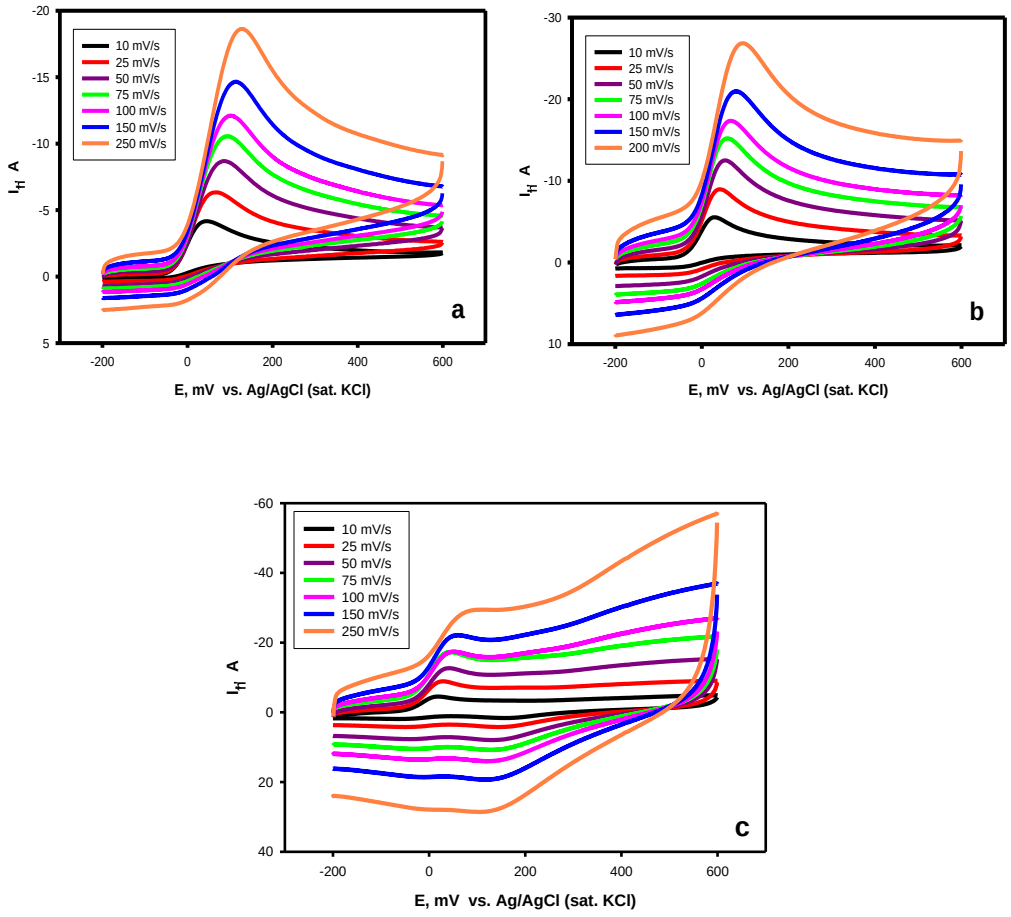

Figure 3.29 Cyclic voltammograms of AA oxidation at a) GCE, b) Ox-PAP/GCE, c) Pt-Ox-PAP/GCE with various scan rates (10-200 mV/s)

The oxidation peak current increased linearly with the square root of scan rate from 10 to 200 mV/s (Figure 3.30 a), suggesting that the process is similar to those controlled by diffusion at all electrodes. Figur 3.30 b shows that oxidation potential of AA was shifted to more positive values by the increasing of scan rate so this suggested that the oxidation of AA reaction was irreversible.

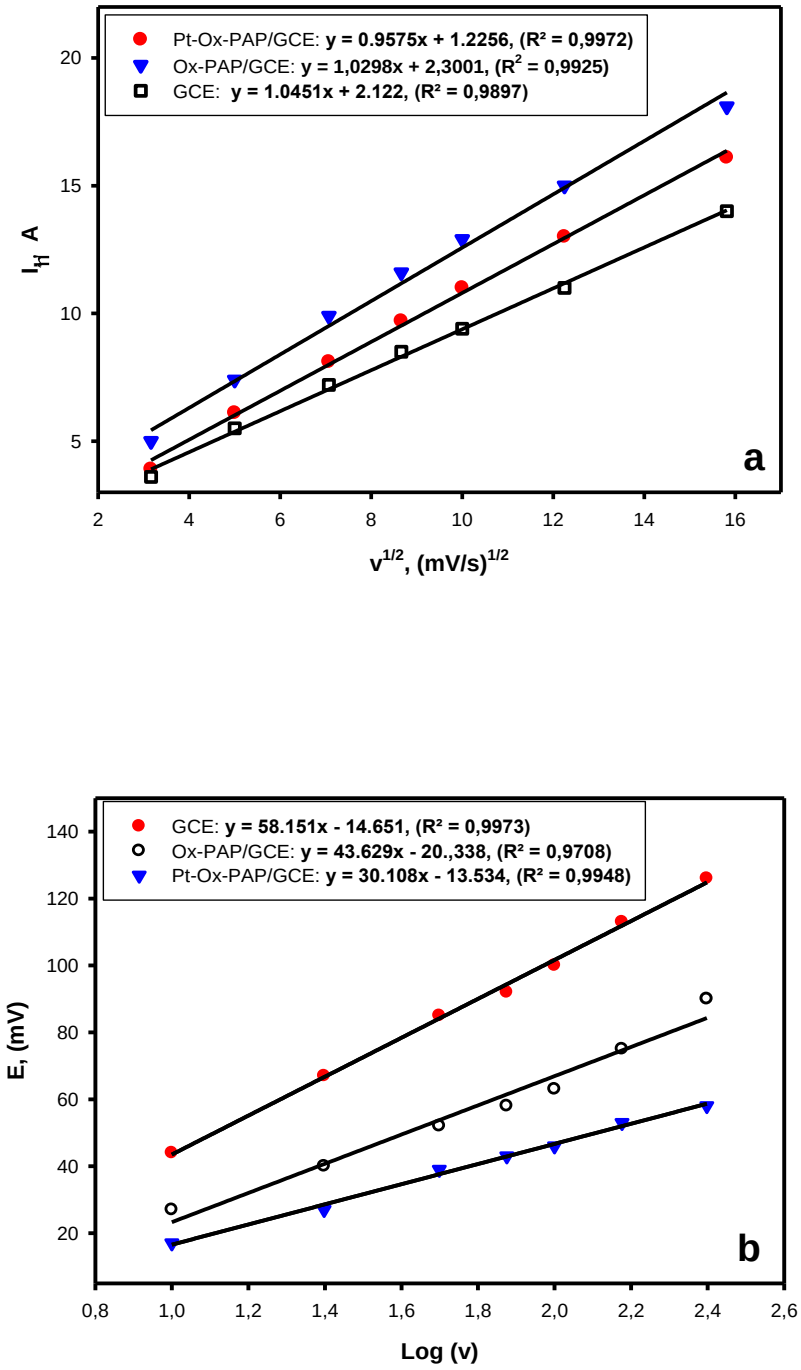

Figure 3.30 Dependence of scan rate on the a) peak current and b) peak potential of AA oxidation at bare GCE, Ox-PAP/GCE and Pt-Ox-PAP/GCE.

3.13.2 Scan Rate Studies of EN

In order to research electrode behaviour on the oxidation of EN, a series of cyclic volatmmograms were recorded at bare GCE, Ox-PAP/GCE and Pt-Ox-PAP/GCE by varying scan rate (Figure 3.31). The anodic and cathodic peak currents increased linearly with the square root of the scan rate (Figure 3.32 a), with correlation coefficients of 0.9969, 0.9992, 0.9992 for bare GCE, Ox-PAP/GCE and Pt-Ox-PAP/GCE, respectively. This indicates that the process is similar to those controlled by diffussion. The oxidation peak potential of EN shifted positive values with increasing the scan rate, indicating that the electron transfer was quasi-reversible (Figure 3.32 b).

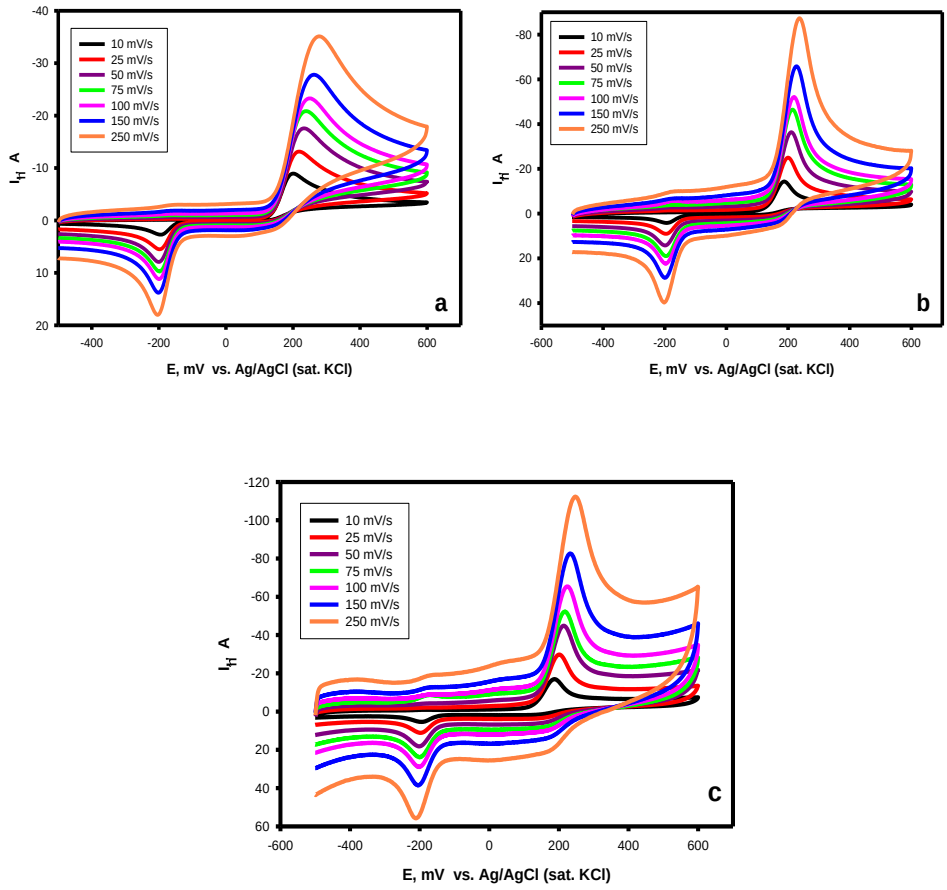

Figure 3.31 Cyclic voltammograms of EN oxidation at a) GCE, b) Ox-PAP/GCE, c) Pt- Ox-PAP/GCE with various scan rates (10-200 mV/s)

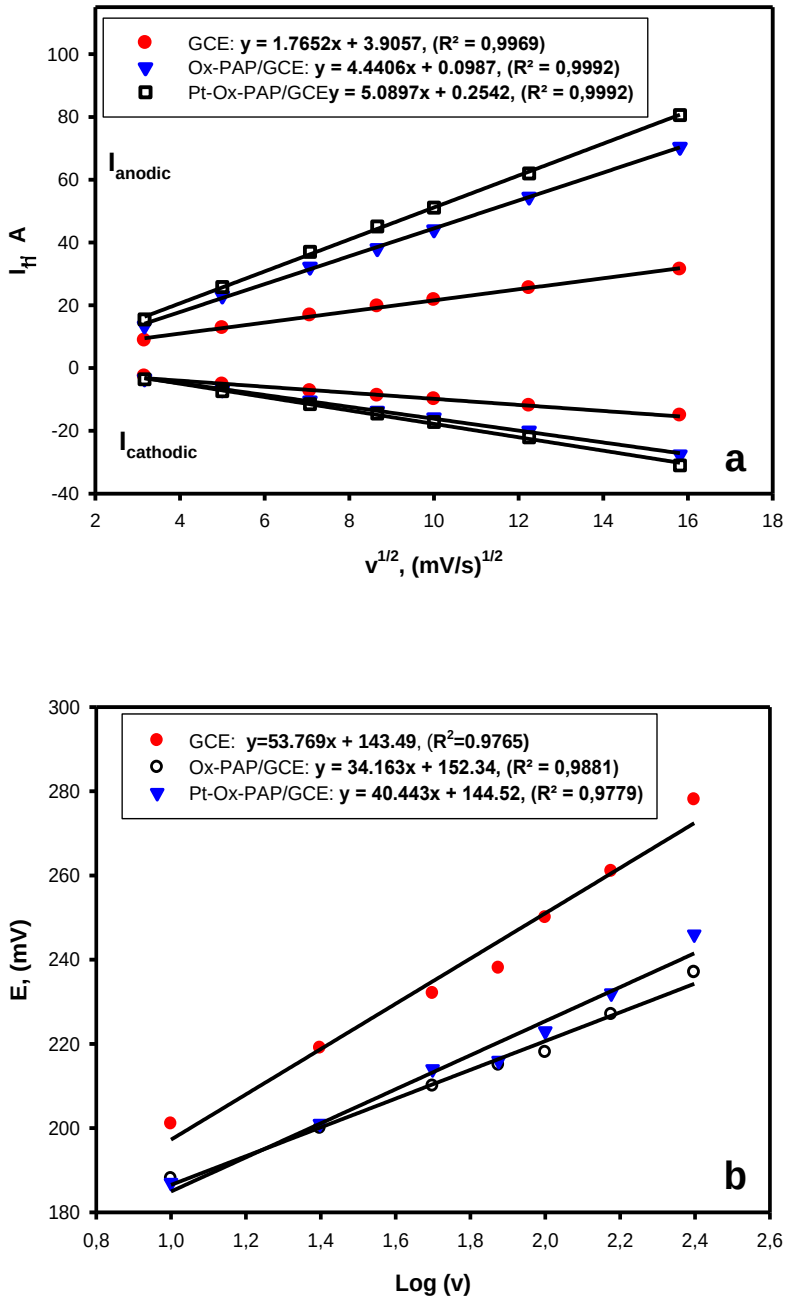

Figure 3.32 Dependence of scan rate on the a) peak current and b) peak potential of EN oxidation at bare GCE, Ox-PAP/GCE and Pt-Ox-PAP/GCE

3.13.3 Scan Rate Studies of UA

For identifying the electrode behaviour on the oxidation of UA, cyclic volatmmograms were recorded at different electrodes as mentioned above for AA and EN by varying potential scan rate (Figure 3.33, 34). The oxidation peak current increased linearly with the square root of scan rate from 10 to 200 mV/s suggesting that the process is similar to those controlled by diffussion. The oxidation peak potential of UA shifted positive values with increasing the scan rate, indicating that the electron transfer was quasi-reversible. A linear regression equation is ipa (μA) = 22.792 v (mV/s) + 302.29 (R^2 = 0.9826) for Ox-PAP/GCE (Figure 3.33 b).

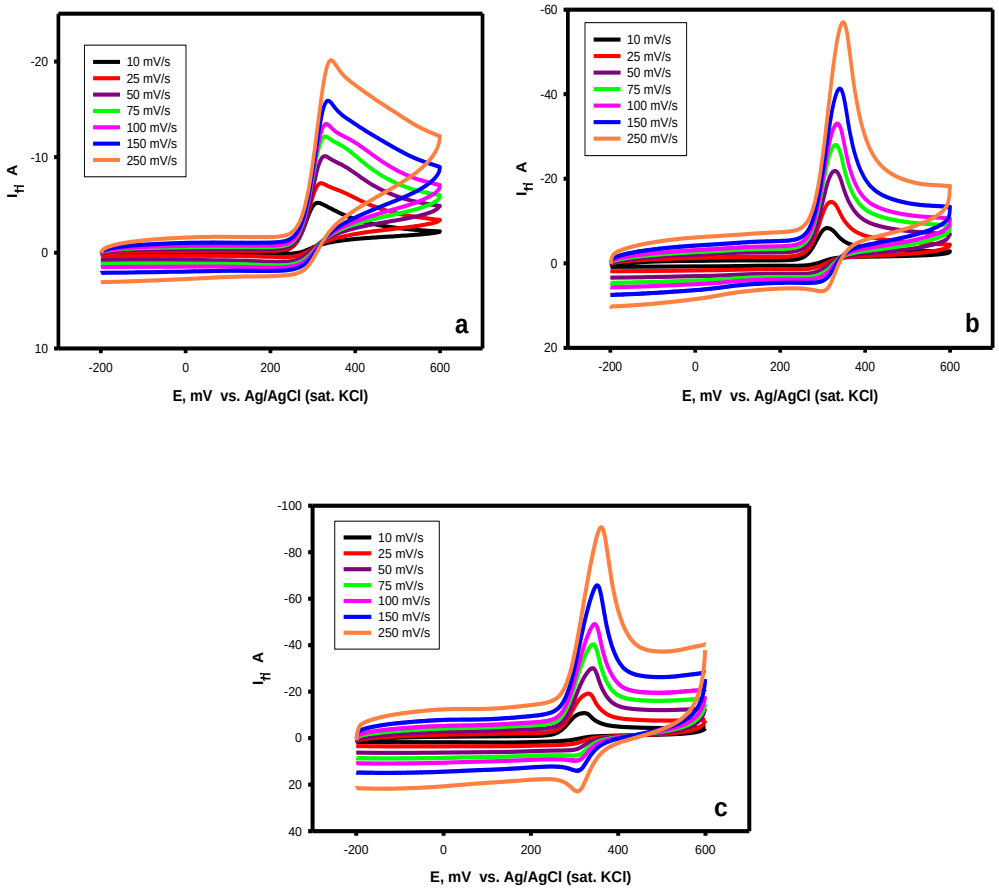

Figure 3.33 Cyclic voltammograms of UA oxidation at a) GCE, b) Ox-PAP/GCE, c) Pt- Ox-PAP/GCE with various scan rates (10-200 mV/s)

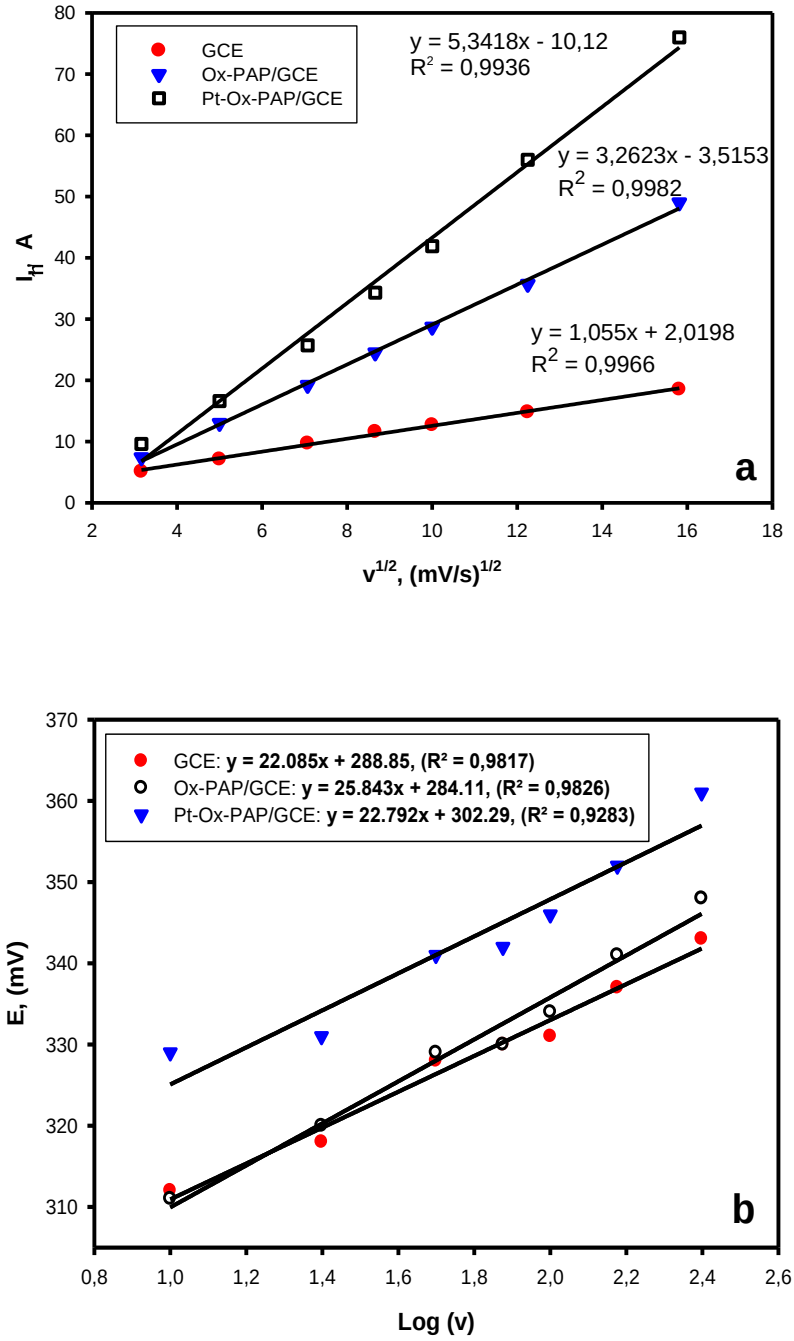

Figure 3.34 Dependence of scan rate on the a) peak current and b) peak potential of UA oxidation at bare GCE, Ox-PAP/GCE and Pt-Ox-PAP/GCE.

3.14 Differential pulse voltammetric determination of AA, EN and UA.

Simultaneous detectermination of EN, AA, and UA is a challenge of critical importance in the field of biomedical chemistry and neurochemistry. However, the simultaneous determination of AA, EN, and UA at conventional solid electrodes (carbon and metal) usually struggles because they undergo an overlapping oxidation potential and electrode fouling takes place due to the adsorption of oxidation products. Since differential pulse voltammetry has a much current sensitivity and better separation the analyte peaks than CV, the electroanalytical technique was used for individual and simultaneous determination of AA, EN and UA.

The main objective of the present study is to obtain a well separated oxidation peaks of AA, EN and UA by using Ox-PAP/GCE and Pt nano particles modified Ox-PAP/GCE in their mixture. Future parts of the study include the individually and simultaneously voltammetric determination of AA, EN and UA in pH 7.40 phosphate buffer solution.

Limit of detection values were calculated from (S/N:3) and calibration curves. The average value of backgroud current estimated from 10 different voltammograms. LOQs and LOLs were calculated for estimation of linear ranges values of all electrodes.

Initial studies with DPV was focused on the electrochemical respons of increasing AA concentrations at bare GCE, Ox-PAP/GCE and Pt-Ox-PAP/GCE in pH 7.40 PBS. Each electrode responses were given in Figure 3.35, Figure 3.36, Figure 3.37. In DPV, a sharp oxidation peak appeared at 210mV, 40mV and 20 mV at at bare GCE, Ox-PAP/GCE and Pt-Ox-PAP/GCE respectively. The oxidation of AA was observed at different potential depending on electrode. The electrochemical respons of AA was increased linearly with the increase of AA concentration in the range of 7x 10^{-6} M – 2x10^{-3} M at bare GCE, 8.1x 10^{-6}– 3x10^{-3} M at Ox-PAP/GCE and 1.8x 10^{-6} – 1x10^{-3} M at Pt-Ox-PAP/GCE. The linear regression equations of bare GCE, Ox-PAP/GCE and Pt-Ox-PAP/GCE could be expressed as R^2=0.9992, R^2=0.9942, R^2=0.9955, respectively.

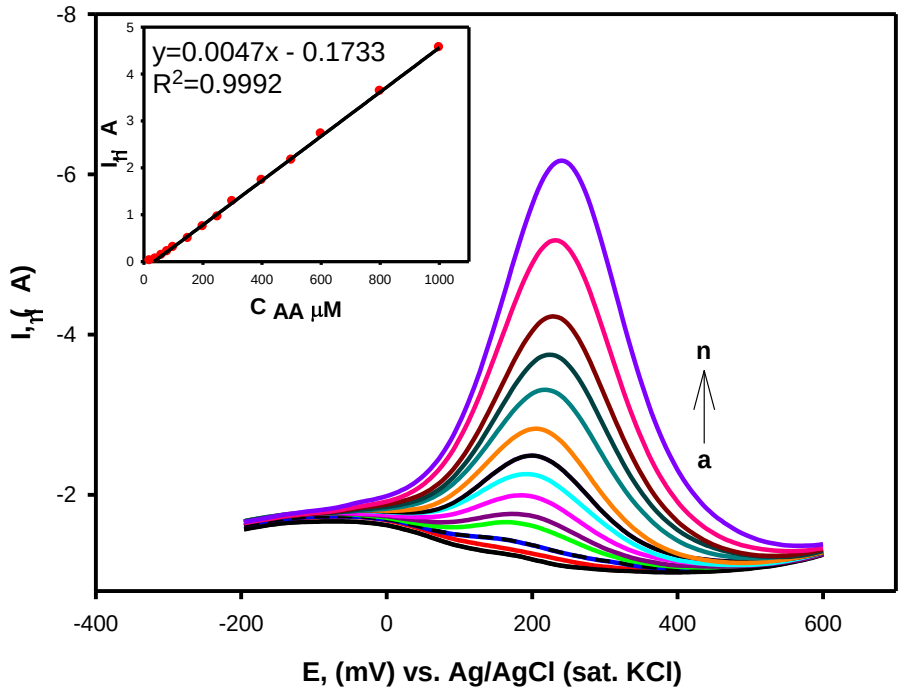

Figure 3.35 Differential pulse voltammograms at GCE for increasing concanterations of AA in 0.1 M pH 7.40 PBS with scan rate 10 mV/s and pulse amplitude 50 mV.(Inset: Corresponding calibration curve of increasing AA concentrations). AA concentrations (a-n) 0 M, 2x10^{-5} M, 8x10^{-5}M, 1x10^{-4}M, 1.5x10^{-4}M, 2.0x10^{-4} M, 2.5x10^{-4} M, 3.0x10^{-4} M, 3.5x10^{-4}M, 4.0x10^{-4}M, 5x10^{-4} M, 6x10^{-4}M, 8 x10^{-4}, 1 x10^{-3} M.

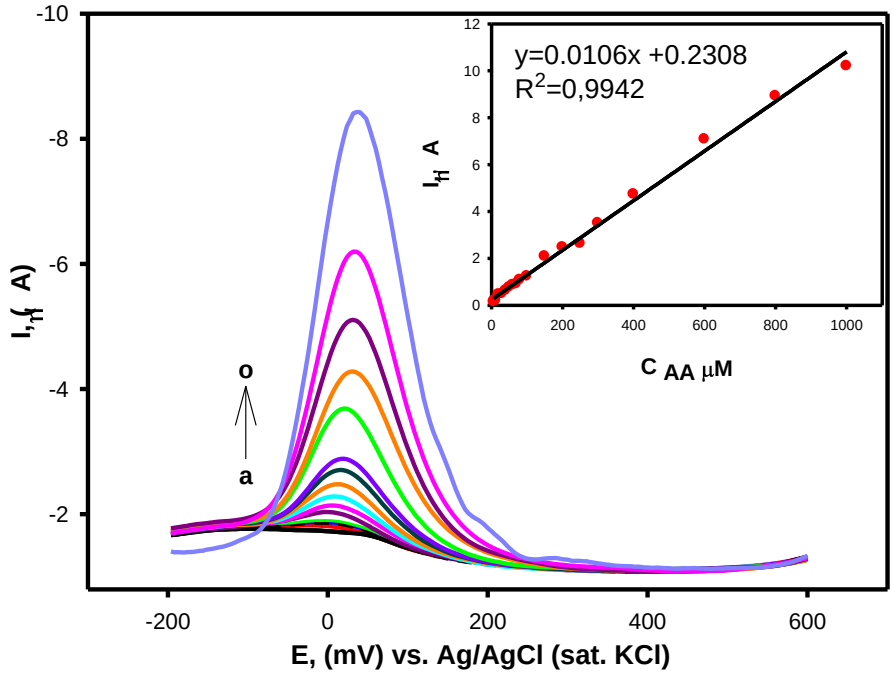

Figure 3.36 Differential pulse voltammograms at Ox-PAP/GCE for increasing concanterations of AA in 0.1 M pH 7.40 PBS with scan rate 10 mV/s and pulse amplitude 50 mV.(Inset: Corresponding calibration curve of increasing AA concentrations). AA concentrations (a-0) 0 M, $2x10^{-5}$ M, $4x10^{-5}$M, $6x10^{-5}$M, $7x10^{-5}$M, $8x10^{-5}$ M, $1x10^{-4}$ M, $1.5x10^{-4}$ M, $2x10^{-4}$M, $2.5x10^{-4}$M, $3x10^{-4}$ M, $4x10^{-4}$M, $6 x10^{-4}$, $8x10^{-4}$, $1 x10^{-3}$ M.

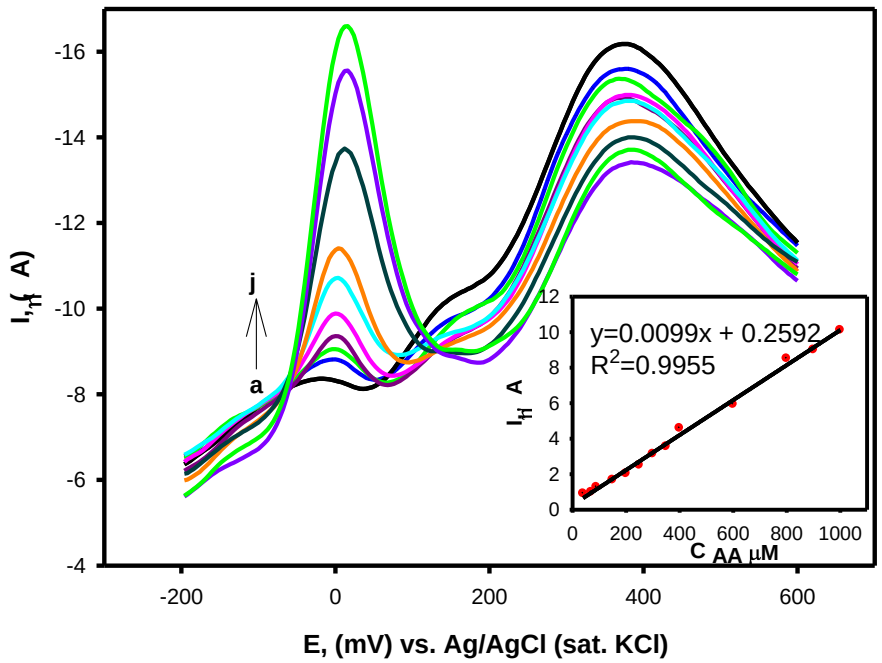

Figure 3.37 Differential pulse voltammograms at Pt-Ox-PAP/GCE for increasing concanterations of AA in 0.1 M pH 7.40 PBS with scan rate 10 mV/s and pulse amplitude 50 mV.(Inset: Corresponding calibration curve of increasing AA concentrations). AA concentrations (a-j) 0 M, $4x10^{-5}$M, $7x10^{-5}$ M, $9x10^{-5}$ M, 2 $x10^{-4}$M, $3x10^{-4}$ M, $4x10^{-4}$M, 6 $x10^{-4}$, $8x10^{-4}$, 1 $x10^{-3}$ M.

Figure 3.38 shows the calibration curves for AA oxidaiton at bare, Ox-PAP/GCE and Pt-Ox-PAP/GCE for the same concentation ranges between 2 $x10^{-5}$- 10^{-3} M . The oxidized polymer modified electrode provide the best catalytic activity towards AA oxidation with a maximum slope value so this was suggested that more sensitive results obtained at Ox-PAP/GCE compared with other electrodes due to this characteristic. From the DPV studies results, limit of detection values were calculated as $8x10^{-6}$ M (S/N=3) and $1.8x10^{-5}$ M (S/N=3) for Ox-PAP/GCE and Pt-Ox-PAP/GCE, respectively. Pt nano particles was also improved the catalytic activit of both bare and polymer film electrodes toward the oxidation potential of AA. The oxidation peak potential was shifted about 250 mV to negative potentials with Pt nano particles modification compare with bare GCE due to the faster electron transfer kinetics during the electrode reaction.

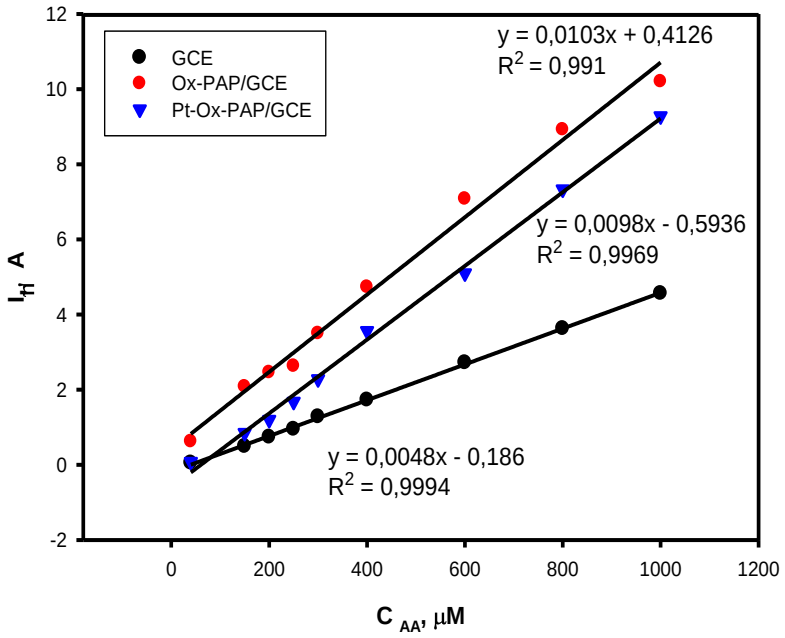

Figure 3.38 Calibration curves for AA oxidation at bare, Ox-PAP/GCE and Pt-Ox-PAP/GCE for the same concentration ranges between 8 $x10^{-5}$- 10^{-3} M

A comparative DPV behaviour of EN was investigated depending on increasing EN concentration at bare GCE, Ox-PAP/GCE and Pt-Ox-PAP/GCE, and the oxidation current changing was shown in Fig 3.39, Fig 3.40 and Fig 3.41 respectively. However a broad oxidation peak appeared at 250 mV at bare GCE, but a well-defined oxidation peak was obtained at 180 mV with both modified electrodes which can be attributed the catalytic activity of polymer and Pt nano particles. The current respons with concentration of EN was found to be linear in the range of $7x10^{-6}$ M – $2.2x10^{-4}$ M bare GCE, $7.8x10^{-9}$ – $8x10^{-5}$M at Ox-PAP/GCE and 4x 10^{-7} – $1.5x10^{-4}$M at Pt nano particles modified Ox-PAP/GCE with correlation coefficients of 0.9916, 0.9907 and 0.9932, respectively.

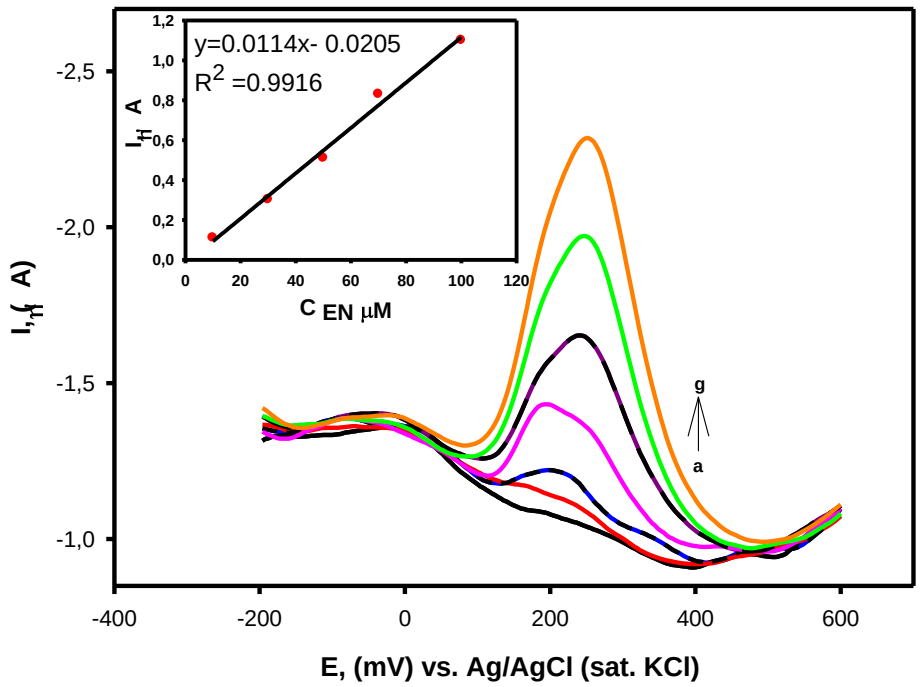

Figure 3.39 Differential pulse voltammograms at GCE for increasing concanterations of EN in 0.1 M pH 7.40 PBS with scan rate 10 mV/s and pulse amplitude 50 mV.(Inset: Corresponding calibration curve of increasing EN concentrations). EN concentrations (a-g) 0 M, $1x10^{-5}$M, $2x10^{-5}$M, $3.0x10^{-5}$M, $5x10^{-5}$ M, $7x10^{-5}$M, $1 x10^{-4}$ M.

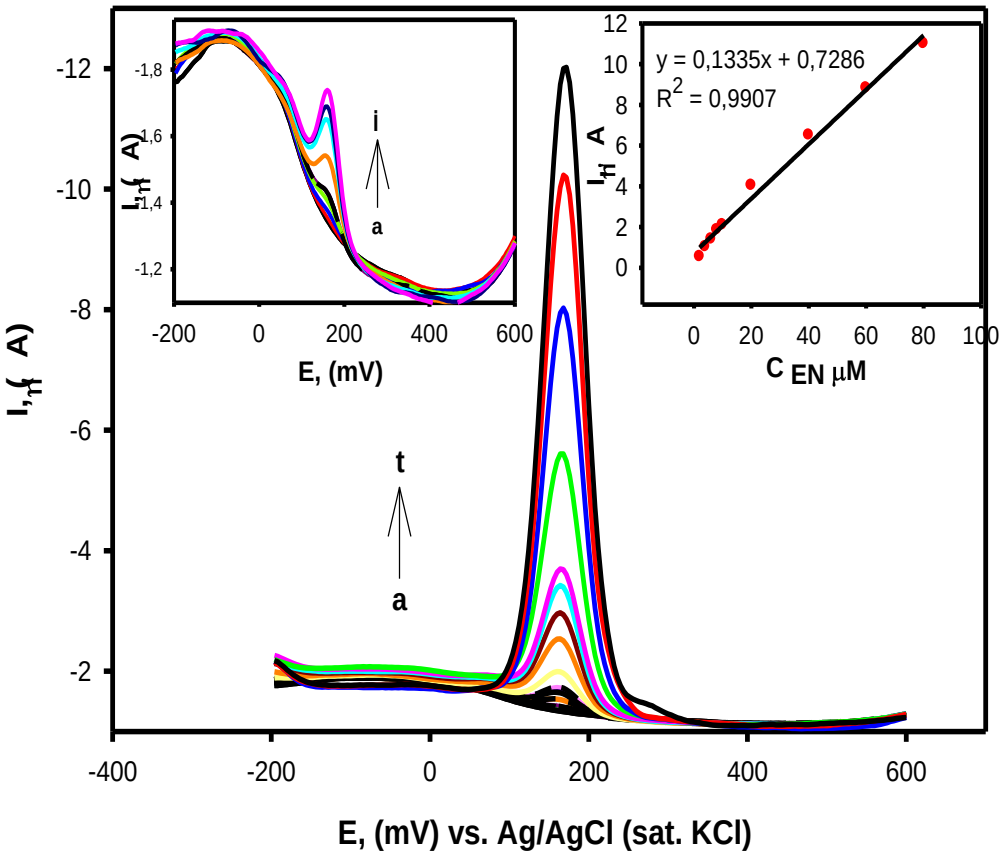

Figure 3.40 Differential pulse voltammograms at Ox-PAP/GCE in the presence of increasing concentration of Epinephrine 0.1 M pH 7.40 PBS with scan rate 10 mV/s, (a) 0 (b) $1.0x10^{-8}$, (c) $4.0x10^{-8}$, (d) $8.0x10^{-8}$, (e) $1.2x10^{-7}$, (f) $2.0x10^{-7}$, (g) $4.0x10^{-7}$, (h) $6.0x10^{-7}$, (i) $8.0x10^{-7}$, (j) $1.0x10^{-6}$, (k) $2.0x10^{-6}$, (l) $4.0x10^{-6}$, (m) $6.0x10^{-6}$, (n) $8.0x10^{-6}$, (o) $1.0x10^{-5}$, (p) $2.0x10^{-5}$, (r) $4.0x10^{-5}$, (s) $6.0x10^{-5}$, (t) $8.0x10^{-5}$ M

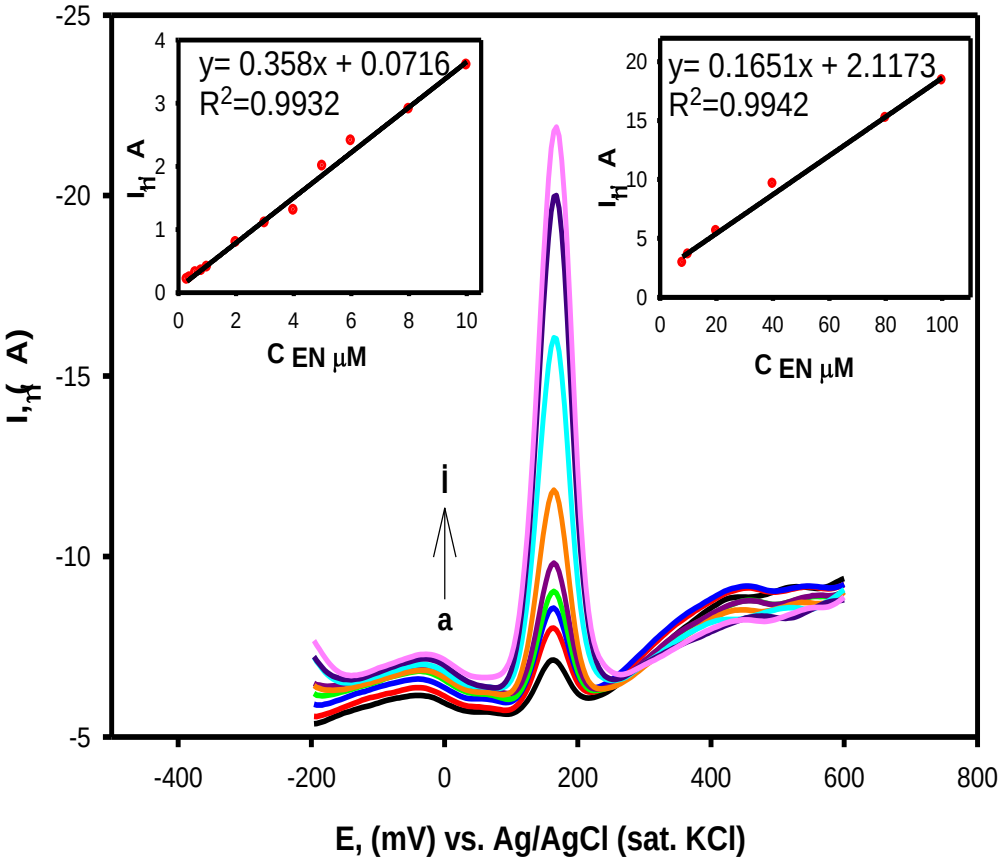

Figure 3.41 Differential pulse voltammograms at Pt-Ox-PAP/GCE for increasing concanterations of EN in 0.1 M pH 7.40 PBS with scan rate 10 mV/s and pulse amplitude 50 mV.(Inset: Corresponding calibration curve of increasing EN concenrations.) EN concentrations (a-i) $4x10^{-6}$M, $5x10^{-6}$ M, $6x10^{-6}$ M, $8x10^{-6}$M, $1x10^{-5}$, $2x10^{-5}$ M, $4x10^{-5}$M, 6 $x10^{-5}$ M, $8x10^{-5}$M, 1 $x10^{-4}$ M.

Figure 3.42 shows the calibration curves for EN oxidation at bare, Ox-PAP/GCE and Pt-Ox-PAP/GCE for the same concentation ranges between 8 $x10^{-6}$- 10^{-4} M . The Pt nano particles modified Ox-PAP/GC electrode provide the best catalytic activity towards EN oxidation with a maximum slope value. From the DPV studies results, limit of detection values were calculated as $6.5x10^{-9}$M (S/N=3) and $1.8x10^{-7}$ M for Ox-PAP/GCE and Pt-Ox-PAP/GCE, respectively. More sensitive results obtained from Ox-PAP/GCE compared to the Pt-Ox-PAP/GCE because Pt has a characteristic wide peak on oxidized polimer film electrode in 0.1 M PBS that was increase the background current

of Pt-Ox-PAP/GCE. This characteristic peak overlapped with EN oxidation potential that explains the less sensitivity of Pt-Ox-PAP/GCE.

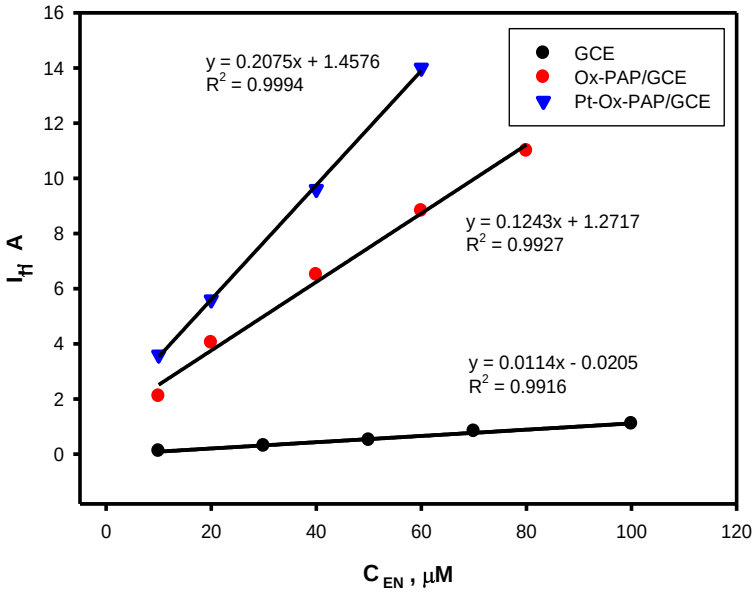

Figure 3.42 Calibration curves for EN oxidation at bare, Ox-PAP/GCE and Pt-Ox-PAP/GCE for the same concentration ranges between 8 $x10^{-6}$- 10^{-4} M

The DPV curves of UA with increasing concentration at bare GCE, Ox-PAP/GCE and Pt-Ox-PAP/GCEs were studied in pH 7.40 PBS solution and corresponding results were shown in Figure 3.43, Figure 3.44, Figure 3.45. However a broad oxidation peak appeared at 240 mV at bare GCE, well-defined sharp oxidation peaks were obtained at nearly same potentials with both modified electrodes which can be attributed the catalytic activity of polymer and Pt nano particles.The oxidation peak current was increased linearly with the increasing of UA concentration in the range of 4 x 10^{-6} M – $1x10^{-4}$ M at bare, $9.8x10^{-8}$ – $6x10^{-5}$M at Ox-PAP/GCE and 2.4x 10^{-6} – $1.5x10^{-4}$ M at Pt nano particles modified Ox-PAP/GCE with correlation coefficient of 0.9992, 0.9926, 0.9903, respectively.

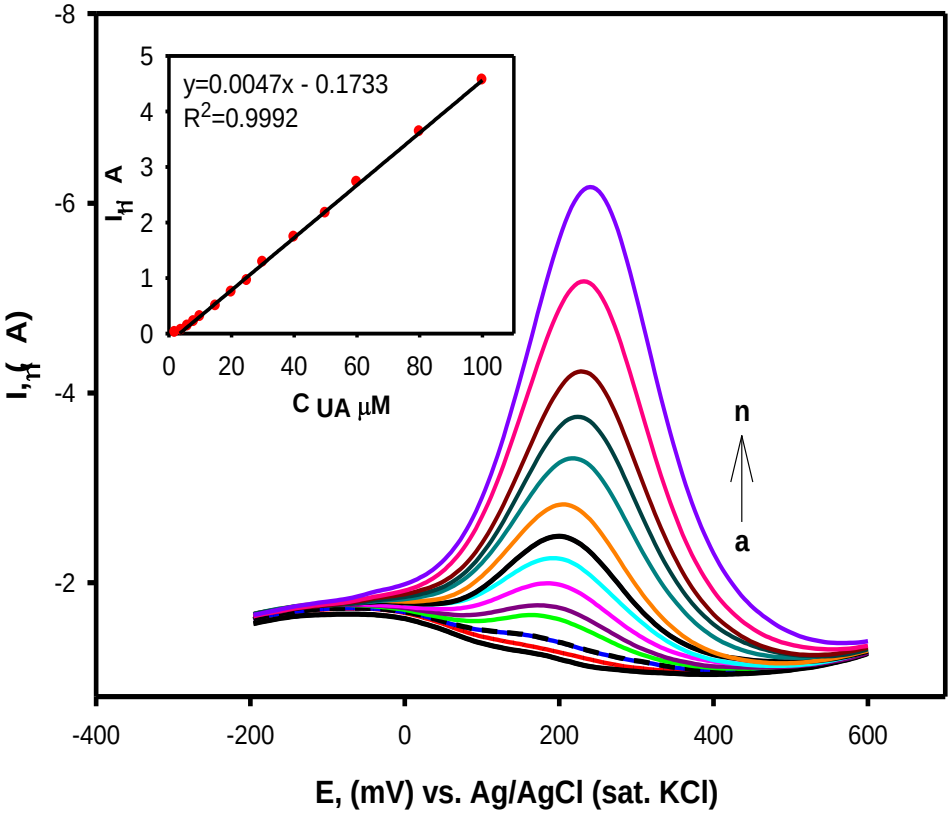

Figure 3.43 Differential pulse voltammograms at GCE for increasing concanterations of UA in 0.1 M pH 7.40 PBS with scan rate 10 mV/s and pulse amplitude 50 mV.(Inset: Corresponding calibration curve of increasing UA concentrations). UA concentrations (a-n) 0 M, $4x10^{-6}$M, $6x10^{-6}$M, $7x10^{-6}$M, $8.0x10^{-6}$M, $1x10^{-5}$ M, $2x10^{-5}$M, $4x10^{-5}$ M, $6x10^{-5}$M, $8x10^{-5}$M, $1.0x10^{-4}$M, $5x10^{-5}$ M, $7x10^{-5}$M, 1 $x10^{-4}$ M UA.

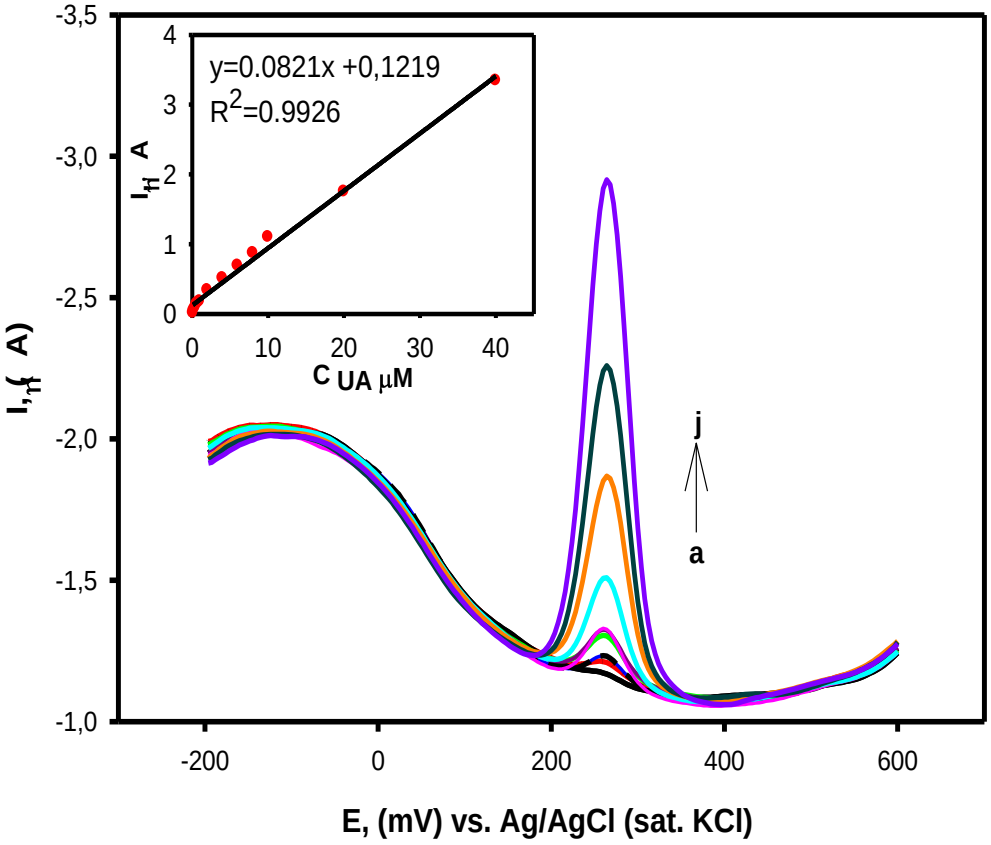

Figure 3.44 Differential pulse voltammograms at Ox-PAP/GCE in the presence of increasing concentration of Uric Acid in 0.1 M pH 7.40 PBS with scan rate 10 mV/s, (a) 0 (b) $1.0x10^{-7}$, (c) $2.0x10^{-7}$, (d) $4.0x10^{-7}$, (e) $6.0x10^{-7}$, (f) $8.0x10^{-7}$, (g) $1.0x10^{-6}$, (h) $2.0x10^{-6}$, (i) $4.0x10^{-6}$, (j) $8.0x10^{-6}$, (k) $1.0x10^{-5}$, (m) $2.0x10^{-5}$, (n) $4.0x10^{-5}$ M. (Inset: Corresponding calibration curve of increasing UA concentrations).

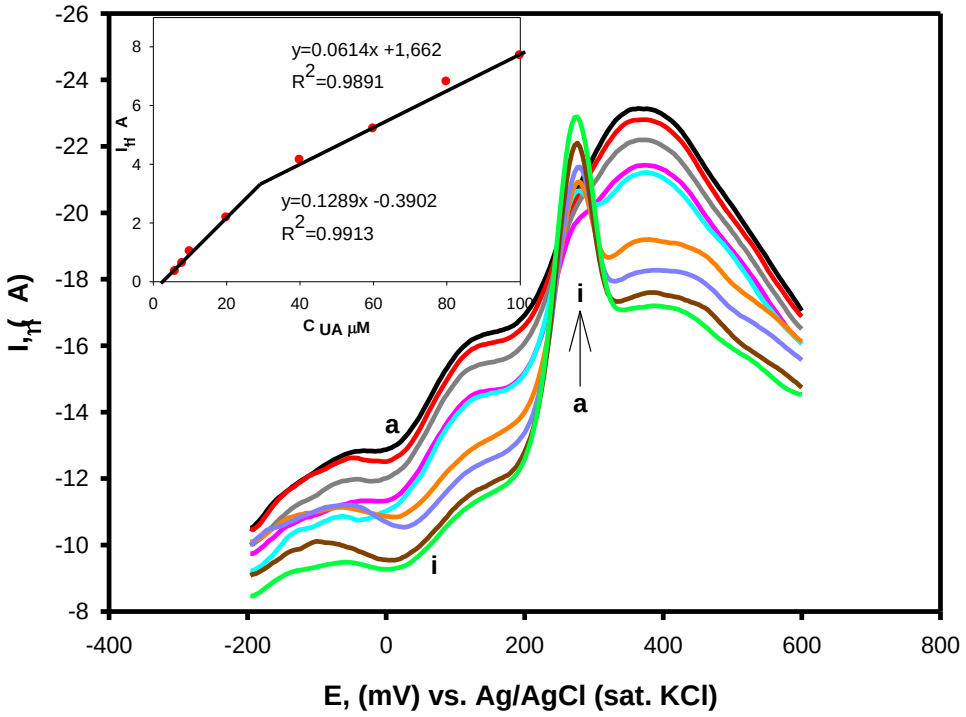

Figure 3.45 Differential pulse voltammograms at Pt-Ox-PAP/GCE for increasing concanterations of UA in 0.1 M pH 7.40 PBS with scan rate 10 mV/s and pulse amplitude 50 mV.(Inset: Corresponding calibration curve of increasing UA concenrations.) UA concentrations (a-i) $4x10^{-6}$M, $6x10^{-6}$ M, $8x10^{-6}$ M, $1x10^{-5}$, $2x10^{-5}$ M, $4x10^{-5}$M, 6 $x10^{-5}$ M, $8x10^{-5}$M, 1 $x10^{-4}$ M.

Figure 3.46 shows the calibration curves for UA oxidation at bare, Ox-PAP/GCE and Pt-Ox-PAP/GCE for the same concentation ranges between 4 $x10^{-6}$- $1x10^{-4}$ M. The Pt nano particles modified Ox-PAP/GC electrode provide the best catalytic activity towards UA oxidation with a maximum slope value compared to the other electrodes. From the DPV studies results, limit of detection values were calculated as $6.4x10^{-8}$ M and $2.2x10^{-6}$M for Ox-PAP/GCE and Pt-Ox-PAP/GCE, respectively. More sensitive results obtained from Ox-PAP/GCE with the same reason as mentioned above for EN.

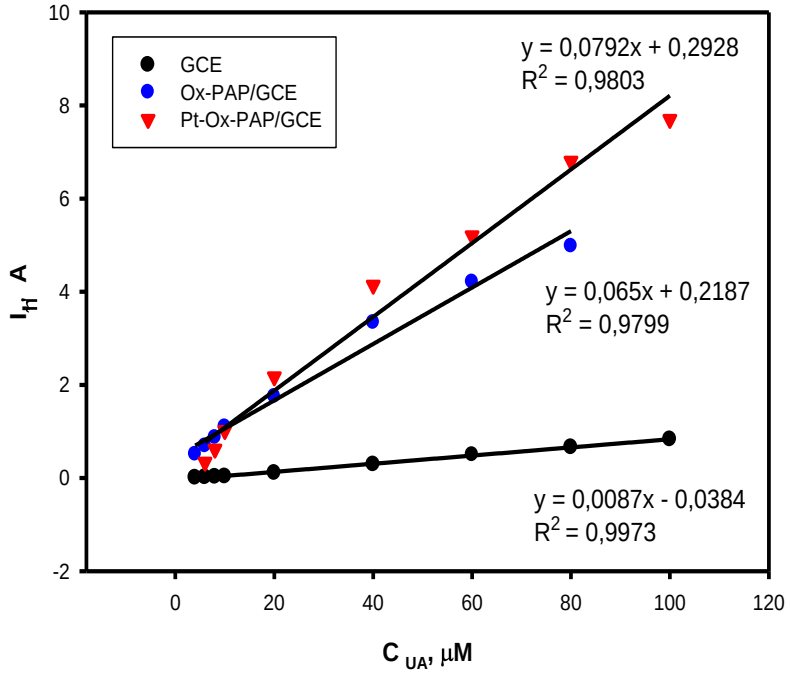

Figure 3.46 Calibration curves for UA oxidation at bare, Ox-PAP/GCE and Pt-Ox-PAP/GCE for the same concentration ranges between 4 $x10^{-6}$- 10^{-4} M

3.15 Simultaneous Voltammetric Determination of AA, EN and UA by Differential pulse voltammetry.

It is well known that the oxidation potential of AA, EN and UA are too close at conventional electrodes due to the homogeneous electron transfer in the results of their sluggish electron kinetics. The above CV results show that, the oxidation peaks of AA, EN and UA in their mixture could be easily separated by using both Ox-PAP/GCE and Pt nano particles modified Ox-PAP/GC electrodes. The comparison of differential pulse voltammetry with cyclic voltammetry, DPV generally shows a much current sensitivity and better separation to the analytes response than CV in the simultaneous determination of AA, EN and UA.

Figure 3.47 and Figure 3.48 exhibits DP voltammograms obtained for only AA concentration varying, while the concentration of EN and UA was kept constant as $2x10^{-5}$ M at Ox-PAP/GCE and Pt-Ox-PAP/GCEs, respectively in phosphate buffer solution. In addition that, well resolved oxidation peaks for all compounds can be seen at -10 mV for AA, 108 mV for EN and 249 mV for UA at Ox-PAP/GCE and -20 mV for AA, 116 mV for EN and 252 mV for UA

at Pt-Ox-PAP/GCE (Figure 3.48). The separation between the three peak potentials with a value of ~120-150 mV were suitable for enabling determination of AA, in the presence of UA and EN while only 60 mV peak seperation was large enough for DPV studies. As shown in Figures, the electrochemical respons of AA increased linearly with increasing of AA concentration. The varying of AA concentration did not have significant influence the peak potential and peak current of EN and UA.

The dependence of peak current on the concentration of AA was a linear relationship in the range of $9.8x10^{-6}$ M – $1x10^{-3}$ M for Ox-PAP/GCE and $6.1x10^{-5}$ – $1.2x10^{-3}$M for Pt-Ox-PAP/GCE. The linear regression equation of AA can be expressed as y= 0.0043x+ 0.1531 R^2=0.9925 for Ox-PAP/GCE and y= 0.0058x + 0.33, R^2=0.9947 for Pt-Ox-PAP/GCE. The detection limit values $9.5x10^{-6}$ and $5x10^{-5}$M for Ox-PAP/GCE and Pt-Ox-PAP/GCE,respectively.

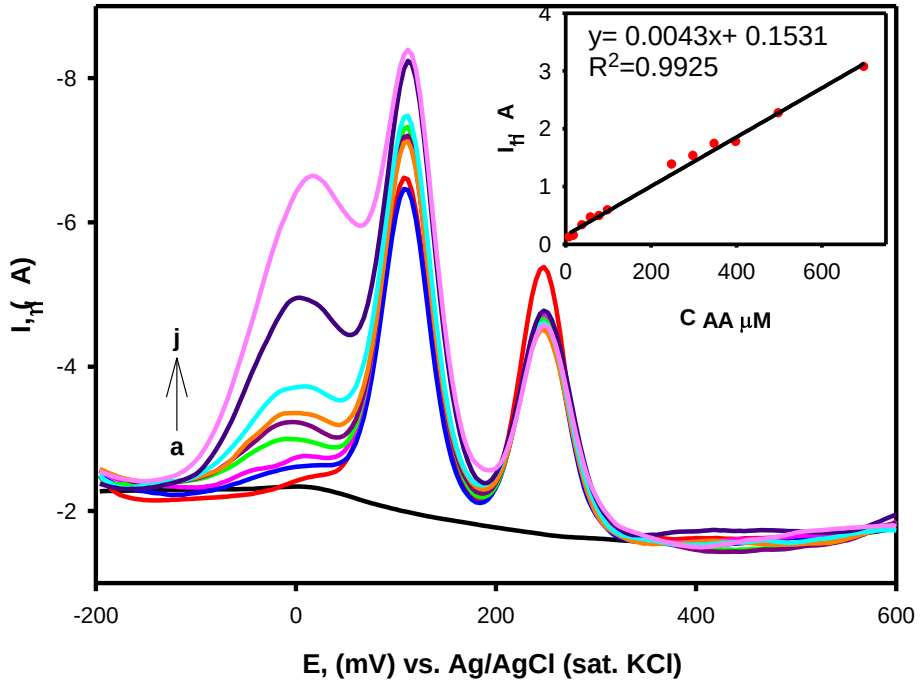

Figure 3.47 Differential pulse voltammograms at Ox-PAP/GCE in the presence of EN ($2x10^{-5}$ M) and UA ($2x10^{-5}$ M) for increasing concanterations of AA in 0.1 M pH 7.40 PBS with scan rate 10 mV/s and pulse amplitude 50 mV.(Inset: Corresponding calibration curve of increasing AA concenrations). (a) 0 M AA, EN, UA, (b-j) $1x10^{-5}$M, $2x10^{-5}$ M, $4x10^{-5}$ M, $6x10^{-5}$, $8x10^{-5}$ M, $1x10^{-4}$M, 2.2 $x10^{-4}$ M, $4x10^{-4}$ M, $7x10^{-4}$ M AA.

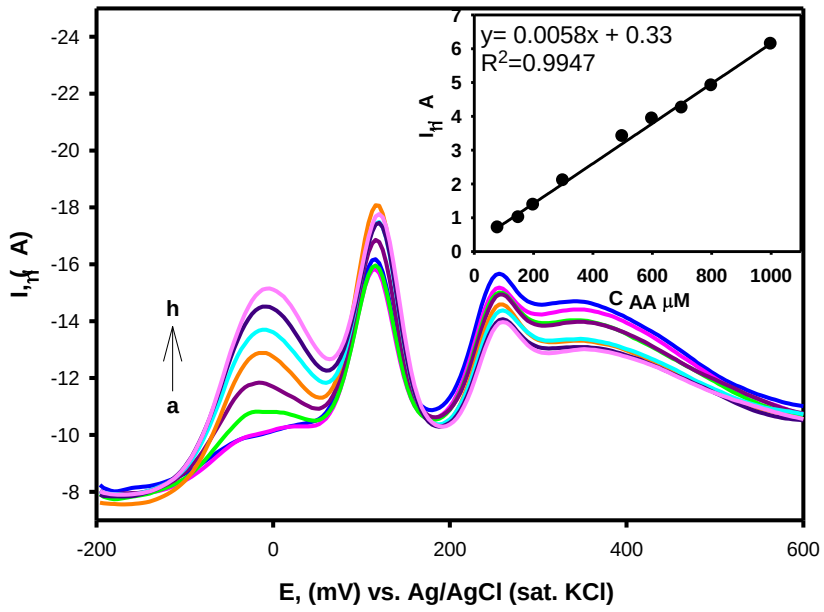

Figure 3.48 Differential pulse voltammograms at Pt-Ox-PAP/GCE in the presence of EN ($2x10^{-5}$ M) and UA ($2x10^{-5}$ M) for increasing concanterations of AA in 0.1 M pH 7.40 PBS with scan rate 10 mV/s and pulse amplitude 50 mV. (Inset: Corresponding calibration curve of increasing AA concenrations). AA, EN, UA: (a-h) $8x10^{-5}$M, $1x10^{-4}$ M, $2x10^{-4}$ M, $3x10^{-5}$ M, $5x10^{-5}$ M, $6x10^{-5}$ M, $7x10^{-5}$ M, $1x10^{-3}$ M.

Figure 3.49 and Figure 3.50 shows the DP voltammograms that were recorded for increasing concentration of EN in the presence of $5x10^{-4}$ M AA and $5x10^{-5}$ M UA at Ox-PAP/GCE and Pt-Ox-PAP/GCEs. The oxidative peak current increased linearly with the concentration of EN in the range of $1.3x10^{-7}$ M – $1x10^{-5}$M for Ox-PAP/GCE and $4.3x10^{-7}$ – $3x10^{-5}$M for Pt-Ox-PAP/GCE. The linear regression equation of EN can be expressed as y = 0,2793x + 0,0153, R^2 = 0,9928 for Ox-PAP/GCE and y= 0.5142x + 0.0042, R^2=0.9908y= 0.0058x + 0.33, R^2=0.9947 for Pt-Ox-PAP/GCE.

The detection limit values $9x10^{-8}$ and $3.6x10^{-7}$ M for Ox-PAP/GCE and Pt-Ox-PAP/GCE, respectively which were calculated from calibration curve in insets of Figure 3.49-50. The peak currents of especially AA were decreased due to the increasing concentration of EN. At Pt-Ox-PAP/GCE AA current decrease value was less obtained from Ox-PAP/GCE.

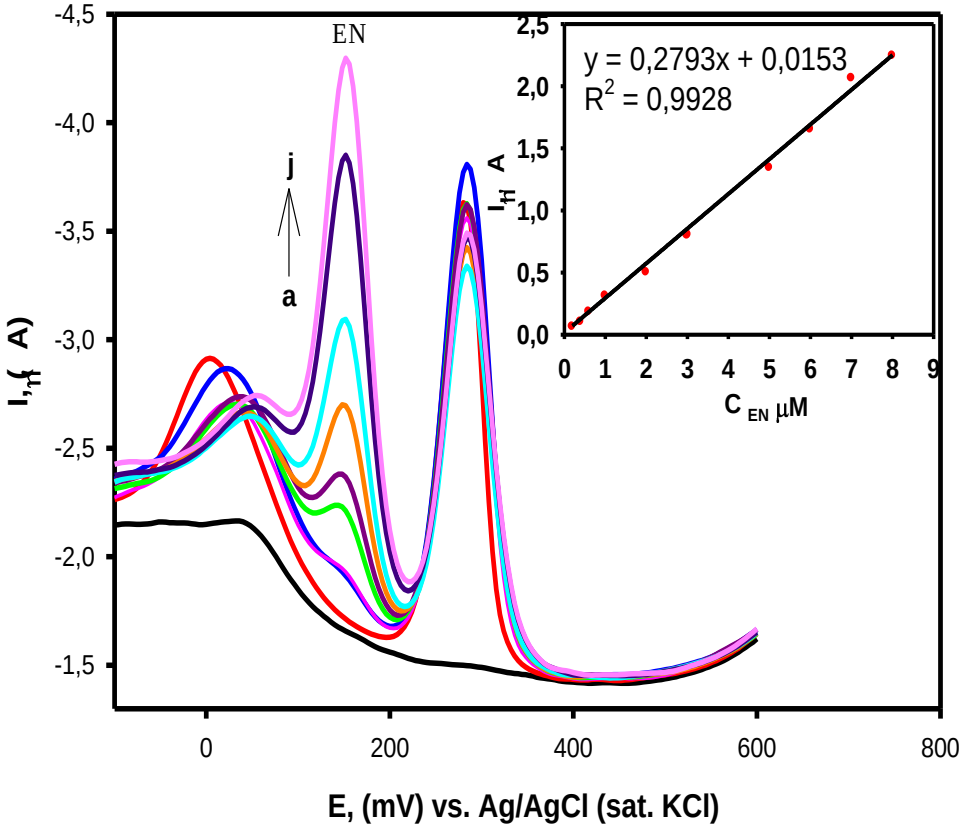

Figure 3.49 Differential pulse voltammograms at Ox-PAP/GCE in the presence of AA ($5x10^{-4}$ M) and UA ($5x10^{-5}$ M) for increasing concanterations of EN in 0.1 M pH 7.40 PBS with scan rate 10 mV/s and pulse amplitude 50 mV.(Inset: Corresponding calibration curve of increasing EN concenrations). (a) 0 M AA, EN, UA, (b-j) $6x10^{-7}$M, $8x10^{-7}$ M, $3x10^{-6}$ M, $6x10^{-6}$ M, $7x10^{-6}$, $8x10^{-6}$ M.

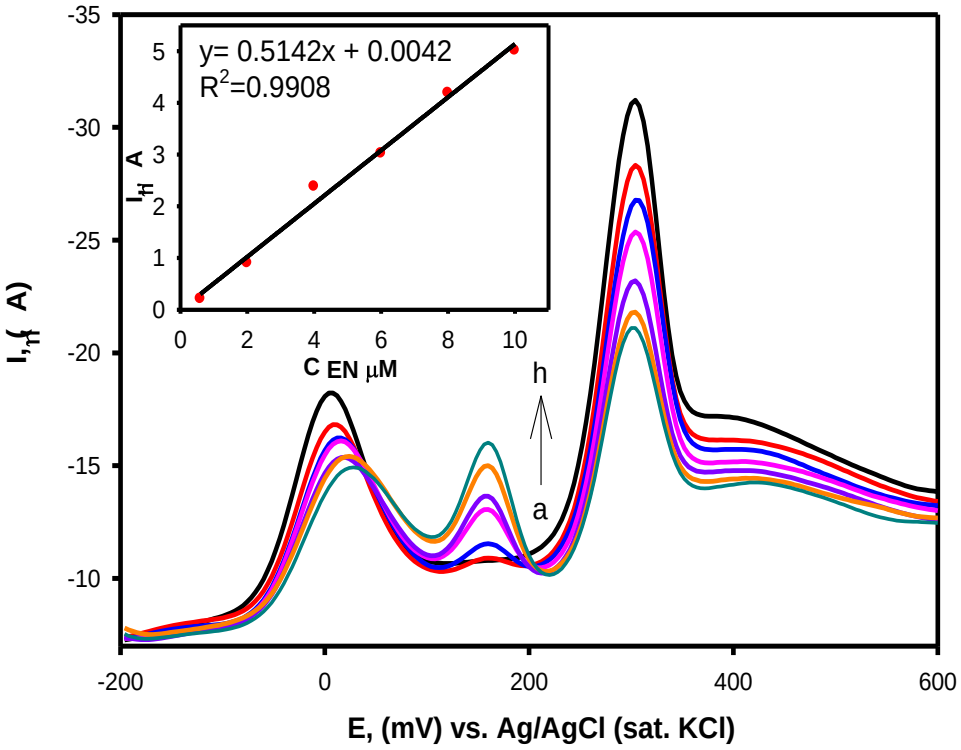

Figure 3.50 Differential pulse voltammograms at Pt-Ox-PAP/GCE in the presence of AA ($5x10^{-4}$ M) and UA ($5x10^{-5}$ M) for increasing concanterations of EN in 0.1 M pH 7.40 PBS with scan rate 10 mV/s and pulse amplitude 50 mV.(Inset: Corresponding calibration curve of increasing EN concenrations). (a) 0 M AA, EN, UA, (b-j) $6x10^{-7}$M, $8x10^{-7}$ M, $2x10^{-6}$ M, $4x10^{-6}$ M, $6x10^{-6}$, $8x10^{-6}$ M, $1x10^{-5}$ M.

Figure 3.51 and 3.52 diplays the DPV obtained for different concentration of UA in the presence of $5x10^{-4}$ M AA and $2x10^{-5}$ M EN at Ox-PAP/GCE and Pt-Ox-PAP/GCEs, respecticely. The oxidations peaks with adequate resolution for three compounds were appeared at 10 mV for AA, 144 mV for EN, 280 mV for UA using Ox-PAP/GCE and 2 mV for AA, 170 mV for EN, 285 mV for UA using Pt-Ox-PAP/GCE. These oxidation peak separations were large enough to achieve determination of UA in homogeneous solution containing excess concentration of AA and EN. More sensitive results obtained from Ox-PAP/GCE compared to the Pt-Ox-PAP/GCE due to the overlapping of UA and Pt signals. The linear regression equations were expressed as y=0,0823x - 0.3956, R^2=0.9909 for Ox-PAP/GCE and y=0,0969x -1.0403,R^2=0.9930 for Pt-Ox-PAP/GCE

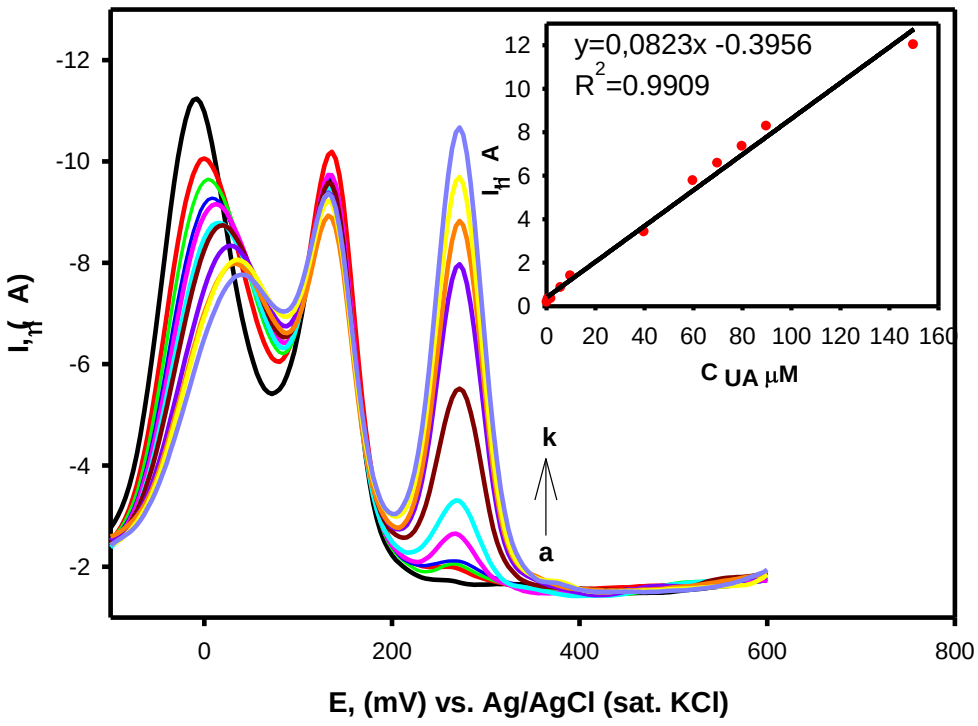

Figure 3.51 Differential pulse voltammograms at Ox-PAP/GCE in the presence of AA ($5x10^{-4}$ M) and EN ($2x10^{-5}$ M) for increasing concanterations of UA in 0.1 M pH 7.40 PBS with scan rate 10 mV/s and pulse amplitude 50 mV.(Inset: Corresponding calibration curve of increasing UA concentrations) (a) 0 M UA, $5x10^{-4}$ M AA, $2x10^{-5}$ M EN, (b-k) $4x10^{-7}$M, $2x10^{-6}$ M, $6x10^{-6}$ M, $1x10^{-5}$ M, $4x10^{-5}$, $6x10^{-5}$ M, $7x10^{-5}$ M, $8x10^{-5}$, $9x10^{-5}$ M, $1.5x10^{-4}$ M.

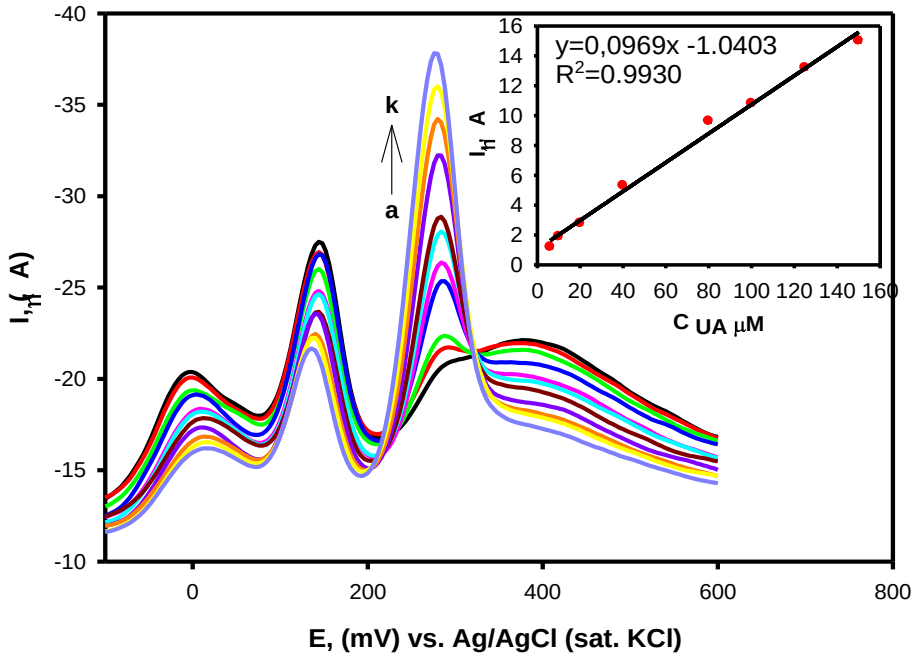

Figure 3.52 Differential pulse voltammograms at Pt-Ox-PAP/GCE in the presence of AA (5x10-4 M) and EN (2x10-5 M) for increasing concanterations of UA in 0.1 M pH 7.40 PBS with scan rate 10 mV/s and pulse amplitude 50 mV.(Inset: Corresponding calibration curve of increasing UA concenrations). (a-k) $1x10^{-5}$ M, $1.3x10^{-5}$ M, $1.5x10^{-5}$ M, $1.8x10^{-5}$ M $2x10^{-5}$ M, $4x10^{-5}$ M, $6x10^{-5}$, $8x10^{-5}$ M, $1x10^{-4}$ M, $1.25x10^{-4}$, $1.5x10^{-4}$ M UA.

The ability of the oxidized polymer film and its Pt nano particles deposited form promote the separation and oxidation peak currents of AA, EN and UA depending on each analyte concentration was investigated at same conditions. Figure 3.53 and Figure 3.54 show the DPV obtained at Ox-PAP/GCE and Pt-Ox-PAP/GCE respectively during the simultaneous increase of the concentration of AA + EN+ UA mixture at similar conditions.

The oxidation peak currents were enhanced with increasing the mixture concentration. Three well-defined oxidation peaks were appeared for AA, EN and UA in simultaneous increasing concentration of the mixture. The voltammograms demonstrated that the peak currents for AA, EN and UA were for a wide range of increasing concentrations: 10^{-5} to $2x10^{-4}$ M for AA and $9x10^{-8}$ to 10^{-5} M for EN and $4x10^{-7}$ M to 10^{-4} M for UA observed at Ox-PAP/GCE. Also at Pt-Ox-PAP/GCE wide range linearity was obtained for all three sunstance with values of $2x10^{-5}$ to $2x10^{-3}$ M for AA and $2x10^{-6}$ to 10^{-4} M for EN and $4x10^{-6}$ M to $4x10^{-4}$ M for UA.

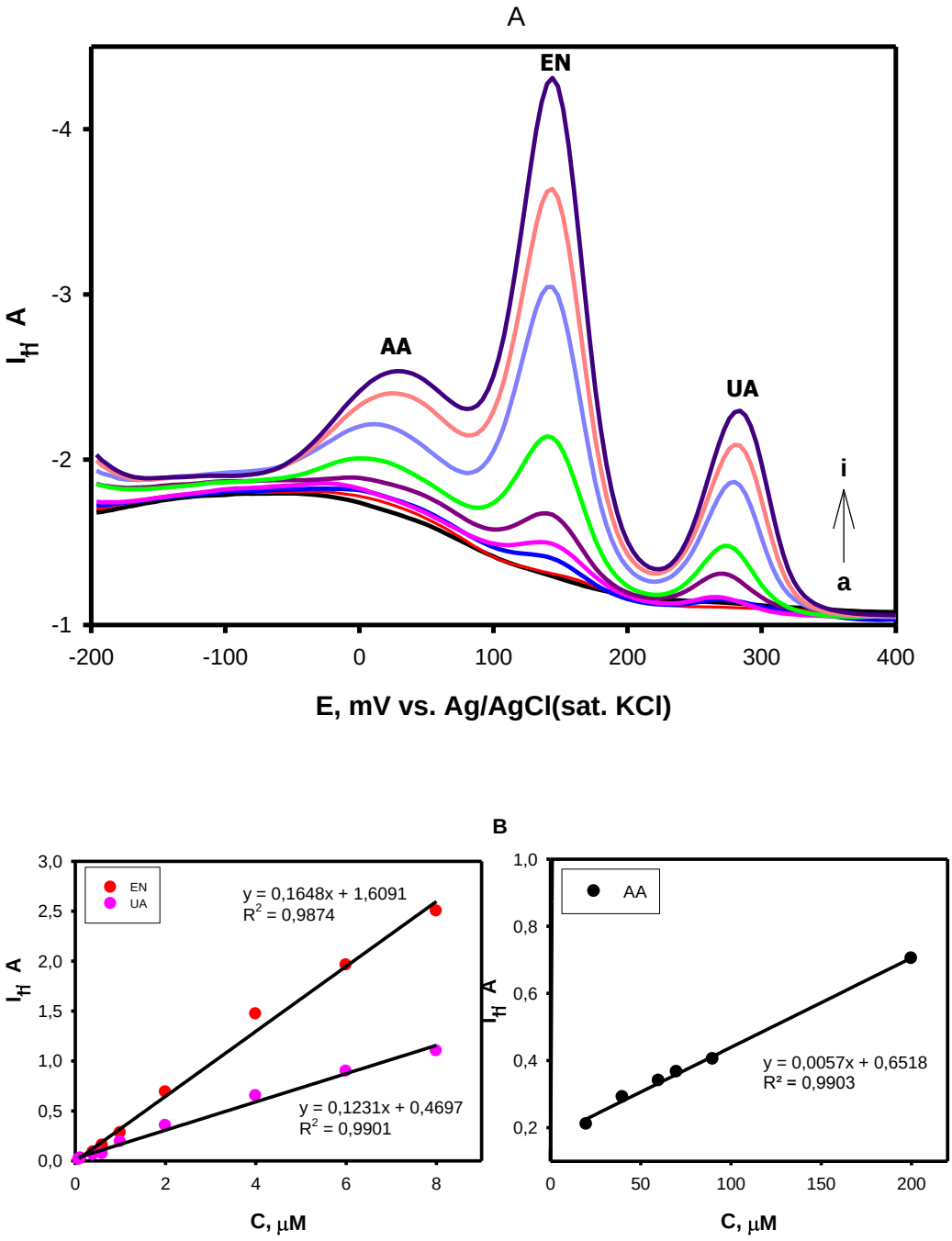

Figure 3.53 A) Differential pulse voltammograms at Ox-PAP/GCE in the presence of increasing concentrations of AA, EN and UA in 0.1 M pH 7.40 PBS with scan rate 10 mV/s, analyte concentrations: (a) 0 (b) $4.0x10^{-6}$ AA, $1.2x10^{-7}$ M EN and UA, (c) $6.0x10^{-6}$ AA, $4x10^{-7}$ M EN and UA (d)$7.0x10^{-6}$ AA, $6x10^{-7}$ M EN and UA, (e) $1.0x10^{-5}$ AA, $1x10^{-6}$ M EN and UA (f) $2.0x10^{-5}$ AA, $2x10^{-6}$ M EN and UA (g) $4.0x10^{-5}$ AA, $4x10^{-6}$ M EN and UA (h) $6.0x10^{-5}$ AA, $6x10^{-6}$ M EN and UA (i) $7.0x10^{-5}$ AA, 8 $x10^{-6}$ M EN and UA. B) Calibration curves of AA, EN and UA.

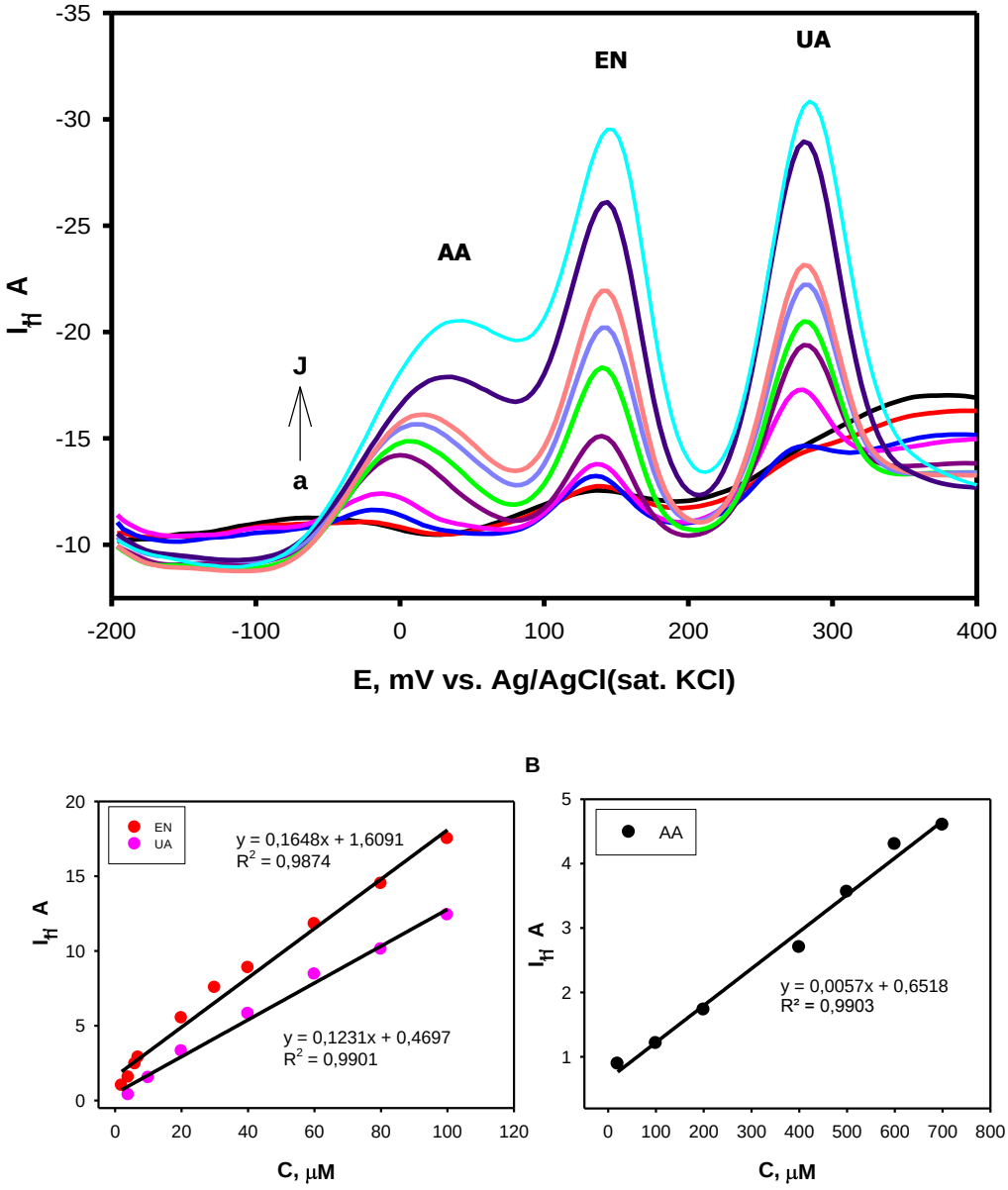

Figure 3.54 A) Differential pulse voltammograms at Pt-Ox-PAP/GCE in the presence of increasing concentrations of AA, EN and UA in 0.1 M pH 7.40 PBS with scan rate 10 mV/s, analyte concentrations: (a) 0 (b) $4.0x10^{-5}$ AA, $4x10^{-6}$ M EN, $4x10^{-6}$ M UA, (c) $1.0x10^{-4}$ AA, $6x10^{-6}$ M EN, $1x10^{-5}$ M UA, (d) $2.0x10^{-4}$ AA, $7x10^{-6}$ M EN, $2x10^{-5}$ M UA, (e) $4.0x10^{-4}$ AA, $1x10^{-5}$ M EN, $4x10^{-5}$ M UA, (f) $5.0x10^{-4}$ AA, $2x10^{-5}$ M EN, $6x10^{-5}$ M UA, (g) $6.0x10^{-4}$ AA, $3x10^{-5}$ M EN, $8x10^{-5}$ M UA, (h) $7.0x10^{-4}$ AA, $4x10^{-5}$ M EN, $1x10^{-4}$ M UA, (i) $1.0x10^{-3}$ AA, $6x10^{-5}$ M EN, $2.5x10^{-4}$ M UA,. (j) $1.5x10^{-3}$ AA, $8x10^{-5}$ M EN, $3x10^{-4}$ M UA, (k) $2.0x10^{-3}$ AA, $1x10^{-4}$ M EN, $4x10^{-4}$ M UA, B) Calibration curves of AA,EN and UA.

Finally, to comparisons of the sensitivity, limit of detection (LOD) and linear concentration range of AA, EN and UA detections on the all electrodes were listed in Table 3.4.

Table 3.4 Limit of detection (LOD) and linear concentration range of bare GCE, Ox-PAP/GCE and Pt-Ox-PAP/GCE for AA, EN, UA and their mixture in this thesis

Analytes	**Ascorbic Acid (AA)**	**Epinephrine (EN)**	**Uric Acid(UA)**
Electrode	**Bare GCE**		
Linear Range	$7x\ 10^{-6}$ M – $2x10^{-3}$ M	$7x10^{-6}$ M – $2.2x10^{-4}$ M	$4\ x\ 10^{-6}$ M – $1x10^{-4}$ M
LOD	$6.9x\ 10^{-6}$ M	$4{,}9x10^{-6}$	$3.1\ x\ 10^{-6}$
Electrode	**Ox-PAP/GCE**		
Linear Range	$8.1x\ 10^{-6}$– $3x10^{-3}$ M	$7.8x10^{-9}$ – $8x10^{-5}$M	$9.8x10^{-8}$ – $6x10^{-5}$M
LOD	$8x\ 10^{-6}$ M	$6{,}5x10^{-9}$ M	$6.4x10^{-8}$ M
Electrode	**Pt-Ox-PAP/GCE**		
Linear Range	$1.8x\ 10^{-6}$ – $1x10^{-3}$ M	$4x\ 10^{-7}$ – $1.5x10^{-4}$M	$2.4x\ 10^{-6}$ – $1.5x10^{-4}$M
LOD	$1.8x\ 10^{-5}$ M	*$1.8x\ 10^{-7}$ M	*$2.2x\ 10^{-6}$ M
Analytes	**MIXTURE OF AA, EN, UA at Ox-PAP/GCE**		
	$2x10^{-5}$ M EN and UA+AA↑	**$5x10^{-4}$ M AA $5x10^{-5}$ M UA +EN↑**	**$5x10^{-4}$ M AA+$4x10^{-5}$M EN +UA↑**
Linear Range	$9.8x10^{-6}$ M – $1x10^{-3}$ M	$1.3x10^{-7}$ M – $1x10^{-5}$M	$2.2x10^{-7}$ M – $1.8x10^{-4}$ M
LOD	$9.5\ x10^{-6}$ M	*$9x10^{-8}$ M	*$1.4x10^{-7}$ M
Analytes	**MIXTURE OF AA, EN, UA at Pt-Ox-PAP/GCE**		
	$2x10^{-5}$ M EN and UA+AA↑	**$5x10^{-4}$ M AA $5x10^{-5}$ M UA +EN↑**	**$5x10^{-4}$ M AA+$4x10^{-5}$M EN +UA↑**
Linear Range	$6.1x10^{-5}$ – $1.2x10^{-3}$M	$4.3x10^{-7}$ – $3x10^{-5}$M	$6.6x10^{-6}$ – $5x10^{-4}$M
LOD	$5x10^{-5}$ M	*$3{,}6x10^{-7}$ M	*$4.1x10^{-6}$ M

*LOD values calculated from calibration curve.

3.17 Stability of Pt nano particles modified Ox-PAP/GCE

A long-term storage stability of the Pt nano particles modified Ox-PAP/GCE was studied by keeping above the electrode in vapour of phosphate buffer solution (pH 7.40) at room temperature. The respons of the electrode in the buffer solution containing $5x10^{-4}$ M AA, EN and UA, maintained 90 %, 90.3 %, 93.5 % of the original peak current value after 3 days for AA, EN, UA, respectively

Table 3.5. Peak current values of Pt nano particules modified Ox-PAP/GCE

	I (µA)		
Days	**AA**	**EN**	**UA**
1	5,96	32,1	27,15
2	5,98	35,4	26.35
3	5,3	31	25,4

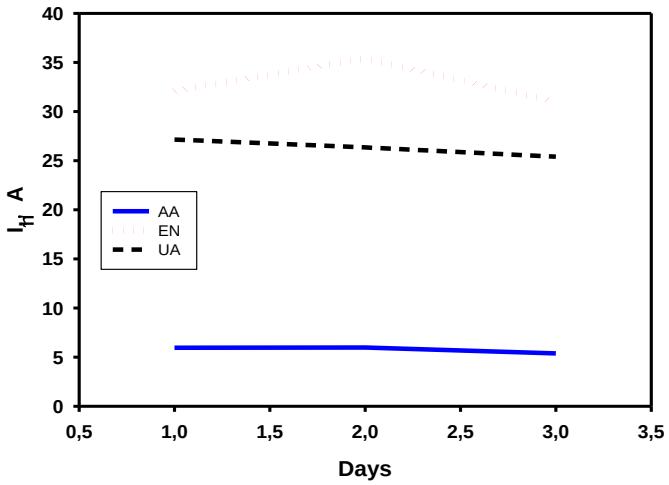

Figure 3.55 Variation of peak current for AA, EN, UA mixture during 3 days.

3.18 Sample Analysis

The method was applied to the EN injection solution which was contain 4.00 µM EN that known from the prospectuse. Figure 3.56 shows the standard addition DP voltammograms obtained for EN sample. The sample was treated as given in experimental section. As can be seen from the figure, standard addition graph was constructed. 3.97± 0.07 (n=3, 95% CI) µM EN concentration was obtained at Ox-PAP/GCE and results were found in agreement with EN injection content (4.00 µM).

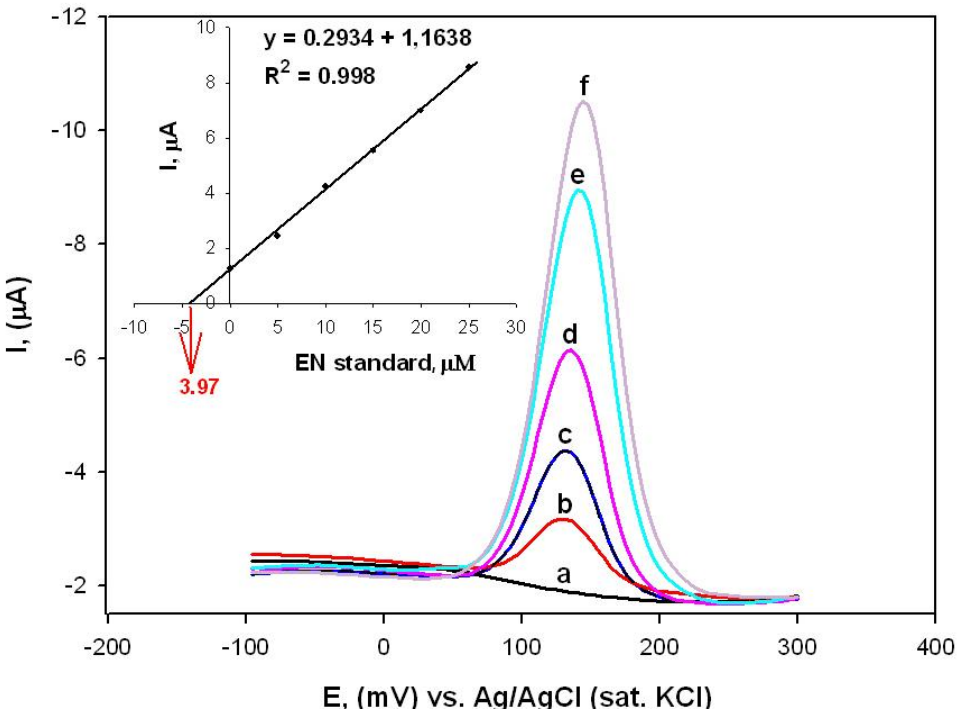

Figure 3.56 Differential pulse voltammograms at Ox-PAP/GCE **A)** (a) pH 7.40 phosfate buffer, (b) EN sample in pH 7.40 phosfate buffer, (c) $5x10^{-6}$, (d) $10x10^{-6}$, (e) $15x10^{-6}$, (f) $20x10^{-6}$, inset: standart addition curves.

Figure 3.57 shows the standard addition at Pt- Ox-PAP/GCE obtained for EN samples. The calibration curve for EN samples at Pt-Ox-PAP/GCE was found linear y=0.279x+1.1211 (R^2 = 0.9918). EN amount of sample was detected 4.02± 0.04 (n=3, 95% CI) µM. The results were found in agreement with for Pt-Ox-PAP/GCE as compared to Pt-Ox-PAP/GCE.

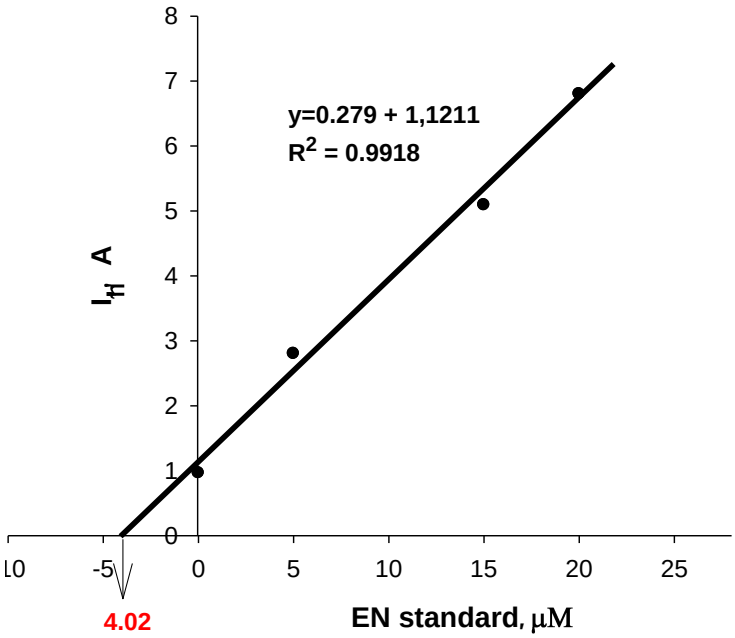

Figure 3.57 Standart addition curves for EN sample in pH 7.40 phosfate buffers at Pt-Ox-PAP/GCE, EN standard solution ($5x10^{-6}$, $10x10^{-6}$, $15x10^{-6}$, $20x10^{-6}$ M).

4. GENERAL DISCUSSION AND CONCLUSION

Electrochemistry and analytical chemistry requires new type of electrode materials for catalytic and selective electrode reactions. For this aim, nano materials have been used in last decade. Nanoparticles are different from bulk materials and isolated molecules because of their unique optical, electronic, magnetic, chemical properties and high effective surface area. Therefore, nano structured materials have been used in diverse applications such as catalysis, nanodevices, optoeletronics and biosensors.

The extraordinary role of nanometarials in modern analytical chemistry is supported by the electrocatalytic ability of carbon nanotubes modified electrodes. The modification is enhanced the analytical properties such as the active surface area, high electronic conductivity and the anti-fouling capability of the surface. Furthermore, to improve the unique properties of CNTs, the modification could be combined with metal nano particles which they can be synthesized and modified chemically or electrochemically. To prepare an effective metal nano particles which is attached on the CNT modified electrodes, an electrochemically deposition procedure is rapid, simple and reproducible.

The electrochemical reduction of oxygen is one of the most important reaction in electrochemistry; because of interest in the corrosion, electrocatalysis, biological systems (respiratory chain and enzymatic reactions), organic electrosynthetic processes, electrochemical devices and especially in energy conversion (fuel cells and metal air bateries). Oxygen reduction reaction can proceed by two electron or four-electron pathways depending on electrode material. Preparation of higher catalytic electrode surface is a key factor for enhancing the performance of the electrodes. For this aim, in this thesis, new electrode materials were prepared using multiwall carbon nanotube modified with alone Cu, Au or Au-Cu bimetallic nano particles on GCE surface for catalytic reduction of oxygen. The Cu-Au bimetalic nano particles modified MWCT/GCE showed best catalytic activity for oxygen reduction. The remarkably enhanced signal of oxygen reduction the modified electrode can be attributed increasing the conductivity and effective

surface area electrode which can be played important role to accelerate the electron transfer.

AA, EN and UA usually coexist in the biological fluids. The individual and simultaneous determination of each compound is important problem in biomedical chemistry and neurochemistry. It is well known that, the oxidation potentials of AA, EN and UA on bare and some modified electrodes overlaps. Therefore, it is essential to develop a new electrode material for selective and sensitive determination of AA, EN and UA. In this thesis, Ox-PAP/GCE and Pt nano particles modified Ox-PAP/GCE have constructed by covering GCE surface with polymer film and Pt nano particles by electrochemically.

The topographic image with AFM, SEM (SEM-EDX) and CV techniques exhibited that a characteristic Ox-PAP and Pt nano clusters were successfully constituted on the Ox-PAP/GCE /GCE surface. The electrochemical oxidation of AA, EN and UA or their mixtures on Ox-PAP/GCE /GCE and Pt nano particles modified Ox-PAP/GCE /GCE were carried out by diffussion controlled conditions which obtained with a series of CV by varying potential scan rates. The Ox-PAP/GCE and Pt nano particles modified Ox-PAP/GCE showed a strongly electrocatalytic activity towards individual and simultaneously oxidation of AA, EN and UA in pH 7.40 of PBS. On the other hand, higher peak potential separation was obtained at the Pt nano particles modified Ox-PAP/GCE /GCE. The results showed that, Pt nano particles has a highest synergic effect with Ox-PAP/GCE on the electrode surface compare to bare GCE due to the well-defined seperated oxidation peaks and higher currents for oxidation of AA, EN and UA mixtures.

Finally, for the individualy and simultaneously determination of AA, EN and UA; the Pt nano particles modified Ox-PAP/GCE showed good characteristics such as excellent selectivity, sensitivity and good stability at least for three days.

REFERENCES

Alexeyeva, N., Matisen, L., Saar, A., Laaksonen, P., Kontturi, K., Tammeveski, K., 2010, Kinetics of oxygen reduction on gold nanoparticle/multi-walled carbon nanotube hybrid electrodes in acid media, *Journal of Electroanalytical Chemistry*, 642:6-12.

Anzai, J., Wang, B., Noguchi, T., 2007, Layer-by-layer thin film-coated electrodes for electrocatalytic determination of ascorbic acid, *Talanta*, 72: 415-418.

Aoun, S. B., Dursun, Z., Koga, T., Bang, G.S., Sotomura, T., Taniguchi, I., 2004, Effect of metal ad-layers on Au(111) electrodes on electrocatalytic reduction of oxygen in an alkaline solution, *J. Electoanal. Chem*. 567:175–183.

Bagotsky, V. S., 2006, Fundamentals of Electrochemistry, *John Wiley & Sons, Inc.*

Bard, A. and Faulkner, L. R., 2001, Electrochemical methods, *John Wiley&Sons*, Newyork

Biallozor, S. and Kupniewska, A., 2005, Conducting polymers electrodeposited on active metals-A Review, *Synthetic Metals*, 155: 443–449.

Buruni, G., 2007, Development of a quantitative method for the analysis of total l-ascorbic acid in foods by high-performance liquid chromatography, *Journal of Chromatography A*, 1154:97-102.

Cao, G., Nanostructures and Nanomaterials, *Synthesis*, Properties and Applications, 2004, Imperial College Press

Cheetham, A.K., Rao, C.N.R., Müller, A., 2004, The Chemistry of Nanomaterials, Wiley, VCH

REFERENCES(continue)

Chen, Der-chang, Zhan, Dian-Zhen, Cheng, Chun-Weng, Liu, An-Chiang, Chen, Chun-hsien 2001, Determination of urine catecholamines by capillary electrophoresis with dual-electrode amperometric detection, *Journal of Chromatography B: Biomedical Sciences and Applications,* 750,(1, 5),33-39

D'Eramo, Fabiana, Moressi, M. B., Fernández, H., María A., Arévalo, A Sereno, Álvarez-Lueje, L.E.A., Studies based on the electrochemical response of 2-(2-nitrophenyl)-1H-benzimidazole at chemically modified electrodes with over-oxidized poly-1-naphthylamine, 2010, *Electrochimica Acta*, 55 (15) 4421-4427,

Dresselhaus, M.S., Dresselhaus, G., Eklund, P.C., 1996, Science of Fullerenes and Carbon Nanotubes, Elsevier

Dresselhausa, M.S., Linb, Y.M., Rabinc, O., Jorioa, A., Filho, A. G. S., Pimentad, M. A., Saitof, R., Samsonidzeb, Ge.G., Dresselhaus G., 2003, Nanowires and nanotubes *Materials Science and Engineering* C 23:129–140.

Dursun, Z., Gelmez, B., 2010, Simultaneous Determination of Ascorbic Acid, Dopamine and Uric Acid at Pt Nanoparticles Decorated Multiwall Carbon Nanotubes Modified GCE *Electroanalysis* Volume 22:1106–1114.

Ensafi, A.A. Taei, M. Khayamian, T., 2010, Simultaneous determination of ascorbic acid, epinephrine, and uric acid by differential pulse voltammetry using poly(p-xylenolsulfonephthalein) modified glassy carbon electrode, *Colloids and Surfaces B: Biointerfaces* 79:480–487.

Galban, J., Andreu, Y., Almenara, M. J., Marcos, S. and Castillo, J. R., 2001, Direct determination of uric acid in serum by a fluorometric-enzymatic method based on uricase, *Talanta* 54: 847–854.

REFERENCES(continue)

Gosser, D.K., 1994, Cyclic Voltammetry, *VCH Publisher*, Newyork

Haudy, P., Brechignac, C. and Lahmani, M., 2006, Nanomaterials and Nanochemistry, *European Materials Research Society*, Belin, France

Heflin. J.R., Ventra, M., Evoy, S., 2004, Introduction to Nanoscale Science and Technology, *Kluwer Academic Publisher*, Boston.

Hernández, P., Sánchez, I. Patón, F. Hernández, L. 1998, Cyclic voltammetry determination of epinephrine with a carbon fiber ultramicroelectrode, *Talanta, 46:(5),985-991*

Hu, P., Wang, R.Y., Liang, Q. L., Luo, G. A. and Wang, Y. M., 2007, Voltammetric determination of uric acid by using gold nanotubule electrode, *Chinese Chemical Letters* 18: 1111–1114.

Huaibing He, C. Michael S., Brian C, Alastair J. J. W., 1997, Determination of catecholamines in sheep plasma by high-performance liquid chromatography with electrochemical detection: comparison of deoxyepinephrine and 3,4-dihydroxybenzylamine as internal standard, *Journal of Chromatography B: Biomedical Sciences and Applications*, 701:(1,7), 115-119.

Inzelt, G., 2008, Conductive Polymers, *Springer*, Germany, 262p

Janghel, E.K., Rai, J.K., Rai, M.K., Gupta, V., K., 2007, Micro determination of ascorbic acid using methyl viologen, *Talanta*, 72:1013-1016

Jin, B., Zhang, H., 2002, Nano-Gold Modified Glassy Carbon Electrode for Selective Determination of Epinephrine in the Presence of Ascorbic Acid, *Analytical Letters*, 35(12):1907-1918.

REFERENCES(continue)

Jing, L., Xiangqin, L., 2007, Simultaneous determination of dopamine and serotonin on gold nanocluster/overoxidized-polypyrrole composite modified glassy carbon electrode, *Sensors and Actuators* B 124:486–493).

Kelsall, R.W., Hamley, I.W., Geoghegan, M., 2005, Nanoscale Science and Technology, *John Wiley & Sons, Inc.*

Kruusenberg, I., Matisen L., Jiang, H. Huuppola, M., Kontturi K., Tammeveski, K., 2010, Electrochemical reduction of oxygen on double-walled carbon Nanotube modified glassy carbon electrodes in acid and alkaline solu tions, *Electrochemistry Communications,* 12 (7), 920-923.

Kumar, S. A., Lo, Po-Hsun, Chen, S., 2008, Electrochemical selective determination of ascorbic acid at redox active polymer modified electrode derived from direct blue 71, *Biosensors and Bioelectronics*, 24:518-523.

Lima, L. F. C., Garcia, M. B., Silva, M. L. and Sousa, J. P., 2004, Automatic determination of uric acid in urine in a FIA system with a tubular amperometric detector, *Portugaliae Electrochimica Acta*, 22:249-262.

Lin, Y., Liu, G., Riechers, S. L., Mellen, M. C., 2005, Sensitive electrochemical detection of enzymatically generated thiocholine at carbon nanotube modified glassy carbon electrode, *Electrochemistry Communications*, 7:1168-1169.

Liu, C. C., Luo, Y. C., Do, J. S., 2006, An amperometric uric acid biosensor based on modified Ir–C electrode, *Biosensors and Bioelectronics* 22: 482–488.

Liu, Li-P., Yin, Z., Yang, Z., 2010, A L-cysteine sensor based on Pt nanoparticles/poly (o-aminophenol) film on glassy carbon electrode , *Bioelectrochemistry* 79:84–89.

REFERENCES(continue)

Łuczak T., 2009, Comparison of electrochemical oxidation of epinephrine in the presence of interfering ascorbic and uric acids on gold electrodes modified with S-functionalized compounds and gold nanoparticles *Electrochimica Acta* 54:5863–5870.

MacDiarmid, Alan G., 1997, Polyaniline and polypyrrole: Where are we headed?, *Synthetic Metals*,Volume 84, Issues 1-3, January, Pages 27-34.

Mahjani, M.G., Ehsani, A. Jafarian, M.. 2010, Electrochemical study on the semiconductor properties and fractal dimension of poly ortho aminophenol modified graphite electrode in contact with different aqueous electrolytes,, *Synthetic Metals 160*:1252–1258.

Matos, R. C., Angnes, L., Araujo, M. C. V., Saldanha, T. C. B, 2000, Modified microelectrodes and multivariate calibration for flow injection amperometric simultaneous determination of ascorbic acid, dopamine, epinephrine and dipyrone, *Analyst*, 12: 2011–2015

Michałowski, P. H, 2001, Flow-injection chemiluminescence determination of epinephrine in pharmaceutical preparations using raw apple juice as enzyme source , *Talanta*, 55, (6, 24)1165-1171

Muraviev, D.N., 2005, Inter-matrix synthesis of polymer stabilised metal nanoparticles, *Contributions to Science,* 3 (1): 19-32.

Nagaiah, T. C., Kundu, S., Bron, M., Muhler, M., Schuhmann W., 2010, Nitrogen-doped carbon nanotubes as a cathode catalyst for the oxygen reduction reaction in alkaline medium, *Electrochemistry Communications*, Volume 12:338-341,

Nakazawa, H., Inoue, K., Namiki, T., Iwasaki, Y., Yoshimura, Y., 2003, Determination of uric acid in human saliva by high-performance liquid chromatography with amperometric electrochemical detection, *Journal of Chromatography B*, 785: 57-63.

REFERENCES(continue)

Ojani, R., Raoof, J.-B., Fathi, S., 2009, Poly (o-aminophenol) film prepared in the presence of sodiumdodecyl sulfate: application for nickel ion dispersion and the electrocatalytic oxidation ofmethanol and ethylene glycol, *Electrochim. Acta*. 54:2190–2196.

Reed, S.J.B., 2005, Electron microprobe Analysis and Scanning electron microscopy in geology, Reed, *Cambridge.*

Rivas, G. A., Rubianes, M.D., 2007, Dispersion of multi-wall carbon nanotubes in polyethylenimine: A new alternative for preparing electrochemical sensors, *Electrochemistry Communications*, 9:480-484.

Shahrokhiana, S. Ghalkhania M,. Aminic M. K., 2009, Application of carbon-paste electrode modified with iron phthalocyanine for voltammetric determination of epinephrine in the presence of ascorbic acid and uric acid, *Sensors and Actuators B* 137 :669–675.

Sorouraddin, M. H. Manzoori, J. L., Kargarzadeh, E. Shabani A. M H., 1998, Spectrophotometric determination of some catecholamine drugs using sodium bismuthate, *Journal of Pharmaceutical and Biomedical Analysis*, 18(4-5), 877-881

Tanaka, K., Yamabe, T., Fukui, K., The Science and Technology of Carbon Nanotubes, 1999, Elsevier

Tietz, W.N., 1987, Fundamentals of Clinical Chemistry, 3rd Edition

Tzontcheva, A., Denikova, N., 2000, Analytical interference of drugs on the fluorimetric determination of urinary catecholamines, Clinica Chimica Acta, 297:(1-2), 217-223.

Ulubay, Ş., Dursun, Z., 2010, Cu nanoparticles incorporated polypyrrole modified GCE for sensitive simultaneous determination of dopamine and uric acid , *Talanta,* Volume 80, Issue 3, Pages 1461-1466

REFERENCES(continue)

Ulubay, Ş., 2008, Preparation of metal nanoparticules modified polypyrrole electrodes and their electrocatalytic activities, Msc thesis, E.U

Valentini, F., Biagiotti, V., Lete, C., Palleschi, G., Wang, J., 2007, The electrochemical detection of ammonia in drinking water based on multi-walled carbon nanotube/copper nanoparticle composite paste electrodes, *Sensors and Actuators B*, 128:(1) 326-333.

Vayenas, C. G., Bebelis, S., Pliangos, C., Brosda, S., Tsiplakides, D., 2002, "Electrochemical Activation of Catalysis Promotion, Electrochemical Promotion, and Metal-Support Interactions, *Kluwer Academic Publishers*.

Wallace, G. G., Spinks, G. M., Kane-Magnuire, L. P., Teasdale, P. R., 2009, Conductive Electroactive Polymers, *CRC pres, Taylor & Francis Group, New York*, 263p.

Walsh, G., 2007, Pharmaceutical Biotecnology: Concepts and Applications, John Wiley&Sons.

Wang, J., 1994, Analytical Electrochemistry", *WILEY-VCH.*

Wang, J., 2001, Analytical Electrochemistry", *WILEY-VCH.*

Wang, J., 2006, Analytical Electrochemistry,3rd ed.,Wiley,VCH

Willard, H. H., Merritt, L.L., Dean, J. A. and Settle, F.A., 1988, Instrumental Methods of Analysis, Wadsworth Publishing Company, California.

Zare H. R., Nasirizadeh, N., 2010, Simultaneous determination of ascorbic acid, adrenaline and uric acid at a hematoxylin multi-wall carbon nanotube modified glassy carbon electrode, *Sensors and Actuators B* 143, 666–672

REFERENCES(continue)

Zen, J. and Chen, P., 1997, A selective voltammetric method for uric acid and dopamine detection using clay-modified electrodes, *Anal. Chem*., 69:5087-5093.

Zen, J., Ke, J., Tseng, H., Hsu, C., Chen, J., Muthuraman, G., 2008, Flow injection analysis of ascorbic acid based on its thermoelectrochemistry at disposable screen-printed carbon electrodes, *Sensors and Actuators B*, 130: 614-619 .

Zhang, J., Xu, H., Wang, Y. and Li, G., 2008, Electrochemical Sensors for Clinic Analysis, Review, *Sensors*, 8: 2043-2081.

Zhao, S., Wang , J., Ye, F., Liu, Y., 2008, Determination of uric acid in human urine and serum by capillary electrophoresis with chemiluminescence detection, *Analytical Biochemistry*, 378: 127-131 .

Zhou, Y.Z, Zhang, L.J. Chen,S.L. Dong, S.Y. Zheng, X.H. , 2009, Electroanalysis and simultaneous determination of dopamine and epinephrine at poly(isonicotinic acid)-modified carbon paste electrode in the presence of ascorbic acid, *Chin. Chem. Lett.* 20 217–220

CURRICULUM VITAE

Name : Çağrı Ceylan BAKIR

Date of Birth **:** September, 30, 1986

Place of Birth **:** İzmir, Turkey

Nationality **:** Republic of Turkish

Marital Status : Single

Adress **:** 32 Sokak No:6 D:3 Güzelyalı İZMİR

Phone Number **:** +90 5556832327

E-mail **:** cagriceylanbakir@hotmail.com

Education **:** 2004-2008, BSc Degree in Chemisty Department of Ege University, İzmir, Turkey

2008-….., MSc Degree in Chemistry Department of Ege University, İzmir, Turkey.

INTERNATIONAL CONFERENCE PAPER

The 8th International Electrochemistry Meeting, 8- 11 October 2009, Antalya, Turkey, Electroreduction of Oxygen on Copper-Gold Nano Particles Doped Multiwalled Carbon Nanotube Modified Glassy Carbon Electrode.

The 8th International Electrochemistry Meeting, 8- 11 October 2009, Antalya, Turkey, Photoelectrocatalytic Oxidation of NADH Using a Poly-methylene Blue Modified Glassy Carbon Electrode.

The 4th International Student Conference on Advance Science and Technology, 25- 26 May 2010, Ege University, İzmir, Turkey, Electrochemical Behavior of Folic Acıd at Metal Nanoparticles Decorated Multıwalled Carbon Nanotube Modified Glassy Carbon Electrode

The 4th International Student Conference on Advance Science and Technology, 25- 26 May 2010, Ege University, İzmir, Turkey, Preparation of Oxidized Poly 4-Aminophenol Modified Glassy Carbon Electrode and Its Analytıcal Applicatıon